

Faculty of Engineering of the University of Porto



**3D Printing and Development of 3D Computational
Models of Biodegradable Meshes**

Maria Francisca Reis Rabaça Vaz

Dissertation elaborated within the scope of the Master's in Bioengineering

Supervisor: Dra. Maria Elisabete Teixeira da Silva

Co-Supervisor: Prof. Emeritus. António Augusto Fernandes

Co-Supervisor: Prof. Dr. Marco Paulo Lages Parente

September 22, 2023

Abstract

The pelvic area of the human body consists of several organs, that can for different reasons, such as natural childbirth or lifting heavy objects, suffer from prolapse, causing pain and discomfort to the person. This problem affects thousands of people in their day-to-day lives worldwide, therefore having a strong negative impact on their quality of life. There are solutions that try to correct the prolapse, however, present several disadvantages and limitations that need to be outdated, and therefore it is essential to develop new alternatives that respond more efficiently to the detected problems and increase the effectiveness of the treatment of pelvic organ prolapse. In order to try to get around this problem, there is the possibility of developing meshes trying to correct pelvic organ prolapse (POP). Initially, repair with synthetic polypropylene meshes was introduced taking into account the high success rates in the correction of abdominal hernias. Until the FDA, Food and Drug Administration prohibited the commercialization of some of these meshes, and, therefore, new approaches are urgent. The development of biodegradable meshes is a new approach to addressing the problems hitherto found with the use of synthetic meshes. This material would be placed in the patient's body through surgical intervention. In addition to its main function of guaranteeing the support of the organs, presents good characteristics regarding its flexibility and resistance, thus ensuring a better reinforcement of the intervened region, avoiding possible injuries in the tissues.

This may be a solution that can respond to the main disadvantages of synthetic meshes, due to the biocompatibility and the biomechanical properties that the biodegradable mesh features. For this, computational models were developed varying pore geometry, pore size, filament thickness, and the presence of filaments around specific mesh areas. Then one of the meshes was printed to validate the results obtained in the simulations performed. Afterwards, an uniaxial tensile test was conducted on sow's vaginal tissue for comparison with simulations, aiming to identify meshes exhibiting behaviour similar to vaginal tissue. Lastly, the most promising results obtained were compared with the uterosacral ligament and with a commercially available mesh.

In conclusion, after analysing all the results obtained, the mesh that best mimics the behaviour of the vaginal tissue features a smaller pore diameter (1.50 mm), filaments around specific areas of the mesh, and the filament thickness varies throughout the mesh. However, when comparing the results with the uterosacral ligament, the meshes do not demonstrate a similar behaviour to

the ligament. Lastly, the commercially available mesh does not appear to be the ideal choice for POP repair, since it does not behave similarly to the vaginal tissue or the uterosacral ligament.

Resumo

A zona pélvica do corpo humano composta por vários órgãos, pode por diversos motivos, por exemplo, o parto natural ou o levantamento de objetos pesados, sofrer prolapso, causando dor e desconforto à pessoa. Este problema afeta milhares de pessoas no seu dia-a-dia por todo o mundo, tendo por isso um forte impacto negativo na sua qualidade de vida. Existem soluções que tentam corrigir o prolapso, contudo ainda apresentam várias desvantagens e limitações que precisam ser ultrapassadas, sendo por isso, essencial desenvolver novas alternativas que respondam de uma forma mais eficiente aos problemas detetados e aumentem a eficácia do tratamento do prolapso dos órgãos pélvicos. De forma a tentar contornar este problema, surge a possibilidade do desenvolvimento de malhas que tentam corrigir o prolapso dos órgãos pélvicos. Inicialmente, o reparo com malhas sintéticas de polipropileno foi introduzido levando em consideração as altas taxas de sucesso na correção de hérnias abdominais. Até que a FDA proibiu a comercialização de algumas destas malhas e, portanto, novas abordagens são urgentes. O desenvolvimento de malhas biodegradáveis são uma nova abordagem para colmatar os problemas até então encontrados com o uso das malhas sintéticas. Este material seria colocado no corpo da paciente através de uma intervenção cirúrgica. Para além da sua principal funcionalidade de garantir a sustentação dos órgãos, apresenta boas características quanto à sua flexibilidade e resistência, garantindo assim, um melhor reforço da região intervencionada, evitando eventuais ferimentos nos tecidos.

A malha biodegradável consegue responder às principais desvantagens das malhas sintéticas, devido à biocompatibilidade e às propriedades biomecânicas que a malha biodegradável apresenta. Para tal, foram desenvolvidos modelos computacionais fazendo variar a geometria e tamanho dos poros, a espessura dos filamentos e a presença de filamentos à volta da malha em zonas específicas. De seguida, foi impressa uma das malhas de modo a validar os resultados obtidos nas simulações realizadas. Posteriormente, foi realizado um teste de tração uniaxial no tecido vaginal de porca para comparar os valores de força-deslocamento obtidos com os resultados das simulações, de modo a identificar quais as malhas que apresentam um comportamento semelhante ao tecido vaginal. Por fim, foram comparados os melhores resultados obtidos com o ligamento útero-sacral e com uma malha comercialmente disponível.

Após a análise de todos os resultados obtidos, a malha que melhor mimetiza o comportamento do tecido vaginal, apresenta menor diâmetro de poro (1,50 mm), filamentos em redor da malha em zonas específicas e a espessura dos filamentos varia ao longo da malha. Contudo, ao comparar os resultados com o ligamento útero-sacral, as malhas não demonstram um comportamento semelhante ao ligamento, sendo este um ponto a melhorar em trabalhos futuros. Por fim, a malha comercialmente disponível não apresenta um comportamento semelhante ao tecido vaginal, nem ao ligamento útero-sacral, logo não é a escolha ideal para o reparo do prolapso.

Acknowledgments

First and foremost, I would like to extend my sincere thanks to my supervisor Dr. Elisabete Silva, and Co-supervisors Prof. Emeritus. António Augusto Fernandes, and Prof. Dr. Marco Paulo Lages Parente, for the dedication, guidance, and motivation provided throughout the development of this thesis. I would also like to take this moment to express my heartfelt appreciation to my colleagues at *Laboratório de Desenvolvimento de Produto e Serviços*, especially to Ana Pais for all the help and support during the past year.

I must also express my gratitude to my family, my boyfriend, and friends, who have been unwavering in their support throughout my academic journey, offering assistance during challenging times, and for turning my years at FEUP into memorable and joyous experiences.

Lastly, I gratefully acknowledge the Emprego Científico 2021.00077.CEECIND, Funded by FCT. This work was supported by FCT, through INEGI, in the scope of LAETA, project UIDB/50022/2020 and UIDP/50022/2020.

Index

Abstract	iii
Resumo	v
Acknowledgments	vii
Index	ix
List of figures	xi
List of Tables	xv
Abbreviations, Acronyms and Symbols	xvii
Chapter 1	1
Introduction	1
1.1 Motivation	1
1.2 Objectives	2
1.3 Dissertation Structure.....	2
Chapter 2	5
State of the Art	5
2.1 Female pelvis	5
2.2 Pelvic Organ Prolapse	9
2.2.1 Classification and Diagnoses	10
2.2.2 Forms of treatment.....	12
2.3 Computational Modelling	15
2.3.1 Finite Element Method.....	15
2.3.2 Finite Element Analysis	17
2.3.3 Abaqus® Software.....	18
2.3.4 Simulations	19
Chapter 3	23
Materials and Methods	23
3.1 Materials	23
3.1.1 Medical-grade PCL	23

3.1.2 Vaginal Tissue	24
3.2 Methodology	25
3.2.1 Instruments and Tools.....	25
3.2.2 Mesh Prototyping	29
3.2.2.1 Synthetic Meshes.....	29
3.2.2.2 Computational Modelling of the Biodegradable Mesh.....	30
3.2.2.3 Experimental Procedures	35
3.2.2.3.1 Uniaxial tensile test - Printed Mesh.....	37
3.2.2.3.2 Uniaxial tensile test - Vaginal tissue.....	37
Chapter 4	39
Results and Discussion	39
4.1 Printed Mesh and the Computational Model	39
4.2 Computational Models	40
4.2.1 Absence and Presence of the Filament around the Mesh	41
4.2.2 Pore Dimension	46
4.2.3 Filament Thickness	47
4.3 Final Remarks Regarding the Computational Models	54
4.4 Main Conclusions.....	55
Chapter 5	57
Conclusions and Future Works	57
5.1 Conclusions	57
5.2 Future Works	58
References	59
Appendix.....	63

List of figures

Figure 2.1 Representation of the women’s and men’s pelvises, respectively (adapted from [8]).	6
Figure 2.2 Representation of the bony framework of the pelvis (adapted from [12]).	7
Figure 2.3 Pelvic floor muscles seen in the sagittal section of pelvis (adapted from [14] and [16]).	8
Figure 2.4 Pelvic floor muscles as seen from the perineal surface (adapted from [16]).	8
Figure 2.5 Types of pelvic organ (adapted from [19]).	9
Figure 2.6 A - Measurements used for this system. B - Points for PQP-Q system examination (adapted from [22]).	10
Figure 2.7 Baden-Walker Halfway Scoring System: grade 0 - no prolapse, grade 1 - descent halfway to the hymen, grade 2 - descent to the hymen, grade 3 - descent halfway past hymen, grade 4 - maximum descent (adapted from [23]).	11
Figure 2.8 Pelvic exam (adapted from [24]).	11
Figure 2.9 Different Pessaries used for the treatment of pelvic organ prolapse (adapted from [24]).	13
Figure 2.10 Illustration displaying the secure anchoring of a mesh through anatomical spaces in the pelvis (adapted from [32]).	14
Figure 2.11 Magnitude of displacement (mm) observed in the uterus and bladder following the complete rupture of USLs and CLs, represented as (a) and (b) respectively. Additionally, the displacement with the incorporation of USLs and CLs implants after the rupture of these ligaments, specifically for the continuous stitch technique, is illustrated as (c) and (d) (adopted from [41]).	20
Figure 2.12 Contour plots depicting the normalized mesh burden for altered DirectFix A geometries are displayed (adapted from [42]).	21
Figure 3.1 The samples of the vaginal tissue.	24
Figure 3.2 Melt electrowriting device.	25
Figure 3.3 Temperature and Humidity control.	26

Figure 3.4 Uniaxial tensile test machine used to perform uniaxial tensile tests in samples of printed meshes.	26
Figure 3.5 Uniaxial tensile test machine used to perform uniaxial tensile tests in samples of vaginal tissue.	27
Figure 3.6 Schematization of the samples' dimensions for the uniaxial tensile tests.	28
Figure 3.7 The micrometre used to verify the filament thickness of the printed meshes.	28
Figure 3.8 A SEM image of the Restorelle® mesh, and an example of the Restorelle® mesh, respectively (adapted from [2][55]).	30
Figure 3.9 Uniaxial tensile test to a filament of medical-grade PCL.	31
Figure 3.10 Stress and strain values obtained from the uniaxial tensile test carried out on the filament.	31
Figure 3.11 Some examples of the different developed meshes. Mesh names: A - Triangle, B - Diamond, C- Octagon, D - Circular, E - Sinusoidal, F- Diagonal, G - Oval, and H - Square.	32
Figure 3.12 Computational models of the circular pore meshes. A - Mesh with 1.50 mm pore diameter and filaments around the mesh in certain areas, B - Mesh with 2.00 mm pore diameter and filaments around the mesh in certain areas, C - Mesh with 2.50 mm pore diameter and filaments around the mesh in certain areas, D - Mesh with 2.50 mm pore diameter and without a filament around the mesh, and E - Mesh with 2.50 mm pore diameter and a filament around the mesh.	34
Figure 3.13 Distribution of filament thickness in the meshes. A - Mesh with 1.50 mm pore diameter, B - Mesh 2.00 mm pore diameter, C - Mesh 2.50 mm pore diameter, D - Mesh with 2.50 mm pore diameter. The red columns represent the filaments with a diameter of 0.08 mm or 0.16 mm, both cases were simulated, and the remaining columns have 0.24 mm of thickness.	34
Figure 3.14 Definition of the boundary conditions of the circular mesh with 2.00 mm of pore diameter.	35
Figure 3.15 Computational model of a mesh with a square pore of 2.00 mm, and a filament with 0.24 mm of thickness.	35
Figure 3.16 Initial part of the g-code for the medical-grade PCL mesh with square pores, 2.00 mm of pore diameter, and 0.24 mm of filament thickness.	36
Figure 3.17 Uniaxial tensile test performed on the printed mesh with square pores of 2.00 mm of diameter, and 0.24 mm of filament thickness.	37
Figure 3.18 Uniaxial tensile test performed on the vaginal tissue.	37
Figure 4.1 Load and displacement values obtained from the computational model and the experimental mesh, both with square pores of 2 mm and 0.24 mm of filament diameter.	40
Figure 4.2 Computational models developed without a filament around the mesh and 0.24 mm filament thickness. 1 - Sinusoidal with a 1.58 mm pore size. 2 - Triangular with a 2.06 mm	

pore size. 3 - Octagon with a 2.10 mm pore size. 4 - Diamond with a 2.00 mm pore size. 5 - Oval with a 2.00 mm by 2.50 mm pore size. 6 - Circular with a 2.00 mm pore size..... 41

Figure 4.3 Load-displacement curves of the computational models created without the filament around them. 41

Figure 4.4 Difference between the pores of the sinusoidal mesh before and after the simulation. 42

Figure 4.5 Computational models developed with a filament around the mesh and 0.24 mm of filament thickness. 1 - Circular with a 2.00 mm pore size. 2 - Octagon with a 2.10 mm pore size. 3 - Oval with a 2.00 mm by 2.50 mm pore size. 4 - Diamond with a 2.00 mm pore size. 5 - Diagonal with a 2.00 mm pore size. 6 - Square with a 2.00 mm pore size. 7 - Triangular with a 2.06 mm pore size. 43

Figure 4.6 Load-displacement curves of the computational models created with the filament around them. 44

Figure 4.7 Difference between the pores of the circular mesh before and after the simulation. 45

Figure 4.8 Circular pore meshes developed with and without a filament around the mesh. 1 and 2 - Meshes with 1.50 mm pore diameter. 3 and 4 - Meshes featuring a pore diameter of 2.00 mm. 5 and 6 - Meshes possessing a pore diameter of 2.50 mm. 46

Figure 4.9 Load-displacement curves of the circular meshes created with different pore sizes. 46

Figure 4.10 Load-displacement curves of the sinusoidal meshes and the circular meshes with a pore diameter of 2.00 mm and a filament around it..... 47

Figure 4.11 Distribution of filament thickness in the circular meshes. A - Mesh with 1.50 mm pore diameter, B - Mesh 2.00 mm pore diameter, C - Mesh 2.50 mm pore diameter, D - Mesh with 2.50 mm pore diameter. The red columns represent the filaments with a diameter of 0.08 mm or 0.16 mm, both cases were simulated, and the remaining columns have 0.24 mm of thickness. 50

Figure 4.12 Force-displacement curves of the circular meshes with and without a filament around it in certain areas, and with the different filament thickness. 51

Figure 4.13 Difference between the pores of the circular mesh with a filament around it in certain areas, and with the different filament thickness before and after the simulation. 52

Figure 4.14 Load-displacement curves of the best mesh results obtained, the vaginal tissue, the ligament uterosacral, and the Restorelle® mesh. 54

List of Tables

Table 1 Number of nodes and elements for each computational model of the meshes.	33
Table 2 Values of pore deformation and maximum values of load in the comfort zone for all the meshes created.....	48
Table 3 Values of pore deformation and maximum values of load in the comfort zone for the circular pore meshes with different filament thickness.	53

Abbreviations, Acronyms and Symbols

CLs	Cardinal Ligaments
EC	European Commission
FEA	Finite Element Analysis
FEM	Finite Element Method
FDA	Food and Drug Administration
FEUP	Faculdade de Engenharia da Universidade do Porto
gh	Genital hiatus
ICS	International Continence Society
INEGI	Instituto de Ciência e Inovação em Engenharia Mecânica e Engenharia Industrial
LDPS	Laboratório de Desenvolvimento de Produtos e Serviços (LDPS)
MEW	Melt Electrowriting
MRI	Magnetic Resonance Imaging
pb	Perineal body
PCL	Polycaprolactone
PEG	Polyethylene glycol
POP	Pelvic Organ Prolapse
POP-Q	Pelvic Organ Prolapse Quantification
PP	Polypropylene
SEM	Scanning Electron Microscope
tvL	Total vaginal length
UK	United Kingdom
UMAT	User MATerial
USA	United States of America
USLs	Uterosacral Ligaments
3D	Three-dimensional
A	Area
D	Filament diameter
<i>E</i>	Young's Modulus
E	Polymer extruded

ε	Strain
F	Force
l	Lenght
L	Lenght of the printed segment

Chapter 1

Introduction

1.1 Motivation

Pelvic organ prolapse (POP) limits people's quality of life and is quite common in women, especially with advancing age, and this condition predominantly affects women between 40 and 60 years of age [1]. POP affects 41% of women over 60 years of age, with one in four cases being symptomatic. It is estimated that 2.9% to 8% of the female population suffers from this condition, and there is a 12.6% lifetime risk that women will need surgery to correct the prolapse [2].

In Portugal, the POP annually affects the lives of approximately 7 thousand women, and this number has been increasing over the years. The number of cases of women suffering from this condition increases significantly as they have children and age. As the average age of the female population in Portugal is increasing, the number of cases is expected to increase by 40% over the next 40 years [3].

In the UK, the prevalence of POP is high. In 2019, in primary care, 8.4% of women had vaginal lumps or lumps and, after examinations, prolapse was found in 50% of patients. It is believed that one in ten women will need at least one surgical procedure, and the percentage of patients who end up needing a second surgery can be as high as 19% [4].

In the United States, about one-third of women in their lifetime will experience vaginal prolapse, and nearly half of women ages 50 to 79 will eventually experience POP, with the severity of prolapse varying from patient to patient. It is estimated that over 12% of American women will require surgery as a treatment for prolapse [5]. It is believed that one in four women over the age of 18 reports suffering from pelvic area disorders, including pelvic organ prolapse. Despite this, most women do not communicate the problem or the symptoms they are experiencing to a doctor, because they feel uncomfortable, embarrassed, or even because they believe that the symptoms, they are experiencing are normal consequences of aging [6]. Around 50% of women who have a normal delivery end up, throughout their lives, experiencing pelvic organ prolapse. This suggests

that by 2050, more than 50 million women in the United States will have problems in the pelvic area related to prolapse [7].

Therefore, POP influences negatively people's daily lives, and the number of cases will increase over the years, becoming urgent the development of new methods of treatment, since there are no viable alternatives to treat severe cases of prolapse. Surgical procedures involving synthetic meshes are associated with a range of complications and therefore new approaches are urgent. The development of biodegradable meshes is a new approach to overcome the problems previously encountered with the use of synthetic meshes.

1.2 Objectives

This dissertation aims to demonstrate the results and discoveries made during the development of computational models of biodegradable meshes for POP repair.

The main goals are:

- Development of computational models through Abaqus® software by varying the pore geometry, pore size, filament thickness, and the presence of filaments around the meshes in certain areas.
- Print at least one of the meshes created and perform a uniaxial tensile test to compare the results with the model results to ensure that the results obtained are similar to the experimental results.
- Perform a uniaxial tensile test on a sow's vaginal tissue in order to compare it with the simulations and determine which meshes have similar behaviour to the vaginal tissue.
- To further advance the research, the intention was to compare the best results obtained with the uterosacral ligament, as well as with a commercially available mesh.

1.3 Dissertation Structure

The dissertation is structured as follows:

- Chapter 2: Describes a review of the female pelvic area and the POP. It also includes an overview of the finite element method, the finite element analysis, the software Abaqus®, and simulations related to POP.
- Chapter 3: This chapter outlines the methodology employed during the development of the computational models and the experimental work, detailing the instruments, tools, and materials used.
- Chapter 4: This chapter presents the results of the uniaxial tensile tests performed, and the results obtained on the simulations carried out on the different meshes created. It also contains the main conclusions drawn from all the work developed.
- Chapter 5: The final chapter comprises the dissertation's conclusions and recommendations for future work.

- Appendix: The appendix contains three articles developed with the findings obtained during the work and a python code created to develop computational models of meshes through g-codes.

Chapter 2

State of the Art

The theoretical fundamentals of this thesis will be reviewed in the following chapter, which should help the reader understand the studies that follow in later chapters. Firstly, it will be given a description of the female pelvic area, which consist of the pelvic floor and vaginal tissue, and an explanation in more detail about the POP. Then, to understand how the simulations performed work, it will be given an overview of the finite element method, the finite element analysis, and the software of preference, Abaqus®. Lastly, it was presented interesting examples of simulations, in order to explore and gain insights from simulations related to POP.

2.1 Female pelvis

To gain a comprehensive understanding of pelvic floor dysfunction, it is crucial to understand the underlying pathophysiological processes. This needs a profound comprehension of the pelvic anatomy and the functions associated with each structure. The pelvis occupies the central region of the human body, placed between the upper lumbar region of the abdomen and the lower extremities, encompassing the bony pelvis, the pelvic cavity, the pelvic floor, and the perineum. This multifaceted framework serves several vital functions, including bearing the weight of the upper body, facilitating the transfer of upper body weight to the lower limbs, and providing anchor points for muscles of the lower limbs and trunk. While the pelvis serves a range of purposes, its primary role is to offer structural support and stability during activities such as standing, walking, and running. Consequently, comprehending the intricacies of each of these structures is essential for a holistic grasp of the pelvic function [8][9].

There are several distinctions between the male and female pelvises (Figure 2.1), for instance, the female pelvis is usually larger and more circular when compared with the male pelvis. This characteristic facilitates vaginal childbirth; however, it weakens the pelvic floor. Another difference between the two pelvises is the angle that the pubic arch creates. In women, the angle normally varies between 80° and 85°, and in men, the angle is only between 50° and 60°. Lastly, in men, the ischial spines typically protrude more prominently into the pelvic cavity compared to women [10].

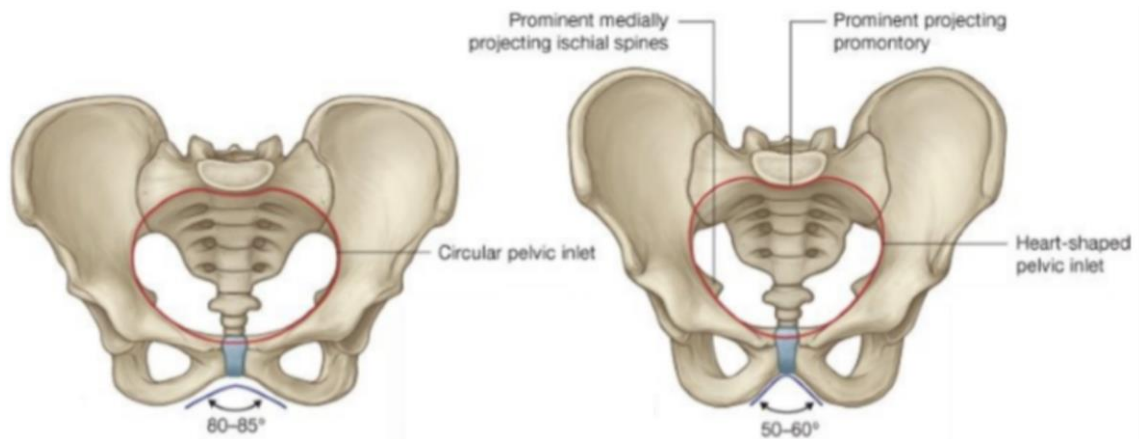


Figure 2.1 Representation of the women's and men's pelvises, respectively (adapted from [8]).

The bones, organs, muscles, ligaments, and other structures that support the pelvic cavity's functionality are collectively referred to as the pelvic cavity. The skeleton's functions include guarding the internal organs, transferring weight from the trunk and upper limbs to the lower limbs, and supporting the attachment of the muscles in the trunk and legs. The pubis, the pelvic bones ilium and ischium, and the sacrum, which articulates inferiorly with the coccyx, serve as the anterior, lateral, and posterior limits of the pelvic cavity (Figure 2.2). The smaller base of the pelvis is a narrower extension of the bigger base, which has two bases that are different sizes. The pelvic floor encloses the lesser pelvis, which is where the bladder, vagina, and rectum are located, and the bigger pelvis houses the abdominal viscera [8][11].

The bony structure has different insertion sites for ligaments, muscles, and fascia. The triangular-shaped sacrospinous ligament runs anterior to the sacrotuberous ligament from the ischial spine to the lateral edge of the sacrum and coccyx. The greater and lesser ischial foramen are located superiorly and inferiorly, respectively. The simultaneous activity of the fascia (connective tissue), ligaments, and muscles, whose integrity is crucial for the normal functioning of the organs, provides the structural organization of the internal organs of the pelvic cavity [8][11].

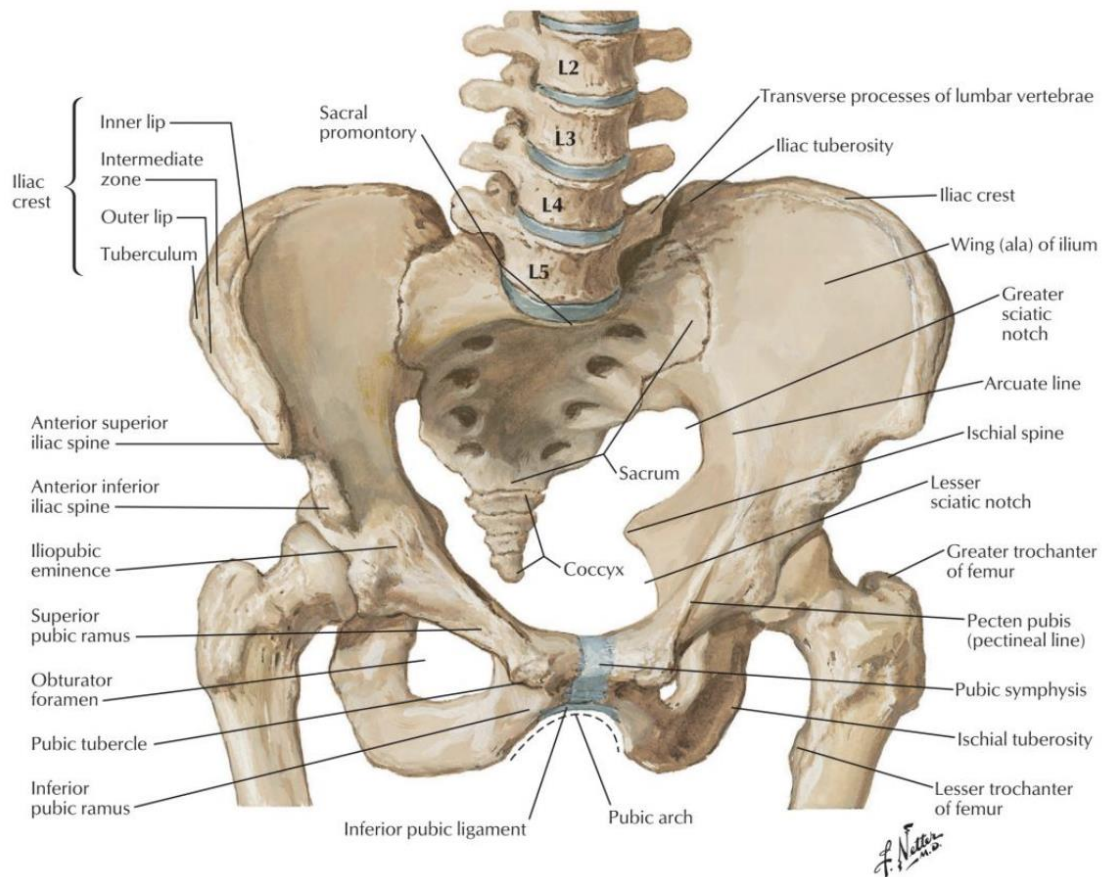


Figure 2.2 Representation of the bony framework of the pelvis (adapted from [12]).

Along with the anal sphincters, the pelvic floor (Figure 2.3), a dome-shaped striated muscle layer that covers the bladder, uterus, and rectum, plays a critical function in controlling the retention and elimination of urine and feces. The pelvic floor is currently defined as a complex of structures, such as muscles, ligaments, and fascia, that supports both the pelvic and abdominal viscera and is located at the lower limit of the pelvic cavity and the upper limit of the perineum, extending from the pubis to the coccyx. Three orifices cross the pelvic floor: the urethra and vagina in the front, and the rectum in the middle. One of the principal functions of the pelvic floor is the ability to help with sexual function as well as urine and fecal continence by constricting its muscles, ligaments, and fascia. Additionally, the pelvic floor supports the abdominal and pelvic organs by pushing them in the opposite direction from the direction of gravity's pull or any potential intra-abdominal pressure, and thus, the internal organs continue to be in their usual places [8][13].

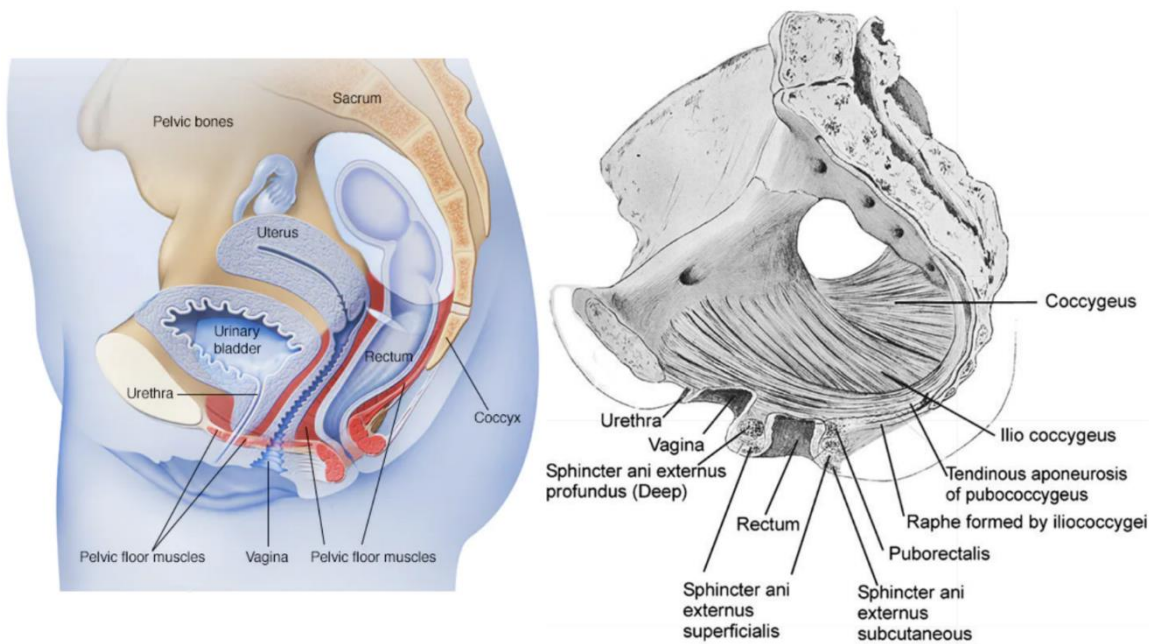


Figure 2.3 Pelvic floor muscles seen in the sagittal section of pelvis (adapted from [14] and [16]).

Finally, the female perineum, illustrated in Figure 2.4, takes on a diamond-shaped form and is situated beneath the pelvic diaphragm, nestled between the symphysis pubis and the coccyx. It comprises two distinct regions: the posterior anal triangle and the anterior urogenital triangle, collectively forming the perineum [15]. This area corresponds to the external genitalia, known as the vulva. Notably, the perineum serves as a critical foundation, providing essential support to the pelvic floor muscles, which, in turn, maintain the proper anatomical positioning of organs like the bladder, colon, and reproductive organs [13].

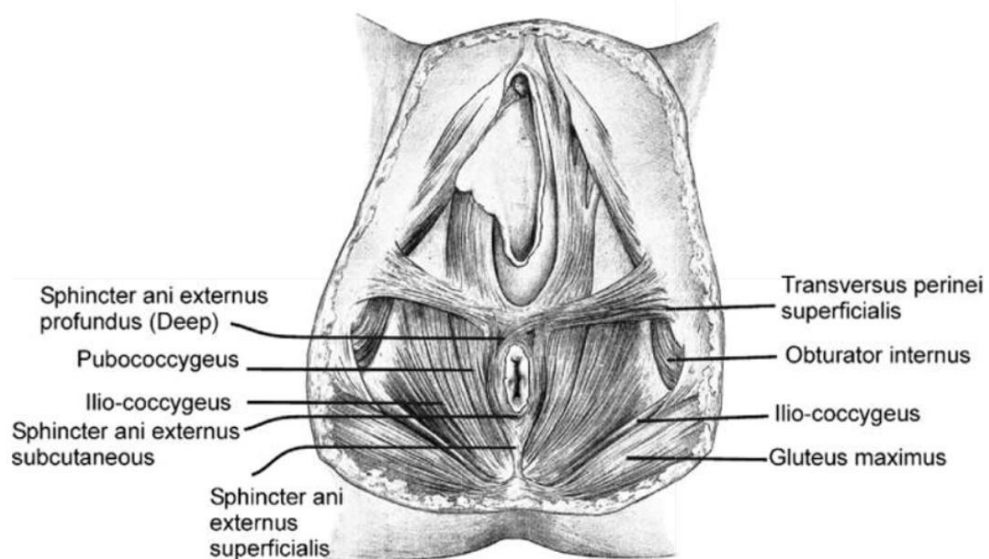


Figure 2.4 Pelvic floor muscles as seen from the perineal surface (adapted from [16]).

2.2 Pelvic Organ Prolapse

POP is the descent of the pelvic organs such as the bladder, urethra, rectum, uterus, and vagina. The prolapse of these organs is caused by lesions or weakness in the muscles, ligaments, and connective tissue, being one of their main functions to support the tissues [17][18].

POP structures may cause a sensation of pressure in the pelvic area or, for women, the sensation that something is descending towards the vagina, and in some cases, a protuberance may appear in the area in question. In addition to these symptoms, this condition may be associated with urinary and fecal incontinence, incomplete defecation, and sexual dysfunction. Other symptoms include pain during sexual intercourse, irregular vaginal bleeding, and back pain. It is important to note that not all patients experience these symptoms, and they vary depending on the organ [17][18].

Usually, it is a combination of several factors that lead to organ prolapses, such as vaginal delivery, obesity, injury to any of the pelvic organs due to surgery, aging, and activities that significantly increase the pressure exerted on the abdomen/pelvic area, such as lifting heavy objects [17]. These factors predispose some women to stretch, disruption, or dysfunction of the *levator ani* complex, connective tissue attachments of the vagina, or both, leading in prolapse [18].

There are different types of POP, the prolapse of the rectum, called rectocele, of the small intestine, also known as enterocele, the prolapse of the bladder, named cystocele, prolapse of the urethra or urethrocele, vaginal dome prolapse, and uterine prolapse (Figure 2.5) [17].

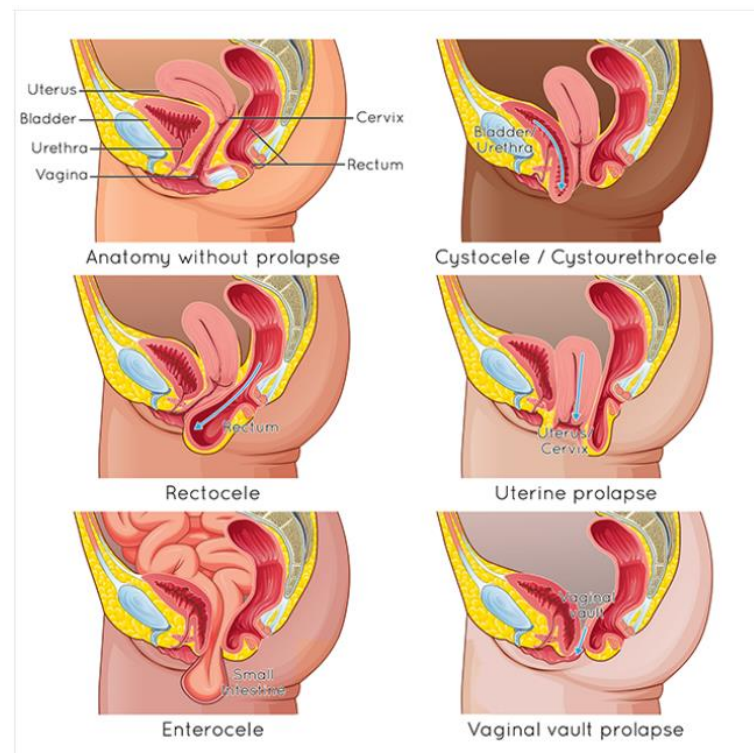


Figure 2.5 Types of pelvic organ (adapted from [19]).

2.2.1 Classification and Diagnoses

The Pelvic Organ Prolapse Quantification system (POP-Q) is a standardized and objective approach used to describe, measure, and stage pelvic support in women. This system provides a consistent tool for documenting clinical findings with proven reliability among different observers and within the same observer. This quantification system has gained global recognition and approval from organizations such as the International Continence Society (ICS) and the Society of Gynecologic Surgeons for characterizing female pelvic organ prolapse, becoming the preferred choice among gynecologists and urogynecologists [20].

This method of quantifying prolapse involves using the hymen as a fixed reference point and six other defined points (Aa, Ba, C, D, Ap, and Bp), as well as considering the genital hiatus (gh), perineal body (pb), and total vaginal length (tvL). Measurements are recorded in centimetres (cm) in relation to the hymen, measurements above or proximal are negative numbers and measurements below or distal are positive numbers [10][20][21]. These measurements can be organized into a grid, as illustrated in Figure 2.6.

According to the POP-Q, the prolapse can be classified into 5 stages [22]:

- Stage 0: no prolapse;
- Stage I: the prolapse is more than 1 cm above the hymen;
- Stage II: the prolapse is approximately 1 cm either above or below the level of the hymen;
- Stage III: the foremost part of the prolapse extends more than 1 cm below the hymen's level but does not bulge beyond 2 cm less than the entire vaginal length.
- Stage IV: vaginal eversion is fully extensive.

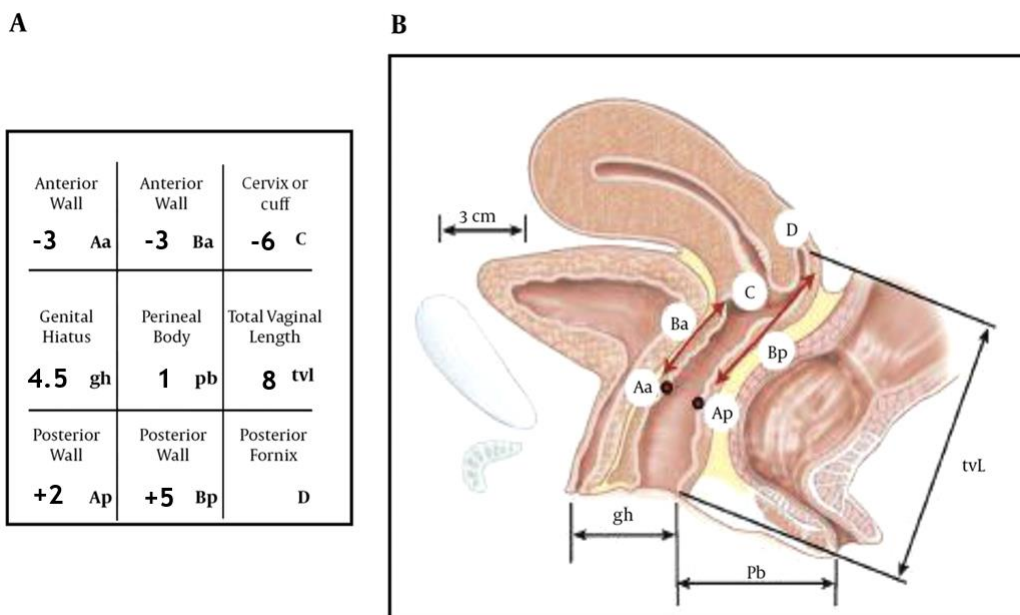


Figure 2.6 A - Measurements used for this system. B - Points for PQP-Q system examination (adapted from [22]).

However, alternative systems have been developed such as the "Baden-Walker Halfway Scoring System" serving as its main competitor [23]. The following figure represents the 4 grades of this quantification system (Figure 2.7).

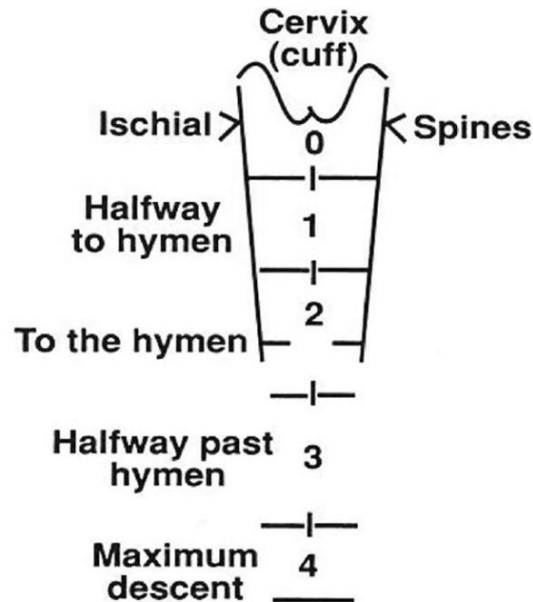


Figure 2.7 Baden-Walker Halfway Scoring System: grade 0 - no prolapse, grade 1 - descent halfway to the hymen, grade 2 - descent to the hymen, grade 3 - descent halfway past hymen, grade 4 - maximum descent (adapted from [23]).

In case the patient exhibits symptoms suggestive of prolapse should undergo a pelvic examination and medical history check.

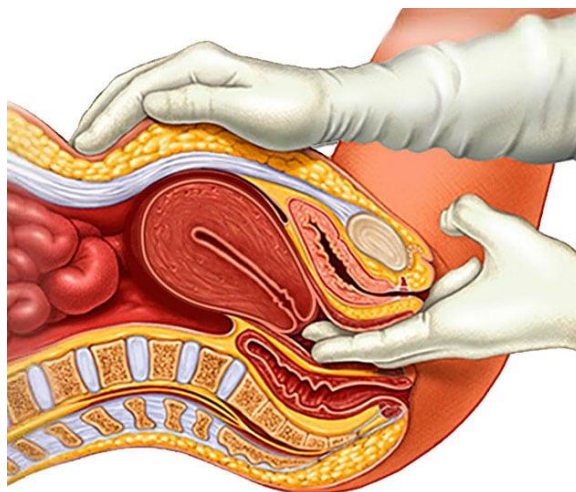


Figure 2.8 Pelvic exam (adapted from [24]).

This examination is done regularly and helps the doctor to check the organs in the pelvic area. During the examination, the doctor will assess the condition of the uterus, vagina, fallopian tubes, ovaries, bladder, and rectum, as shown in Figure 2.8. In any case, if the symptoms presented

indicate that more than one organ has prolapsed, the doctor may request an ultrasound or a magnetic resonance imaging (MRI) examination, thus obtaining images of the pelvic area. In this way, it is possible to determine the degree of severity of the prolapse through the images obtained [1][25].

The ultrasound imaging offers various routes for examining the urethra and bladder, including transvaginal, transabdominal, translabial, transperineal, and transrectal approaches [20]. Translabial ultrasound serves as a cost-effective and widely accessible means for assessing POP. It offers the advantage of being radiation-free while allowing for dynamic evaluation of the pelvic floor. However, the effectiveness of the ultrasound examination relies heavily on the expertise of the sonographer and the familiarity of the interpreting radiologist with the procedure. Additionally, to ensure accurate diagnostics, the examination necessitates bowel preparation because of potential interference from rectal fecal content. It is important to note that translabial ultrasound involves sensitive areas, including the rectum and genitalia. Regardless of these limitations, it remains a readily available, safe, and budget-friendly option for evaluating pelvic prolapse [26].

Another option to assess the POP is the dynamic MRI. The MRI has various advantages such as, surpassing the anatomical detail provided by translabial ultrasound, and it is also valuable as a preoperative tool. Additionally, MRI examinations do not necessitate bowel preparation and do not entail exposing sensitive pelvic areas. Nevertheless, it is important to note that MRI availability is limited, and the procedure can be costly. Moreover, it is contraindicated for patients with MRI incompatible devices or hardware [26][15].

2.2.2 Forms of treatment

There are some forms of treatment for this condition, such as physiotherapy and muscle strengthening exercises in the pelvic area, biofeedback therapy, electrical stimulation therapy, the use of a pessary, and surgery. In order to make the treatment process as less invasive as possible, doctors only resort to surgery as a last option, i.e., if the prolapse is severe [27].

Regarding physiotherapy exercises, Kegel exercises stand out as a prevalent choice during the initial stages, right from the detection of prolapse. Their primary objective is to strengthen pelvic muscles through a regimen of controlled contractions and relaxations. Patients are typically introduced to a range of these exercises during physiotherapy sessions and subsequently instructed to continue practicing them at home [28].

When it comes to biofeedback therapy, it helps to locate and strengthen the muscles in the pelvic area. This is done by placing a sensor in the vagina or rectum and a second sensor in the abdomen. As the patient contracts and relaxes the pelvic muscles, their electrical signals are recorded on a computer to see if the muscles can contract [29].

Electrical stimulation therapy is often used in conjunction with biofeedback therapy. In this treatment, the muscles in the pelvic area contract through stimulation by electrical currents. However, it is important to note that, the patient should do physiotherapy exercises at home as a way to complement the treatment [28][29].

Another solution for the correction of POP is the use of a pessary (Figure 2.9). A pessary is a small device consisting mainly of silicone in various sizes and shapes. It is inserted into the vagina and holds the bladder, uterus, or rectum in place. Pessaries are often recommended as a low-invasive, low-maintenance, and cheaper form of treatment than surgery. It can be used for months, however, it needs to be removed at least once every three months to be cleaned as well as to assess the vagina for possible signs of erosion caused by the pessary [30].

Although this solution is useful in the early stages of the problem, many women experience vaginal irritation due to the use of this device, as well as excessive vaginal discharge. In addition to these disadvantages, the size of the pessary can also become a problem, as it may be too small and end up falling off. In other words, it is not always possible to find a pessary that fits every patient perfectly [16][30].

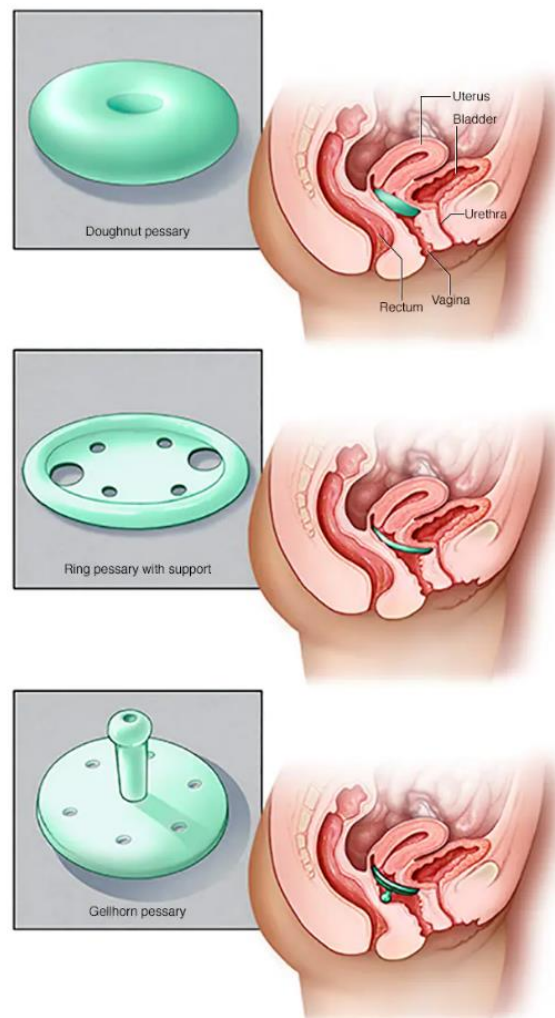


Figure 2.9 Different Pessaries used for the treatment of pelvic organ prolapse (adapted from [24]).

All these solutions, although practically non-invasive, are only useful in the initial phase of the problem, and if the situation worsens, surgery using meshes or native tissue is necessary.

Thus, surgical intervention, although an invasive solution, is the only one that can correct prolapse in more severe cases. In the beginning, the utilization of synthetic polypropylene meshes for repairs was introduced, considering its notable success rates in correcting abdominal hernias. However, in 2019, in the United States, the FDA (Food and Drug Administration) banned the sale and distribution of these meshes for the treatment of transvaginal prolapse due to the high risks associated with this product [31].

Initially, after surgery, the prolapse appears to be corrected, but after a few months, in most cases, the mesh wears out or tears. In the worst case, surgery is needed to remove the damaged part of the mesh or even all of it. The high rate of complications may be due to poor biocompatibility, inadequate biomechanical properties, and other factors such as the person's age, general health, previous surgeries, severity of prolapse, as well as the experience of the surgeon, which is also an important factor [2].

As a result, the use of these meshes can lead to infections, pain, scarring, incontinence, bowel problems, excessive vaginal discharge, muscle problems and more. Many of these complications require additional medical intervention and sometimes further surgical treatment may be necessary [31]. The following image (Figure 2.10) represents the placement of a mesh for the treatment of the prolapse.

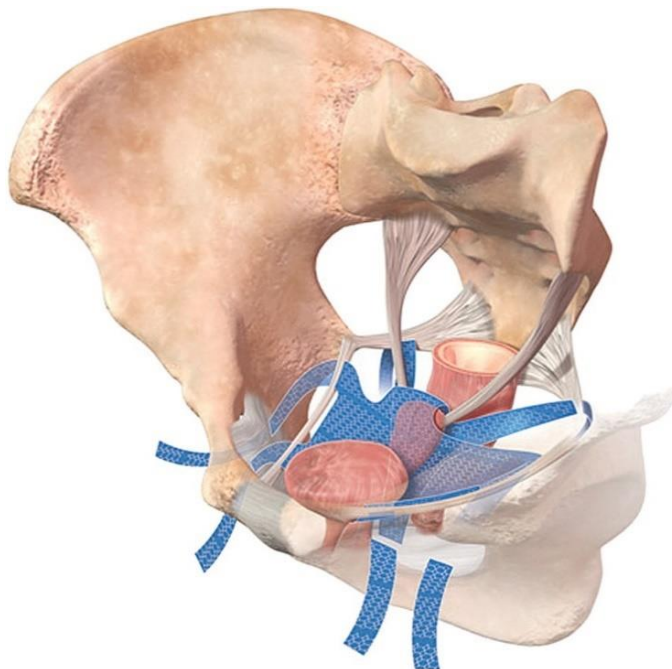


Figure 2.10 Illustration displaying the secure anchoring of a mesh through anatomical spaces in the pelvis (adapted from [32]).

In addition to the use of synthetic mesh, surgical intervention using native tissue can also be used. However, this alternative is also not very feasible as it, like mesh, has high failure rates in prolapse correction. For example, a 2016 study of 4,023 women found that after surgery using native tissue, 38% of women may experience prolapse again, and 11% to 20% of patients who used synthetic mesh may experience prolapse again. In addition, 5% of women who used native tissue will end up needing another surgery, and 7% to 18% of patients who used mesh will need a new intervention [33].

Another example is a study using data from 2008 to 2016 to understand the impact that mesh and native tissue have on people's lives when used to treat POP. The study, conducted at a hospital in New York, aims to assess long-term safety and understand the consequences of a second intervention on the mesh used for treatment [34].

It found that 54,194 women required treatment to correct prolapse, 11,205 of whom used mesh and 41,205 of whom did not use mesh, and that the average age of the women was 59.8 years, and the average follow-up period was 4.7 years. In addition, it is concluded that there is a higher risk of a second intervention when a mesh is used to repair the prolapse than when the correction is made without using the mesh, i.e., using the native tissue. Of the patients who required surgery using the mesh, 18.5% required a further intervention due to complications associated with the mesh [34].

Thus, although transvaginal mesh has been withdrawn from the market, the risk of complications has not decreased over time, and women who still have these meshes need regular monitoring, i.e., it is essential to monitor the mesh to ensure the safety and well-being of patients who still have them [34].

2.3 Computational Modelling

2.3.1 Finite Element Method

Invented during the mid-1950s by engineers, Finite Element Method also known as FEM, offers a numerical approach to tackling intricate problems, accommodating a degree of approximation. Its primary application arises when traditional mathematical approaches prove inadequate due to problem complexity. Conceptually, FEM can be likened to breaking down a substantial problem into a sequence of more manageable components, hence the name finite elements, thereby simplifying the investigation of the overarching problem. FEM becomes a valuable tool for engineers seeking to create a workable design that suits a specific application's practical needs, even if it does not attain absolute perfection [35].

The process of finite element discretization simplifies the problem by partitioning a continuous region—whether it is a substance like a solid, liquid, or gas, or simply a spatial area—into discrete elements. These elements then serve as constituent blocks for expressing the

unknown field variable. This variable is represented using assumed approximating functions unique to each element. These approximating functions, sometimes referred to as interpolation functions, are formulated based on the field variable values at designated points known as nodes or nodal points. Typically, nodes are positioned along the element's borders, connecting adjacent elements. Besides these boundary nodes, interior nodes can also exist within an element. The nodal values of the field variable, along with the interpolation functions assigned to the elements, collectively define how the field variable behaves within those individual elements [36].

In the context of representing a problem using finite elements, the nodal values associated with the field variable take on the role of the variables to be solved for. After these variable values are determined, the interpolation functions define how the field variable behaves across the entirety of the element assembly. It is evident that the nature of the solution and the extent of approximation are influenced not solely by the quantity and size of the elements employed, but also by the specific interpolation functions chosen. It is important to note that these functions cannot be chosen arbitrarily, as they need to adhere to certain compatibility conditions. Frequently, these functions are selected in a way that ensures the field variable or its derivatives remain continuous across the boundaries where elements connect [36].

A distinctive aspect of the finite element method that distinguishes it from alternative numerical techniques is its capacity to devise solutions for individual elements before amalgamating them to depict the entire problem. This implies that when addressing stress analysis, for instance, it is first determined the stiffness or force-displacement characteristics of each discrete element. Subsequently, these elements are assembled to deduce the overall stiffness of the entire structure. In essence, a complex problem undergoes a transformation into a series of considerably simplified predicaments. An additional advantage of the finite element method lies in the range of methods available for shaping the attributes of individual elements. There are a few distinct approaches in this regard [36].

The initial method for deriving element properties is referred to as the direct approach, stemming from its origins in the direct stiffness method employed in structural analysis. While the direct approach is applicable primarily to relatively straightforward problems, it proves to be the most accessible for beginners to the finite element method. This approach emphasizes the utilization of matrix algebra when addressing finite element equations. The element characteristics acquired through the direct approach can also be determined using the variational approach. The variational approach hinges on the calculus of variations. A grasp of the variational approach becomes essential for advancing beyond introductory levels and expanding the application of the finite element method to a wide array of engineering challenges. While the direct approach remains suitable solely for the simplest element shapes, the variational approach accommodates both uncomplicated and intricate element configurations [36].

Lastly, a notably more adaptable technique for deducing element characteristics is rooted in mathematical principles and is termed the weighted residuals approach. The weighted residuals

approach initiates with the governing equations of the given problem and proceeds without relying on a variational statement. This method offers an advantage in that it permits the expansion of the finite element method to situations in which no functional is at hand. The weighted residuals method finds extensive use in deriving element properties for non-structural scenarios, encompassing areas like fluid mechanics and heat transfer [36].

2.3.2 Finite Element Analysis

The mathematical equations underpinning FEM are employed to craft a simulation, known as a finite element analysis (FEA). This simulation serves the purpose of conducting a structural evaluation of how a specific product or design would respond to real-world stress conditions. The simulation dissects the complete model into smaller elements within a mesh, enabling engineers to assess how the distinct design components interact and perform when subjected to simulated stress factors. This analysis can be carried out on tangible objects or on models that emulate facets of the actual object. When models are utilized in place of real objects, the analysis can be executed at earlier stages in the design procedure, even before physical prototypes are constructed. These models can encompass physical renditions such as mock-ups, scaled-down models, and photoelastic models, or they can manifest as mathematical constructs. Simple mathematical models can be solved through analytical methods, whereas more intricate models necessitate the application of numerical approaches. FEA is one of these numerical techniques wielded to address the intricacies of mathematical models. Within engineering practice, the terms Finite Element Analysis (FEA) and Finite Element Method (FEM) have become synonymous and interchangeable [37].

FEA represents an exceptionally useful and powerful yet rigorous instrument in engineering analysis. The proficiency anticipated of FEA practitioners' hinges on the complexity of the analysis, demanding a grasp of several engineering fundamentals, such as engineering design, mechanics of materials, heat transfer, kinematics and dynamics, and other similar subjects [37].

FEM and FEA permit engineers to enhance precision and improve the design of the product, which means, the amalgamation of FEM and FEA yields heightened precision in structural analysis by illuminating intricate interactions among the various components of a design. Furthermore, they afford engineers the opportunity to scrutinize both the internal and external aspects of a design with meticulousness. Another advantage is the possibility to accelerate testing in a cost-effective way, by enabling the craft of virtual simulations, diminishing the necessity for physical testing and the construction of prototypes. Moreover, FEM and FEA have many applications in various fields, such as civil and aerospace engineering, biomechanics, biomedical engineering, electromagnetics, and other disciplines [35].

2.3.3 Abaqus® Software

Finite Element Analysis (FEA) is a widely used computerized method to understand how an object behaves when subjected to various forces, vibrations, temperatures, and other physical components. Through this method, it is possible to grasp and visualize the behaviour of the object based on applied physical properties. For example, it is possible to comprehend when the object becomes deformed or experiences fracture. To conduct these simulations, the Abaqus® software is commonly employed [38].

Abaqus® is a software for finite element analysis and computer-aided engineering, built upon the finite element method. Abaqus® offers numerous tools that make it relatively straightforward to create, edit, monitor, and visualize simulations. The purpose of this software is to comprehend how the created object/model will behave when utilized. One reason engineers employ this software is due to the ability to model, visualize, and analyse results within a single working window. This streamlines the software's utility and ultimately enhances users' productivity [39]. This software is capable of solving diverse problems, ranging from simple linear analyses to complex nonlinear simulations. The software provides various pre-defined elements and materials to assist users in their projects capable of emulating the behaviour of a wide spectrum of engineering materials, encompassing rubber, metals, composites, polymers, and more. Offering an extensive collection of elements, Abaqus® can effectively replicate almost any geometry. However, if needed, the User MATerial (UMAT) can be employed for more intricate issues, considering equations to compute stiffness matrices and stresses. Originally designed as a versatile simulation tool, Abaqus® transcends mere structural concerns, accommodating simulations in diverse domains such as heat transfer, mass diffusion, thermal management of electrical components, acoustics, soil mechanics, and piezoelectricity [19].

Finite element analysis involves breaking down an object/model into a specific number of finite elements and establishing nodes that represent the connections between these finite elements. The combination of finite elements and nodes is referred to as meshes. The accuracy of this software relies on the number of nodes and elements within the developed model, as well as the size and type of mesh employed. In other words, better results are achieved by decreasing the size of elements and increasing their quantity when creating the object's mesh [38].

Despite offering a broad spectrum of capabilities, Abaqus® remains user-friendly, and even intricate issues can be modelled. For instance, complications arising from multiple components are tackled by linking the geometry of each component with the suitable material models. In the majority of simulations, even those characterized by high nonlinearity, users only need to input engineering data, including structural geometry, material behaviour, boundary conditions, and applied loads. During nonlinear analyses, Abaqus® independently determines appropriate load increments and convergence thresholds. Going beyond mere selection, Abaqus® dynamically adjusts these parameters throughout the analysis to guarantee a precise and efficient solution.

Users hardly ever need to define parameters to control the numerical resolution of the problem [40].

A full analysis typically encompasses three distinct phases, preprocessing, simulation, and postprocessing.

In the preprocessing stage, the initial step involves defining the physical problem's model and generating an input file. Typically, the model is created graphically using Abaqus® CAE or another preprocessor [40].

Afterward, in the simulation phase, Abaqus® tackles the numerical problem specified in the input file. The outcomes of the analysis are saved in binary files and can be used for postprocessing. The duration of an analysis run varies depending on the complexity of the problem and the computational power of the computer, ranging from seconds to potentially days [40].

Upon completion of the simulation, it is possible to assess the results obtained through Abaqus® Viewer. This postprocessing tool reads the output file and offers a range of options for visualizing the results, such as animations, X-Y plots, and deformed shape plots [40].

2.3.4 Simulations

As previously mentioned, simulations conducted using software like Abaqus enable us to visualize and understand the behaviour of objects based on their physical properties. Therefore, it is worthwhile to explore and gain insights from simulations related to pelvic organ prolapse.

One example of such simulations revolves around the study of mesh anchoring techniques in uterine prolapse repair surgery, a study made by Silva et al, in 2021 [41]. In this study, a transvaginal reconstructive surgery was simulated to address the repair of apical ligaments, namely the uterosacral ligaments (USLs) and cardinal ligaments (CLs). Various degrees of ligament impairment (90% and 50%) and total rupture were modelled. The implants designed to reinforce or replace these ligaments were crafted according to literature specifications, and their mechanical properties were derived from uniaxial tensile tests [41].

The primary goal of this study was to simulate the impact of different mesh anchoring techniques and compare the extent of pelvic tissue displacement during the Valsalva manoeuvre. The simulations accounted for scenarios with and without synthetic mesh when the CL and USLs were entirely ruptured, resulting in a shift in vaginal displacement. Furthermore, the simulations revealed variations in superior-inferior displacement of the vaginal wall across different anchoring techniques[41].

The computer simulations effectively emulated the biomechanical responses of USLs and CLs to different anchorage techniques, offering valuable insights to enhance the outcomes of prolapse surgery [41].

The image below illustrates the simulations conducted in this study (Figure 2.11).

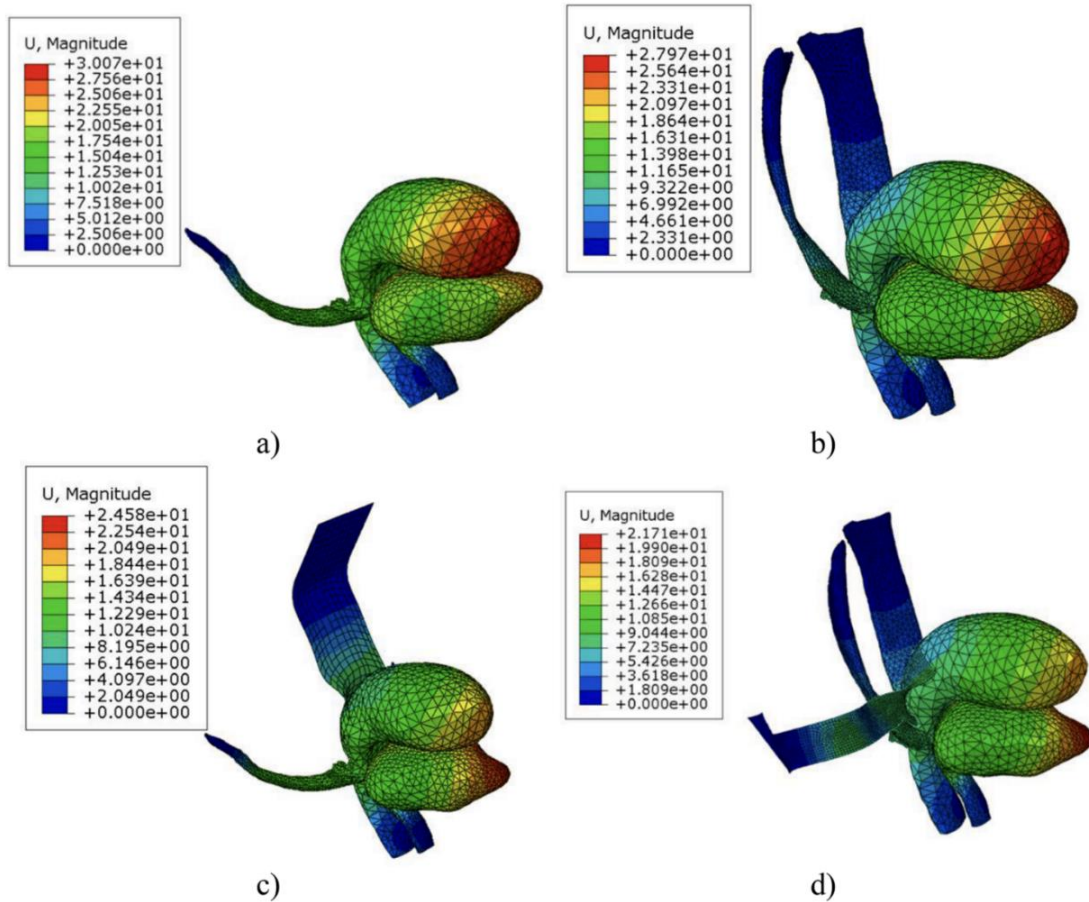


Figure 2.11 Magnitude of displacement (mm) observed in the uterus and bladder following the complete rupture of USLs and CLs, represented as (a) and (b) respectively. Additionally, the displacement with the incorporation of USLs and CLs implants after the rupture of these ligaments, specifically for the continuous stitch technique, is illustrated as (c) and (d) (adopted from [41]).

Another interesting study involves the investigation of pore diameter deformation in transvaginal mesh when subjected to significant multidirectional forces. In pursuit of this goal, a computational model was created to replicate the mesh's response under in vivo loading scenarios [42].

A tensile force was applied to each arm of the mesh to simulate surgical implantation. Two different loading scenarios were investigated by varying the angle of the applied tension. In parallel, a computational model was created to replicate how pores respond to these same loading conditions, allowing for a comparison with experimental results [42].

In both loading scenarios, it was observed that a significant proportion of pores, exhibited diameters less than 1 mm. Notable reductions in pore diameter were particularly evident in the inferior arms and between the two superior arms. This study highlights the potential for clinically applied multiaxial loading to reduce the porosity of transvaginal mesh, thereby increasing the risk of complications. Furthermore, the computational simulations demonstrate the potential for predicting this behaviour under more complex loading conditions [42].

The following image, Figure 2.12, represents the results obtained on the simulations performed.

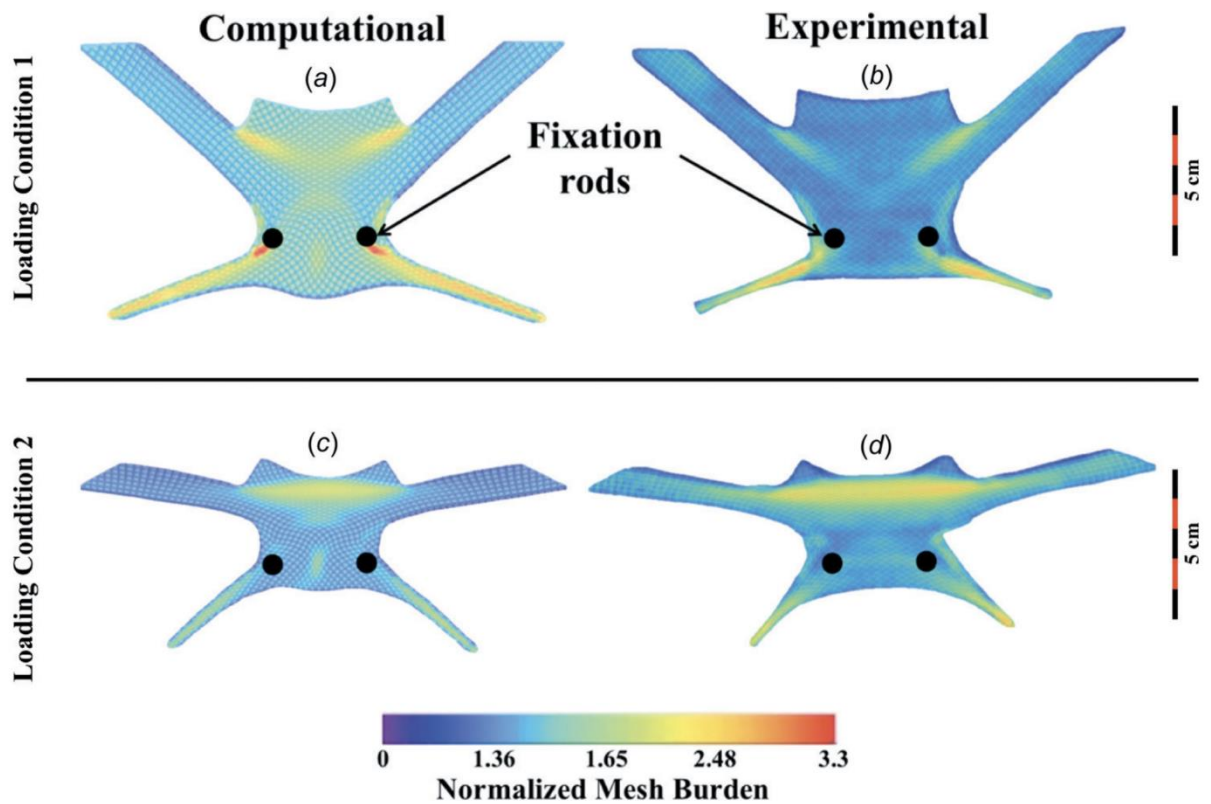


Figure 2.12 Contour plots depicting the normalized mesh burden for altered DirectFix A geometries are displayed (adapted from [42]).

In general, there is a strong concurrence between computational and experimental outcomes for both loading conditions 1 and 2. To normalize the mesh burden values, the maximum mesh burden of the unaltered geometry was used as a reference. In these plots, warmer colours indicate higher percentage increases in mesh concentration [42].

These are merely a couple of the numerous simulations conducted to study the POP. These simulations serve as noteworthy examples of the extensive range of applications achievable through finite element analysis.

Chapter 3

Materials and Methods

This chapter addresses the materials and the methodology adopted to perform simulations on the computational models developed, as well as the mechanical tests done on a medical-grade PCL (polycaprolactone) mesh, and on the sow's vaginal tissue.

3.1 Materials

3.1.1 Medical-grade PCL

PCL is an FDA-approved polymer that has been used in humans and is frequently used in 3D printing processes, ideal for MEW (Melt Electrowriting spinning) due to its low melting temperature and rapid solidification [43]. This polymer, aliphatic semicrystalline, presents a melting temperature that varies between 59°C to 64°C. As a result, at room temperature, this material exhibits improved mechanical properties such as high strength and flexibility. PCL is a non-toxic polymer with high tissue compatibility that is commonly used in resorbable sutures, drug delivery applications, and as a support in regenerative therapies. Another benefit of this biodegradable polymer is its extended degradation period since it is one of the polymers with the lowest rate of erosion, which can range between two and three years [44].

This material is undoubtedly, according to the literature, the most used and studied polymer for MEW is medical-grade PCL, like PC12. In contrast to non-medical PCL, medical-grade PCL offers heightened purity, as well as great printing quality. Furthermore, by opting for medical-grade PCL in MEW over technical-grade PCL, it is possible to obtain excellent control and precision during the process and thus, achieve better structures and designs [45][46].

The biodegradable meshes were printed using the medical-grade PCL from Corbion with the trade name PURASORB PC12. This material is a homopolymer with an intrinsic viscosity ranging

from 1.0 to 1.3 dl/g and it was used in pellet form [45][46]. It is important to mention that during the printing process, the temperature and humidity were controlled.

3.1.2 Vaginal Tissue

Animal models have a crucial role in advancing the understanding of human development and diseases, as well as in discovering effective therapeutics and vaccines. Pigs, due to their similarities with humans in aspects such as anatomical structure and size, genome, immunology, and physiology, provide a more relevant substitute for rodent models in the pursuit of translational and clinical research. Pigs possess notable advantages over primates and other livestock models, attributed to their larger litters, shorter generation times and genomes that can be easily manipulated [47].

The shared characteristics in anatomy and physiology between pigs and humans underscore the suitability of pigs as a valuable biomedical model for studying human biology. Therefore, to compare the results obtained in the simulations, it was used five samples of the vaginal tissue of sow's for the uniaxial tensile tests [47]. Soft tissues of the pelvic floor in sow's were obtained at the Matadouro Carneiro e Salgueirinho Lda slaughterhouse, located in Trofa, Portugal, for research purposes. These procedures were conducted in compliance with the stipulations outlined in Regulation (EC) No. 1069/2009 dated 21 October. The animal components were acquired as a single unit, consisting of the vaginal canal, rectum, muscles, and adjacent fat [48]. Subsequently, the vaginal canal was isolated, and specimens were prepared, as shown in Figure 3.1.



Figure 3.1 The samples of the vaginal tissue.

3.2 Methodology

3.2.1 Instruments and Tools

Several instruments were needed during the experimental work and for the development of the computational models of the biodegradable meshes. All these instruments were available at the Laboratório de Desenvolvimento de Produtos e Serviços (LDPS) at FEUP, except for the machine used for the uniaxial tensile test of the vaginal tissue, the “Mecmesin Multitest 10-í” (Figure 3.5). This machine was available at INEGI’s laboratory.

- **Melt electrowriting device:** This was used to print meshes and filaments, successfully developed within a project “SPINMESH” (Figure 3.2). Recently this device was adapted with pellets’ extruder, with the goal of printing meshes with medica-grade PCL, only available in pellets. This printer is an aluminium structure and consists of a collector plate with X-Y movement where the material is deposited and a Z-movable print head from where the material passes through, due to a heating mechanism that melts the material in a spinneret. These are linked to an external high voltage power supply via electrodes. Furthermore, the instructions are established through a computer and a translation system to define the intended direct writing patterns [46].

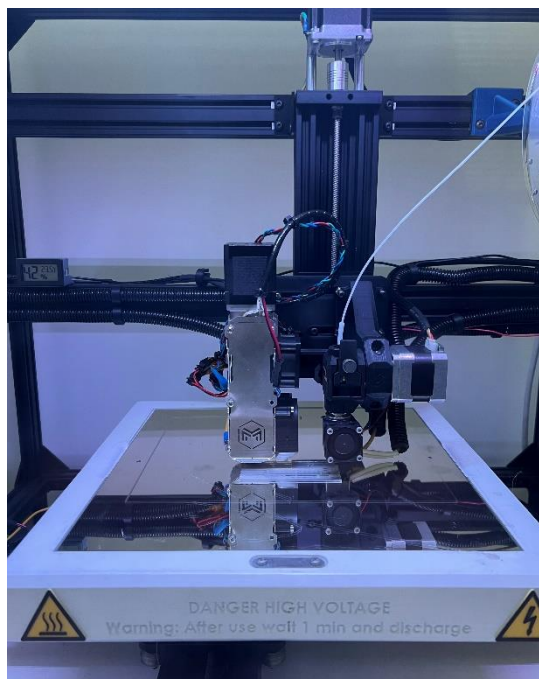


Figure 3.2 Melt electrowriting device.

- **Temperature and Humidity Monitorization:** This tool helps to measure the temperature and humidity of the printer (Figure 3.3).



Figure 3.3 Temperature and Humidity control.

- **Uniaxial tensile test machine and the software for the data acquisition of the tests performed:** The machine used for the mechanical tests was the “Mecmesin Multitest 2.5-dv” with a 100 N load cell set up and a constant elongation rate of 10 mm/min (Figure 3.4). This machine was used for the uniaxial tensile tests of the meshes and filaments printed. During the uniaxial tests the acquisition of data was facilitated by the "VectorPro Lite" software.



Figure 3.4 Uniaxial tensile test machine used to perform uniaxial tensile tests in samples of printed meshes.

Concerning the uniaxial test conducted on the vaginal tissue, it was used the “Mecmesin Multitest 10-i” (Figure 3.5). For the test, it was applied a 100 N load, and a constant elongation rate of 10 mm/min.



Figure 3.5 Uniaxial tensile test machine used to perform uniaxial tensile tests in samples of vaginal tissue.

Uniaxial testing is a procedure in which a sample is subjected to a single-axis force until it reaches failure, it can be either tension or compression. Throughout these tests, the force applied to the specimen is monitored as it relates to the displacement between the grips of the testing machine. Key properties that can be directly assessed through a uniaxial test encompass ultimate tensile/compressive strength, alterations in specimen length, and variations in cross-sectional area. Utilizing these measurements, it becomes possible to calculate the stress, strain, and Young's Modulus (elasticity) of the specimen [49].

The following image, Figure 3.6, demonstrates the dimensions of the meshes and the vaginal tissue samples when submitted to a uniaxial tensile test. The length (a) varies, the meshes' length is 40 mm, and the vaginal tissue length is 50 mm.

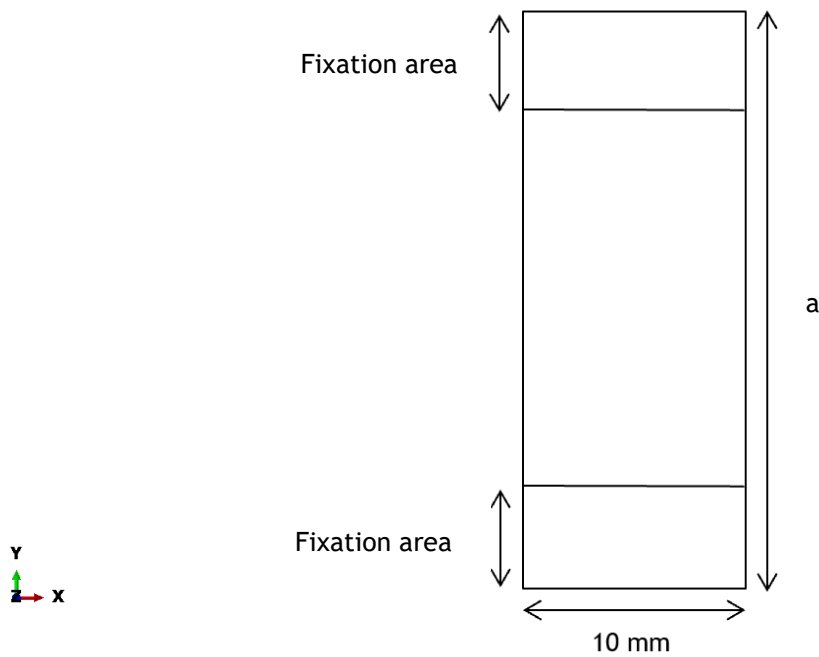


Figure 3.6 Schematization of the samples' dimensions for the uniaxial tensile tests.

- Micrometre:** A micrometre (Figure 3.7), also known as a micrometre caliper, serves as a precision instrument used for accurately measuring linear dimensions such as diameters, thicknesses, and lengths of solid objects. It comprises a C-shaped frame housing a movable jaw, which is controlled by an integrated screw mechanism. The precision of the measurements achievable is contingent upon the pitch of the screw, which signifies how much the spindle advances or retracts in one complete revolution, as well as the mechanisms in place for indicating fractional portions of a revolution. The accuracy of these measurements relies on the precision of the screw and nut combination [50].



Figure 3.7 The micrometre used to verify the filament thickness of the printed meshes.

- Abaqus® software:** For the development of the computational models, it was used the Abaqus software v.2021 (Dassault Systemes Simulia Corp., Providence, RI, USA).

3.2.2 Mesh Prototyping

3.2.2.1 Synthetic Meshes

To better understand the ideal characteristics that the meshes should have, it is important to research about existing meshes and meshes that were once used to treat different cases of pelvic organ prolapse.

Therefore, ideally the mesh thickness would vary between 0.08 mm, 0.16 mm and 0.24 mm, given the dimensions of the meshes described in the literature [43][51]. Furthermore, the pores of the mesh would be approximately 2.00 mm in diameter in order to favour cell growth, thus correcting the prolapse [2].

It is important to highlight that meshes with small pores, that is, smaller than 1.00 mm, and low porosity can lead to increased inflammation and the development of connective tissue, causing pain to the patient. The same does not occur in meshes with more than 1.00 mm in pore size, these being considered large pores with high porosity. On the other hand, contraction of the mesh, that is, the collapse of the pores, is associated with vaginal pain and normally, the problem areas for patients with pain are where the pores of the mesh have collapsed after tension forces have been exerted. Another problem that arises with the collapse of the pores is the reduction in the possibility of cell growth in the initial phase until the mesh degrades. Therefore, it is essential to be able to control and predict the behaviour of the pores when forces are exerted on the mesh and in this way, it is possible to achieve excellent compatibility between the mesh and the patient's tissues [52].

Finally, in contrast to multifilament mesh, a monofilament mesh lacks tiny gaps between its filaments, which limits bacterial growth and consequently lowers the risk of infection. In terms of weight, a lighter mesh typically suggests less tissue involvement, which tends to reduce the likelihood of inflammation [53][54].

Finally, having all this information gathered, and before starting the process of developing meshes, it was analysed existing products, in this case the Restorelle® mesh. This mesh is an ultra-lightweight polypropylene (PP) mesh with a density of 19g/m², made from three knitted monofilaments (0.08 mm diameter), featuring a pore size of approximately 2.00 mm [43]. For visual reference, Figure 3.8 provides an image of the Restorelle® mesh and its SEM image [2][55].

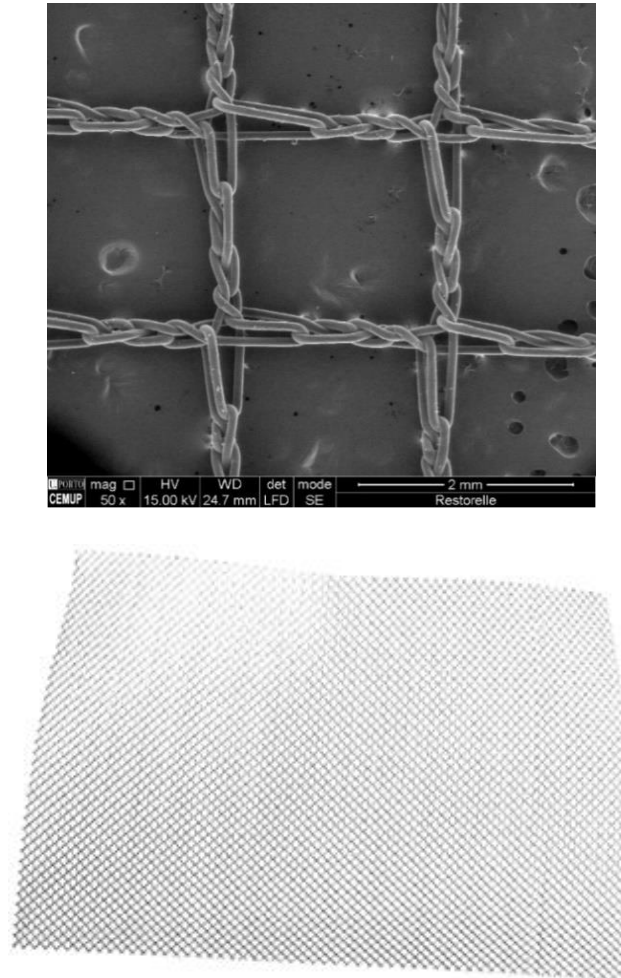


Figure 3.8 A SEM image of the Restorelle® mesh, and an example of the Restorelle® mesh, respectively (adapted from [2][55]).

3.2.2.2 Computational Modelling of the Biodegradable Mesh

Firstly, to simulate the behaviour of the material in Abaqus®, it is necessary to determine its Young's modulus.

Young's modulus (E), or modulus of elasticity, is a characteristic of the material that allows determining the ease with which it stretches and deforms, based on the ratio between stress (σ) and strain (ϵ). Stress is defined by the force exerted per unit area, and strain corresponds to the extension applied to the object per unit length, as shown in the equation (Eq. 1). Typically, Young's modulus is expressed in megapascals (MPa) [56].

$$E = \frac{\sigma}{\epsilon} = \frac{F \times l}{A \times \Delta l} \quad (1)$$

This value is determined by performing a uniaxial tensile test to a filament of medical-grade PCL (Figure 3.9).



Figure 3.9 Uniaxial tensile test to a filament of medical-grade PCL.

The graphic of the Figure 3.10 shows the average of the experimental values obtained in the uniaxial tensile test carried out on a filament of medical-grade PCL with 0.24 mm diameter. The value used in the simulations was 251.56 MPa. According to the literature, the Young's modulus should be higher, and range between 343.9 MPa and 363.4 MPa [57]. The Young's modulus value achieved may be lower due to the temperature that the material is exposed during the printing process, in this case is 200°C, which can alter the properties of the medical-grade PCL. Another potential factor contributing to the discrepancy in Young's modulus values could be attributed to the extensive utilization of the material, as both the laboratory equipment and supplies are shared among multiple users. Therefore, the medical-grade PCL may not have been properly maintained over the past few months. Ideally, this material should be stored in an inert atmosphere and at low temperatures (-15°C). Nevertheless, it is also feasible to preserve the material in its original packaging at room temperature, maintaining its initial properties for a minimum of one year [58].

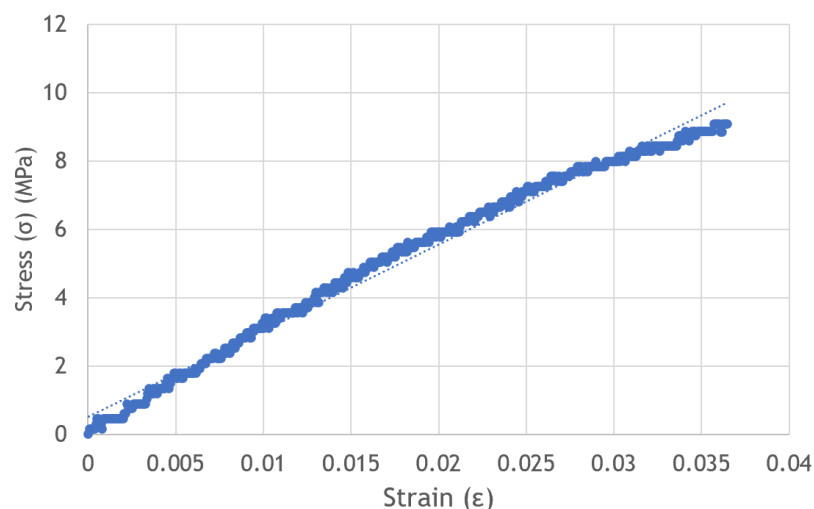


Figure 3.10 Stress and strain values obtained from the uniaxial tensile test carried out on the filament.

It is important to mention that the results were obtained from the average of the stress-strain values from 3 uniaxial tensile tests carried out on 3 medical-grade PCL filaments.

Besides the Young's modulus, it is necessary to determine the Poisson's ratio for the simulations. The Poisson's ratio is determined by the relationship between the change in width and length of a material when subjected to an applied force. In other words, Poisson's ratio is calculated as the ratio of the expansion fraction to the compression fraction. For isotropic materials, the Poisson's ratio typically falls within the range of -1 to 0.5 [59]. Isotropic materials are those whose properties remain consistent when tested in different directions [60].

It is worth emphasizing that the specific value of the Poisson's ratio can vary depending on the material being examined. In the case of a biodegradable polymer like PCL, the Poisson's ratio is approximately 0.3 [61].

After determining the Young's modulus and the Poisson's ratio, the process to develop the meshes began. All of them are medical-grade PCL meshes with 40 mm length, and 10 mm width.

Several meshes were developed to attempt to create a mesh whose load-displacement values are similar to the load-displacement values of the vaginal tissue (Figure 3.11). The models were produced by varying the filaments thickness, the pore geometries and sizes, and by adding a filament around the mesh models in certain areas.

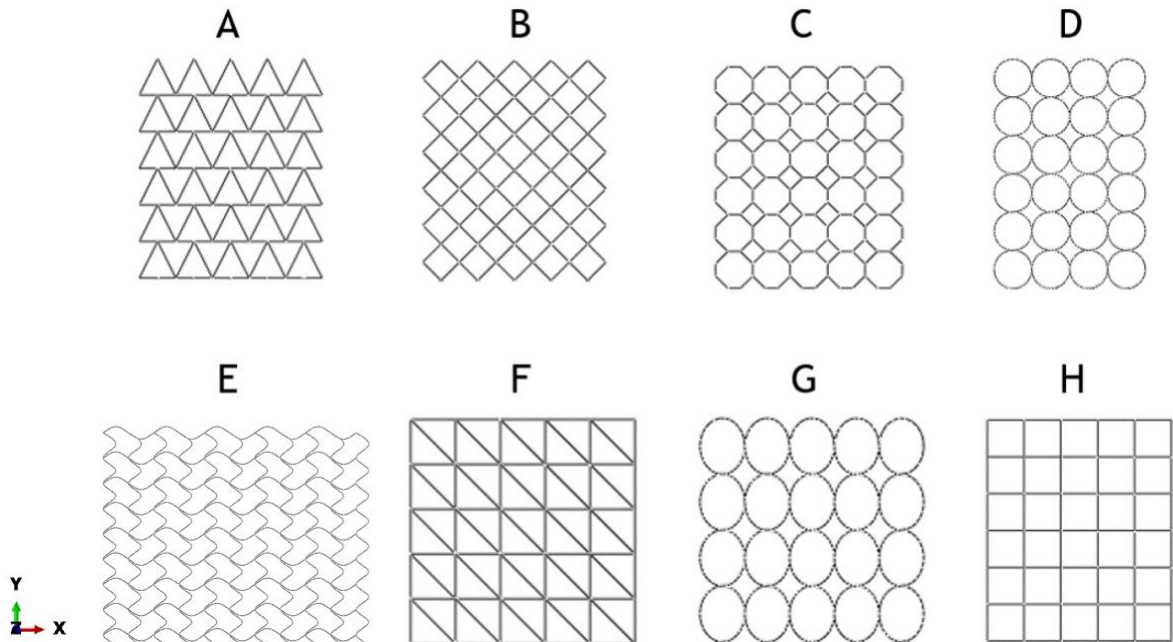
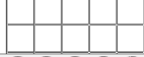
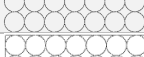


Figure 3.11 Some examples of the different developed meshes. Mesh names: A - Triangle, B - Diamond, C - Octagon, D - Circular, E - Sinusoidal, F- Diagonal, G - Oval, and H - Square.

The Table 1 shows the number of nodes and elements for each computational model of the meshes. The element type applied for these meshes was the beam element “B21”.

Table 1 Number of nodes and elements for each computational model of the meshes.

Type of Mesh		Number of nodes	Number of elements
Sinusoidal		16258	17076
Square		4401	4500
Circular without the filament around the mesh, and with 2.00 mm pore diameter		6197	6372
Circular with the filament around the mesh, and with 2.00 mm pore diameter		7175	7400
Circular without the filament around the mesh, and 2.50 mm pore diameter		4990	5098
Circular with the filament around the mesh, and 2.50 mm pore diameter		5975	6123
Circular without the filament around the mesh, and 1.50 mm pore diameter		8726	9070
Circular with the filament around the mesh, and 1.50 mm pore diameter		9684	10096
Diagonal		7101	7300
Octagon without the filament around the mesh		6750	7100
Octagon with the filament around the mesh		7314	7714
Oval		5597	5736
Oval with the filament around the mesh		6581	6762
Triangle		6225	6400
Triangle with the filament around the mesh		7081	7300
Diamond		5425	5600
Diamond with the filament around the mesh		6375	6600

The pore size of the meshes varied between 1.50 mm, 2.00 mm, and 2.50 mm in order to comprehend how the pore size can influence the final results of load and displacement. As previously mentioned, the ideal pore size should be bigger than 1.00 mm, or around 2.00 mm, thus creating pore sizes of 1.50 mm and 2.00 mm for the meshes. Nevertheless, to understand how the pore deforms, and how it influences the results, meshes with slightly bigger pores were also created, with 2.50 mm. For certain pore geometries, such as the sinusoidal pore represented in Figure 3.11 by the letter E, because the shape of the pore is not easily measured, its size is not exactly 1.50 mm, but rather 1.58 mm. The size of the pore was stipulated by measuring the distance between the two points furthest from the centre of the pore. Furthermore, after creating the meshes pore geometry, a filament wrapped around the meshes in certain areas was added to

try to limit the pores distortion and improve the results obtained, as shown in Figure 3.12. For each geometry, the filament diameter applied was 0.08 mm, 0.16 mm, and 0.24 mm.

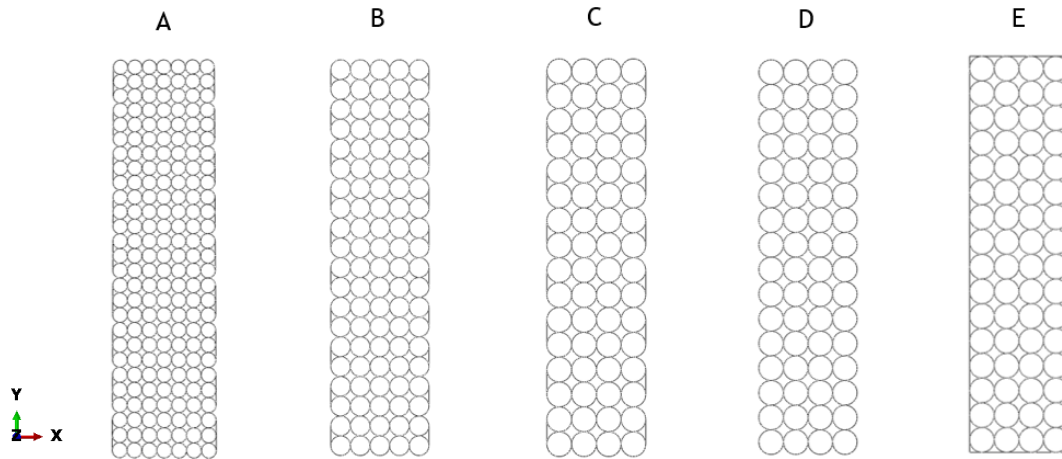


Figure 3.12 Computational models of the circular pore meshes. A - Mesh with 1.50 mm pore diameter and filaments around the mesh in certain areas, B - Mesh with 2.00 mm pore diameter and filaments around the mesh in certain areas, C - Mesh with 2.50 mm pore diameter and filaments around the mesh in certain areas, D - Mesh with 2.50 mm pore diameter and without a filament around the mesh, and E - Mesh with 2.50 mm pore diameter and a filament around the mesh.

The concept of producing meshes with varying filament thickness in different regions of the meshes emerged to improve the results obtained. Filaments with a diameter of 0.08 mm or 0.16 mm were used in the mesh's extremities, and 0.24 mm in the remaining columns (Figure 3.13).

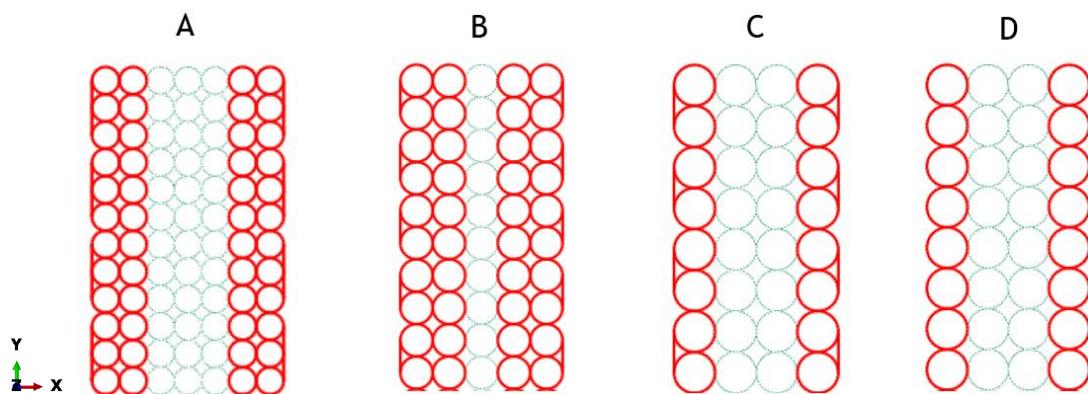


Figure 3.13 Distribution of filament thickness in the meshes. A - Mesh with 1.50 mm pore diameter, B - Mesh with 2.00 mm pore diameter, C - Mesh with 2.50 mm pore diameter, D - Mesh with 2.50 mm pore diameter. The red columns represent the filaments with a diameter of 0.08 mm or 0.16 mm, both cases were simulated, and the remaining columns have 0.24 mm of thickness.

Then, to simulate the uniaxial tensile test, it was defined the boundary conditions. At the lower end of the mesh, the nodes were considered fixed and at the top edge of the mesh, it was applied a displacement of 40% of the mesh length (Figure 3.14).

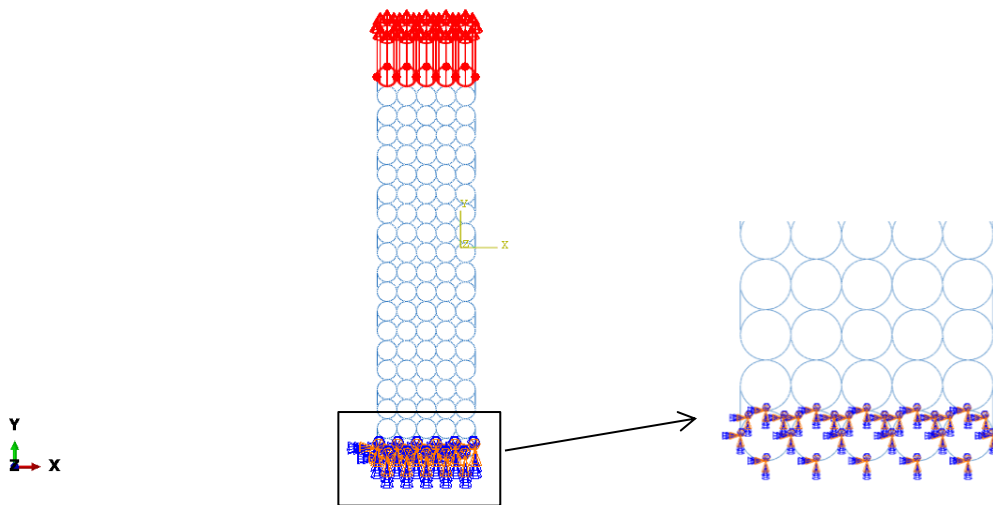


Figure 3.14 Definition of the boundary conditions of the circular mesh with 2.00 mm of pore diameter.

3.2.2.3 Experimental Procedures

To validate the results obtained in the simulations performed, it was printed one of the meshes created. For that and based on a previous study made by Pinto, in 2022 [46], done to calibrate the same pellet's extruder used to print meshes with medical-grade PCL, a g-code was created to print a mesh with a square pore size of 2.00 mm, and a filament with a 0.24 mm of thickness (Figure 3.15).

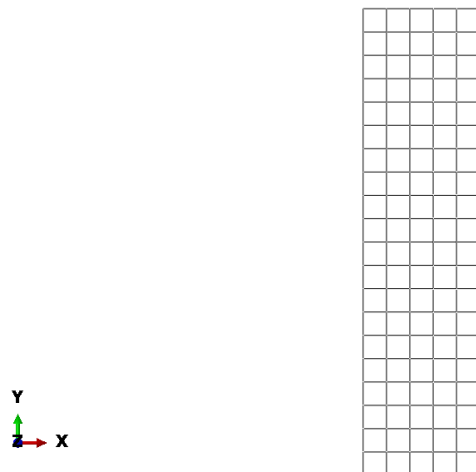


Figure 3.15 Computational model of a mesh with a square pore of 2.00 mm, and a filament with 0.24 mm of thickness.

In order to print the mesh, the printed parameters of the melt electrowriting printer were: (1) temperature of 200°C, (2) speed of 700 mm/min, (3) voltage of 7 kV, and (4) height of the extruder should be determined by the following equation (Eq.2):

$$E = \frac{(D \times 1.5 \times 0.001)^2 \times L}{1.75^2} \quad (2)$$

The E (mm) represents the polymer to be extruded, the D (μm) corresponds to the required diameter, and the L (mm) symbolises the length of the printed segment. The values used in the g-code are expressed on the following figure (Figure 3.16).

```

M107;           %Start Program
M104 S200.0000; %Set Temperature to 200°C
G28;           %Calibrate Axes
G21;           %Set unit in millimeters
G90;           %Set Absolute Coordinates for Position
M83;           %Set Relative Coordinates for Extrusion
M109 S200.0000; %Set Temperature to 200°C and wait for
the temperature to stabilize before moving on to the next command line
G1 Z3;         %Set the height to the minimum dimension
G1 X150 Y75 F3000; %Start of the stabilization route
G91;           %Set Relative Coordinates for Position
G1 X200 E0.4;
G1 Y200 E0.8;
G1 X-250 E0.8;
G1 Y-200 E0.8;
G1 X125 E0.4;
G1 Y5;         %End of the stabilization route
G1 X-42.0000 Y30 E2 F3000;
G4 S2;
G1 F700.0000

G1 X0 Y0 Z0

G1 X84.0000 Y0 E3.9995
G1 X0.0000 Y2.0000 E0.0846
G1 X-84.0000 Y0.0000 E3.9995
G1 X0.0000 Y2.0000 E0.0846
G1 X84.0000 Y0 E3.9995
G1 X0.0000 Y2.0000 E0.0846
G1 X-84.0000 Y0.0000 E3.9995
G1 X0.0000 Y2.0000 E0.0846
G1 X84.0000 Y0 E3.9995
G1 X0.0000 Y2.0000 E0.0846
G1 X-84.0000 Y0.0000 E3.9995
G1 X0.0000 Y2.0000 E0.0846
G1 X84.0000 Y0 E3.9995
G1 X0.0000 Y2.0000 E0.0846
G1 X-84.0000 Y0.0000 E3.9995
G1 X0.0000 Y2.0000 E0.0846
G1 X84.0000 Y0 E3.9995
G1 X0.0000 Y2.0000 E0.0846
G1 X-84.0000 Y0.0000 E3.9995
G1 X0.0000 Y2.0000 E0.0846
G1 X84.0000 Y0 E3.9995

```

Figure 3.16 Initial part of the g-code for the medical-grade PCL mesh with square pores, 2.00 mm of pore diameter, and 0.24 mm of filament thickness.

3.2.2.3.1 Uniaxial tensile test - Printed Mesh

After printing the mesh, it was carried out uniaxial tensile tests to six samples to determine the load-displacement values of the mesh in order to validate the results obtained in the simulation (Figure 3.17).

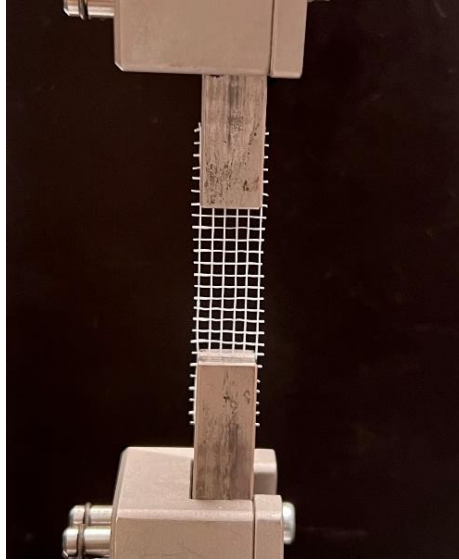


Figure 3.17 Uniaxial tensile test performed on the printed mesh with square pores of 2.00 mm of diameter, and 0.24 mm of filament thickness.

3.2.2.3.2 Uniaxial tensile test - Vaginal tissue

A uniaxial tensile test was performed on five samples of vaginal tissue to determine the values of load-displacement and compare them with the results obtained in the simulations of the meshes (Figure 3.18).

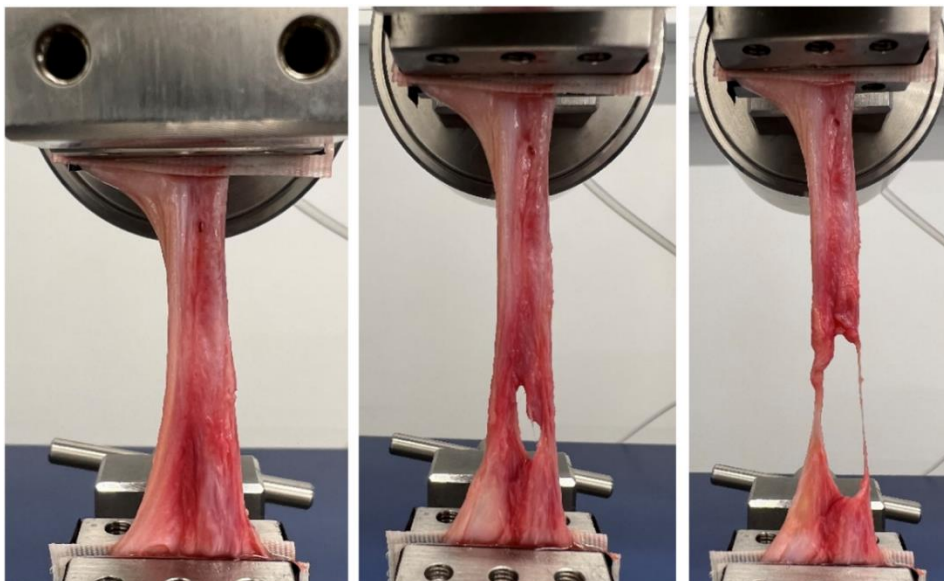


Figure 3.18 Uniaxial tensile test performed on the vaginal tissue.

Chapter 4

Results and Discussion

Chapter 4 starts with the results of the uniaxial tensile tests performed on a square pore mesh, to compare it with the medical-grade PCL printed square pore mesh. Then, it was analysed the results obtained on the different computational models of the meshes, varying their pore size, pore geometry, the filament diameter, and the presence of filaments completely around the meshes, or only in specific points. The results of the simulations were presented in images, tables, and graphics. The graphics also include the results of the uniaxial tensile test made on the vaginal tissue.

4.1 Printed Mesh and the Computational Model

Initially, in order to confirm that the results obtained in the simulation performed in Abaqus® are similar to the experimental results, the values of load and displacement obtained in both cases were compared. It is important to mention that the results were obtained from the average of the load-displacement values from 3 uniaxial tensile tests carried out on 3 medical-grade PCL square meshes, as shown in the subsection 3.2.2.3.1.

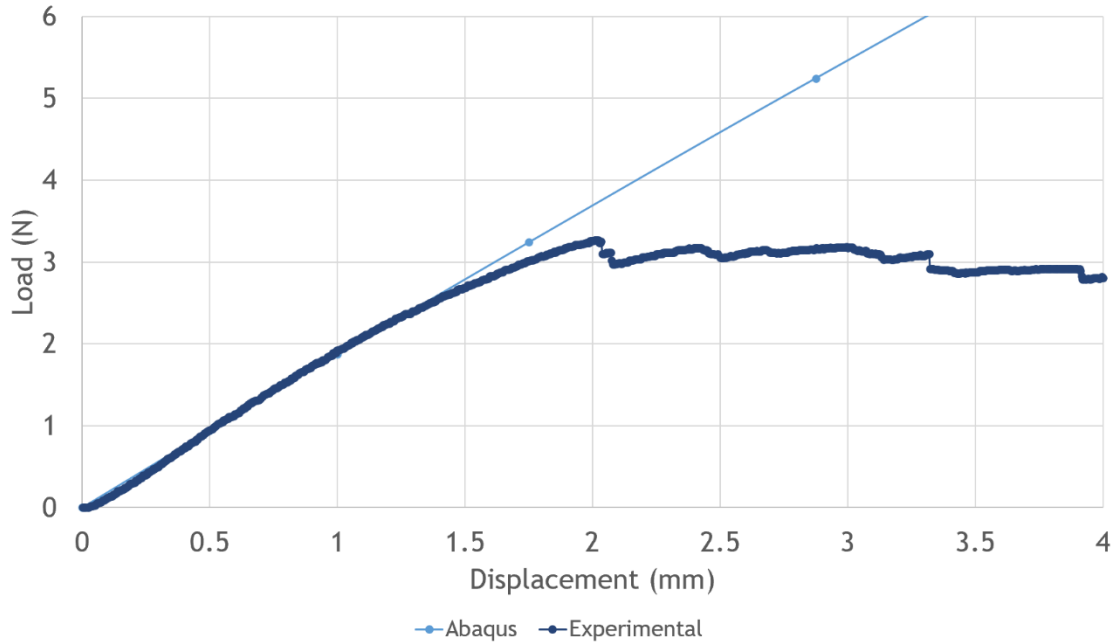


Figure 4.1 Load and displacement values obtained from the computational model and the experimental mesh, both with square pores of 2.00 mm and 0.24 mm of filament diameter.

As observed in the graphic (Figure 4.1), the magnitude is the same and the lines exhibit similar behaviour; additionally, as expected, the behaviour of the developed model is stiffer than that of the experimental model. These results are based on models and testing with a square pore mesh, as shown in the subsection 3.2.2.3. It is important to note that the results may vary based on the geometry and properties of the mesh. The computational model was built and simulated based on the experimental results. An experimental mesh was printed by MEW, using medical-grade PCL. The outcomes demonstrate an extremely close match between the experimental and computational analysis. The difference between the two meshes is the fact that on the moment that the filaments start to rupture during the uniaxial tensile test, the material starts to have a plastic behaviour, while in the simulation it continues to have an elastic behaviour because it does not have into consideration the yield stress.

4.2 Computational Models

Before delving into the analysis of the simulation results, it is crucial to clarify that the graphics depict outcomes within the safety zone, while the images showcasing distorted pores correspond to the comfort zone. The terms "Comfort zone" and "Safety zone" are associated with the expected strains experienced by vaginal tissue. The comfort zone represents the typical stresses encountered during daily activities, typically staying within a range of up to 20% strain. Conversely, the safety zone is designed to account for extreme stress peaks, set at a 40% strain threshold [62][63]. However, more recent research adopts a maximum strain threshold of 23%, aligning it with what is conventionally considered within the comfort zone [64].

4.2.1 Absence and Presence of the Filament around the Mesh

Firstly, it was compared the values of load and displacement obtained by the computational models without a filament around them, and a pore dimension of around 2.00 mm (except for the sinusoidal mesh), comparing them with the values of load and displacement of the vaginal tissue, as shown on the graphic (Figure 4.3). It is worth noting that all these meshes were created using a 0.24 mm filament thickness. The Figure 4.2 represents the computational models of the results presented in the graphic (Figure 4.3):

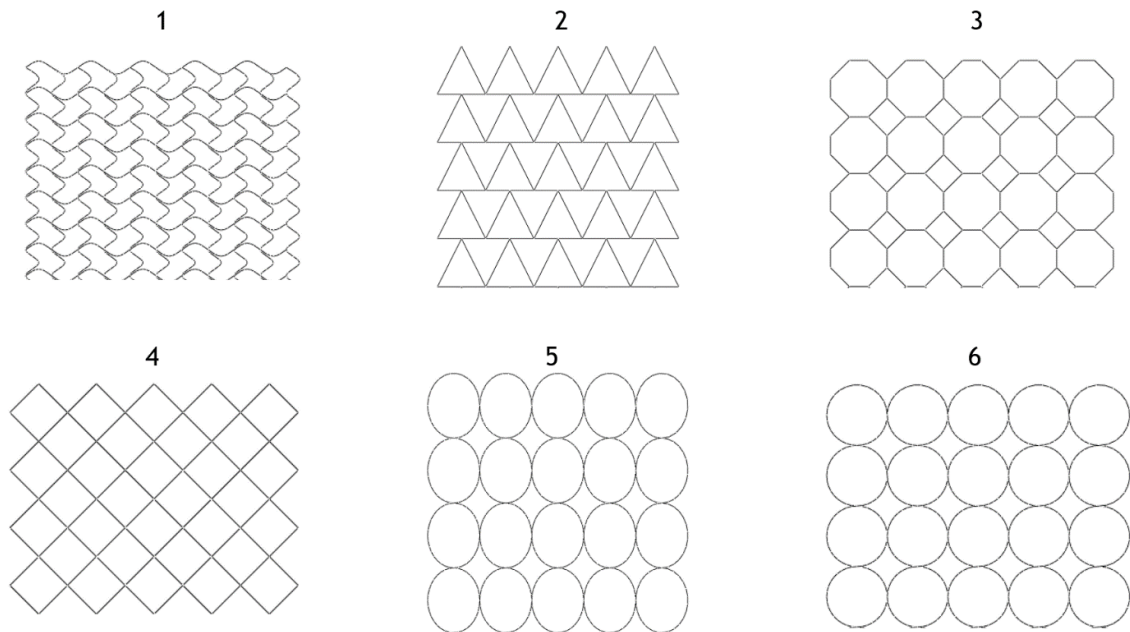


Figure 4.2 Computational models developed without a filament around the mesh and 0.24 mm filament thickness. 1 - Sinusoidal with a 1.58 mm pore size. 2 - Triangular with a 2.06 mm pore size. 3 - Octagon with a 2.10 mm pore size. 4 - Diamond with a 2.00 mm pore size. 5 - Oval with a 2.00 mm by 2.50 mm pore size. 6 - Circular with a 2.00 mm pore size.

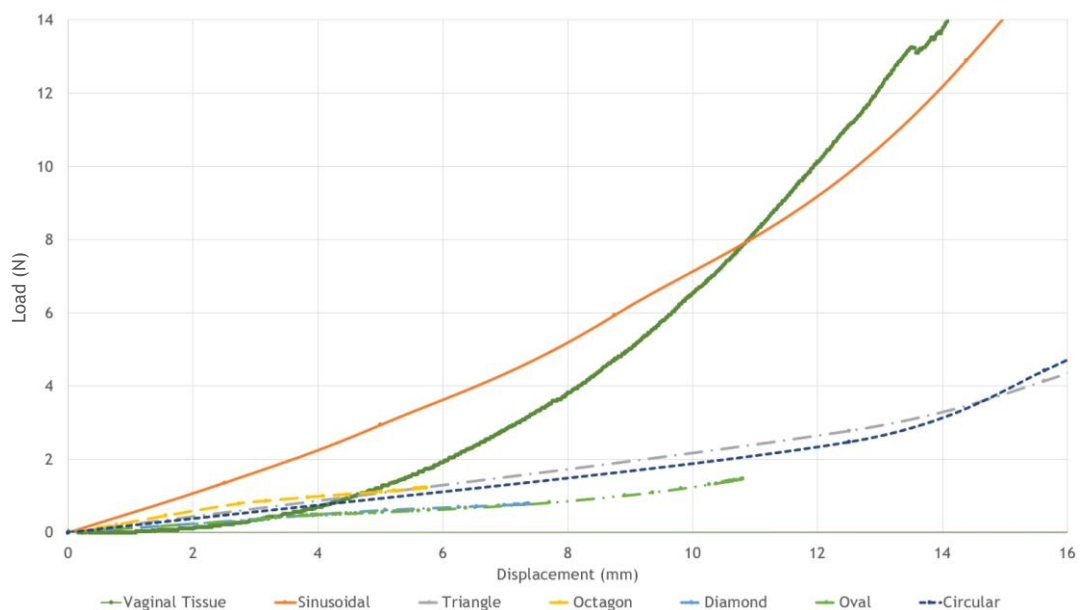


Figure 4.3 Load-displacement curves of the computational models created without the filament around them.

By analysing the graphic (Figure 4.3), for the same displacement values as the vaginal tissue, meshes without the filament around them show low load values, with the exception of the sinusoidal mesh that presents a nonlinear mechanical behaviour similar to vaginal tissue.

So, in addition to these results, it is also important to analyse the pore deformation of the computational models. For this, it was analysed the pore distortion of the mesh that displays the best results, which is the sinusoidal mesh (Figure 4.4).

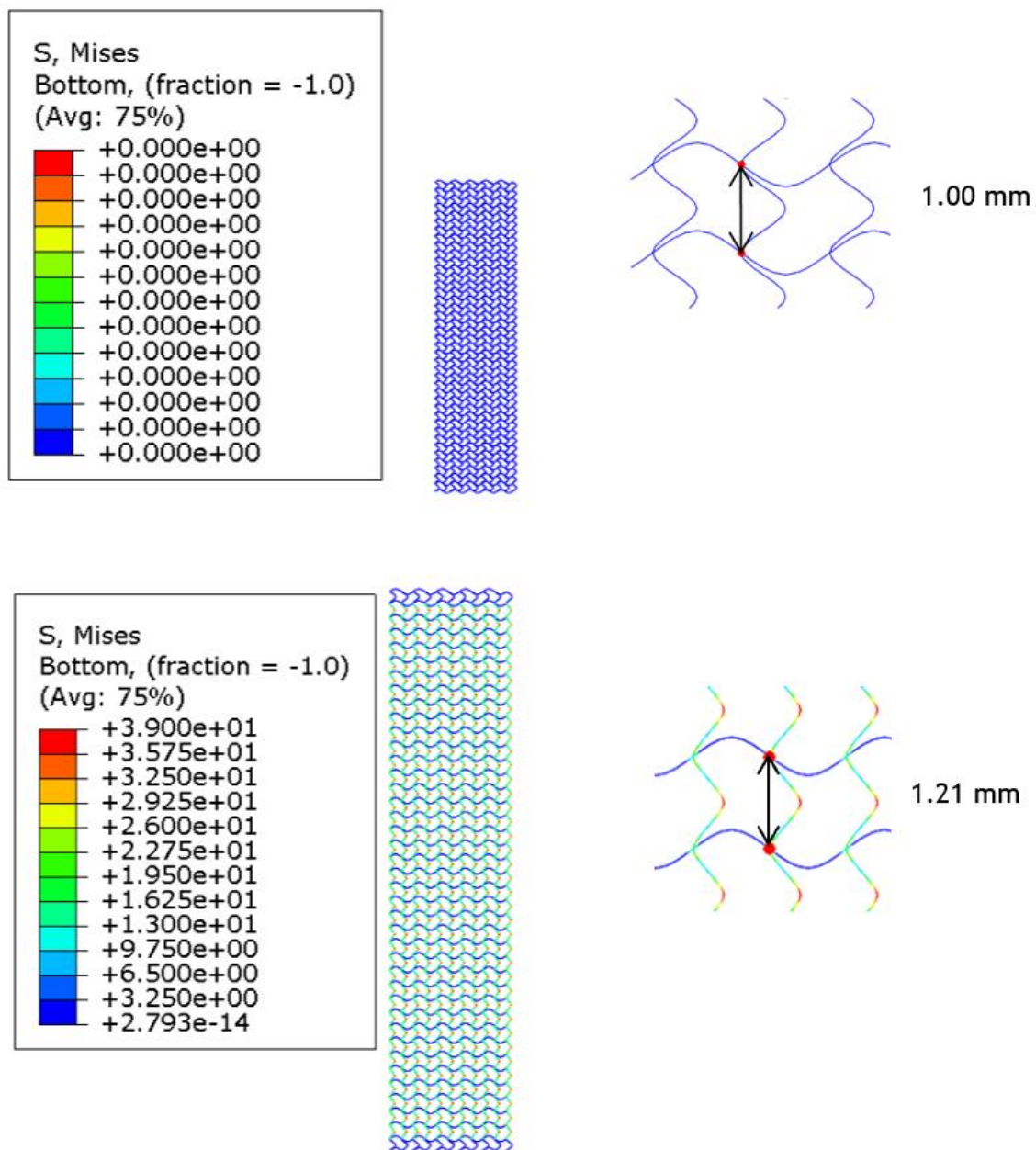


Figure 4.4 Difference between the pores of the sinusoidal mesh before and after the simulation.

As it can be observed, during the uniaxial tensile test, the filaments that are in a horizontal position have a minimal impact on the outcome. In this test, the filaments positioned vertically bear nearly all the applied force on the mesh. Consequently, when examining only the pores, one can observe that the filament undergoes a transformation from its initial sinusoidal shape to elongation in the vertical direction of 21.60%, thereby modifying the pore dimensions as depicted in the Figure 4.4. Horizontally, the filament experiences almost no alteration, approximately 1%, transitioning from 1.00 mm to 0.99 mm. In summary, its geometry and shape deform, causing it to lose its original shape. As vital as it is to pay attention to load and displacement values, it is also crucial to consider the deformation of each mesh after experiencing a specific level of load, which can result in an unusable mesh due to its degree of distortion.

Therefore, in an attempt to increase the load values and reduce the deformation of the models' pores, it was added a filament around the meshes (Figure 4.5). The results of the simulations made to these meshes are represented in Figure 4.6.

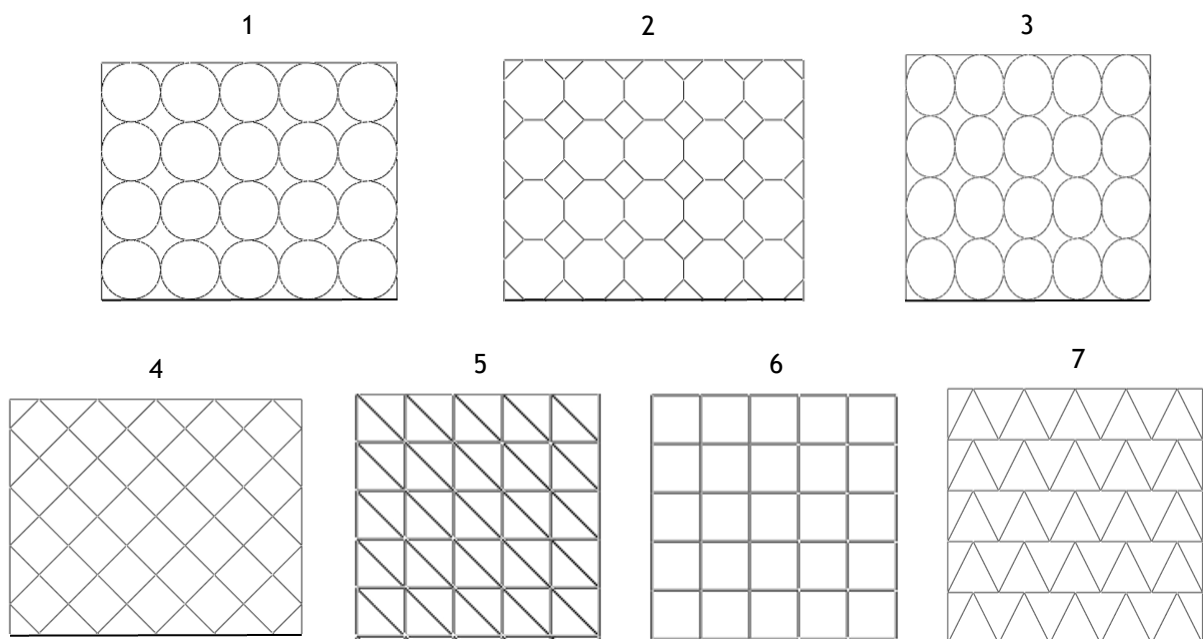


Figure 4.5 Computational models developed with a filament around the mesh and 0.24 mm of filament thickness. 1 - Circular with a 2.00 mm pore size. 2 - Octagon with a 2.10 mm pore size. 3 - Oval with a 2.00 mm by 2.50 mm pore size. 4 - Diamond with a 2.00 mm pore size. 5 - Diagonal with a 2.00 mm pore size. 6 - Square with a 2.00 mm pore size. 7 - Triangular with a 2.06 mm pore size.

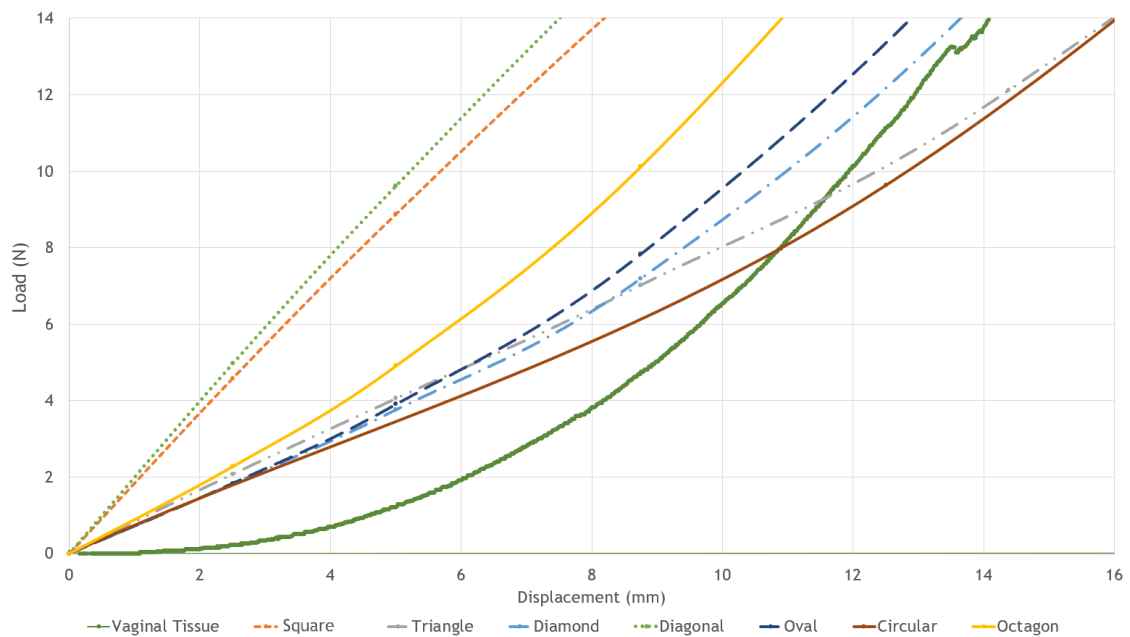


Figure 4.6 Load-displacement curves of the computational models created with the filament around them.

As shown in the graphic (Figure 4.6), it is possible to conclude that meshes with a filament around them present higher load values, in comparison with the meshes without the filament around them, meaning that the presence of a filament around the mesh influences the obtained load values.

Drawing from the acquired results, it is possible to eliminate the square and diagonal meshes from consideration going forward. These meshes present considerably higher load values than the vaginal tissue when exposed to the same displacement, indicating that these are not the ideal choice for POP repair.

The remaining computational models present promising results, however, the circular mesh is the one with a mechanical behaviour more similar to the vaginal tissue.

Lastly, it was examined the deformation of the pores within the circular mesh, as it presents values that resemble those of the vaginal tissue (Figure 4.7).

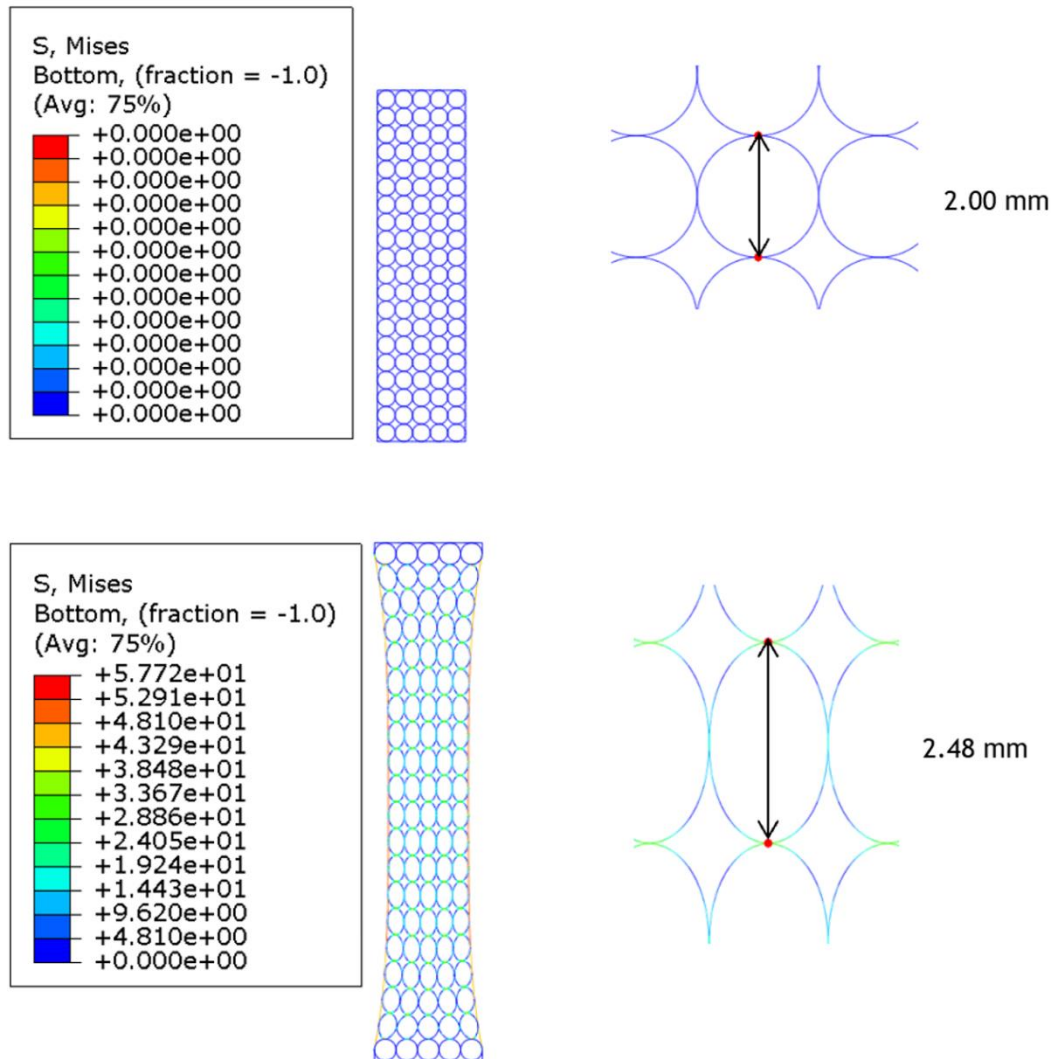


Figure 4.7 Difference between the pores of the circular mesh before and after the simulation.

The Figure 4.7 reveals a bigger contrast in pore deformation within this mesh when compared to the sinusoidal mesh. It is crucial to emphasize that pore deformation is not uniform across the entire mesh. In proximity to the fixed regions, the pores experience minimal deformation, whereas at the mesh's centre, the pores undergo a more substantial deformation of 24.15%, as illustrated in the Figure 4.7. In this scenario, the regions capable of withstanding most of the force applied during the uniaxial test are the filaments around the mesh, and the areas where the pores are connected.

In conclusion, while the inclusion of filaments around the computational models has shown promise in reducing pore deformation and enhancing load-displacement values, it is essential to investigate alternative approaches and make adjustments to other mesh characteristics to further improve the obtained results.

4.2.2 Pore Dimension

To enhance the meshes performance, it was examined how varying the dimensions of the pores can impact the load and displacement values of the meshes. For this purpose, it was developed three models with circular pores, one with 1.50 mm, another with 2.00 mm and one more with 2.50 mm diameter (Figure 4.8). It is important to mention that all the meshes were created with 0.24 mm filament thickness.

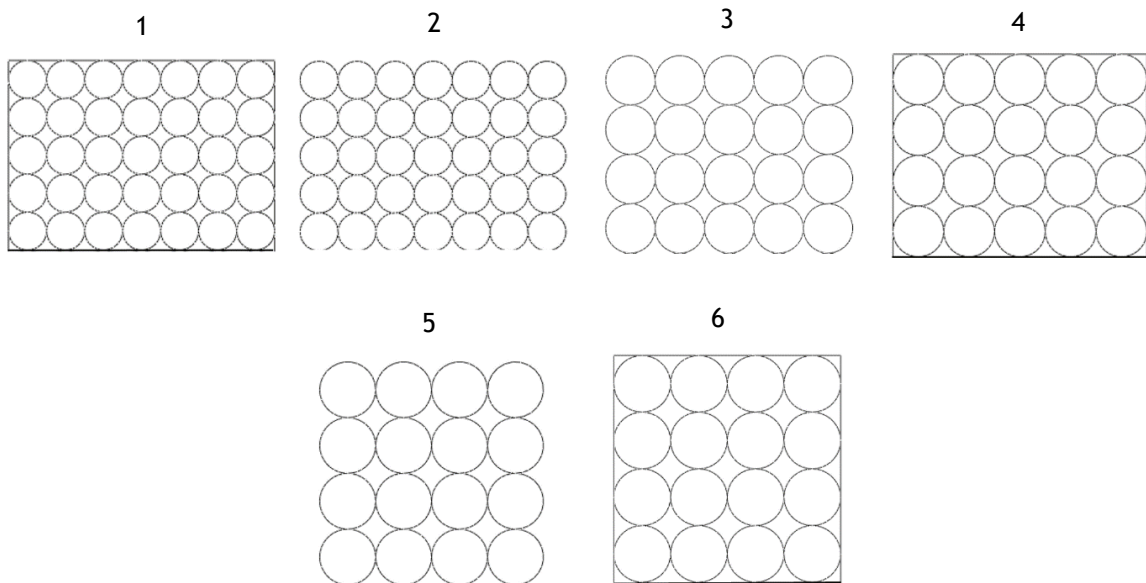


Figure 4.8 Circular pore meshes developed with and without a filament around the mesh. 1 and 2 - Meshes with 1.50 mm pore diameter. 3 and 4 - Meshes featuring a pore diameter of 2.00 mm. 5 and 6 - Meshes possessing a pore diameter of 2.50 mm.

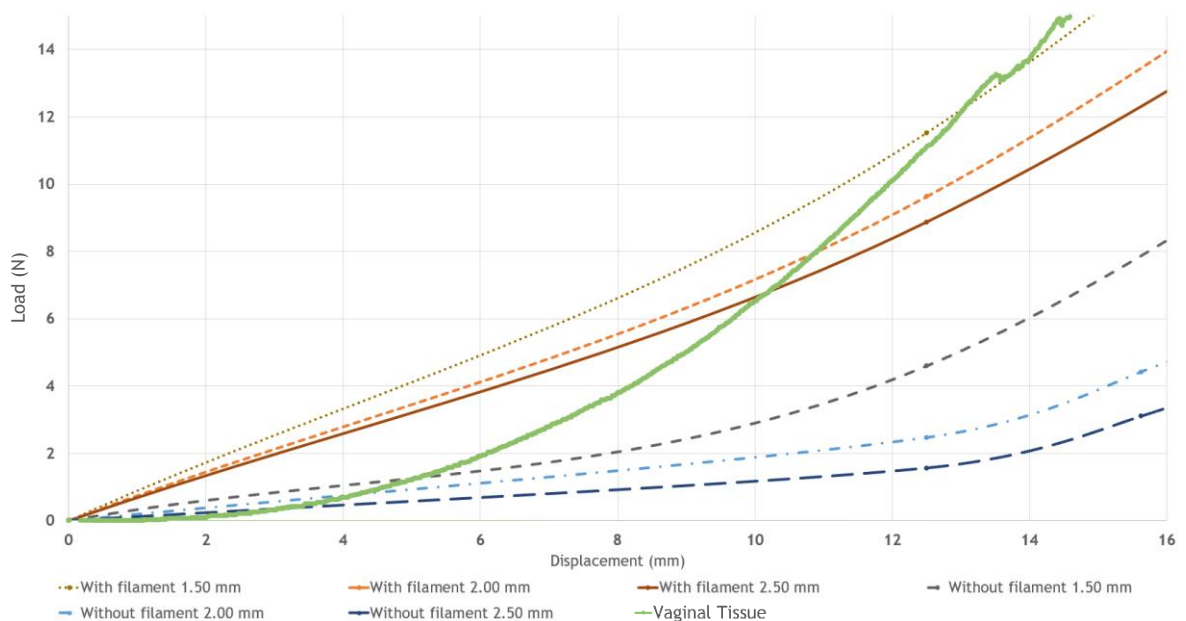


Figure 4.9 Load-displacement curves of the circular meshes created with different pore sizes.

By examining the graphic (Figure 4.9), it becomes evident that there exists a direct correlation between the pore size of the mesh and the resulting load values. Therefore, the mesh featuring the smallest pore diameter, 1.50 mm, exhibits greater load values compared to the other meshes.

This experiment has led to the conclusion that as the mesh's pore size decreases, the number of mesh columns increases. Consequently, the mesh becomes more resistant to the applied force, resulting in higher values of load-displacement.

Based on the results showcased, a possibility emerges: the notion of creating meshes with strategically positioned filaments around specific regions, aiming to achieve values that align with the range of results obtained while minimizing pore distortion to the greatest extent possible. In the upcoming section, section 4.2.3, it will be presented the outcomes of meshes designed with filaments strategically placed around specific areas.

4.2.3 Filament Thickness

The filament thickness is another important aspect to take into consideration when developing meshes. Several meshes with the same geometries presented previously in the section 4.2.1 were created with different filament diameters. Thus, for each pore geometry, three meshes with filaments of different thicknesses were developed, one with 0.08 mm, another with 0.16 mm and another with 0.24 mm. Although three meshes for each pore geometry were created, only the results for the meshes which have a similar behaviour as the vaginal tissue were presented in the following graphic (Figure 4.10).

Figure 4.10 represents the results obtained from the simulations carried out on the different mesh models that demonstrated the best results in the section 4.2.1, which are the sinusoidal mesh and the circular mesh with a pore diameter of 2.00 mm and a filament around it.

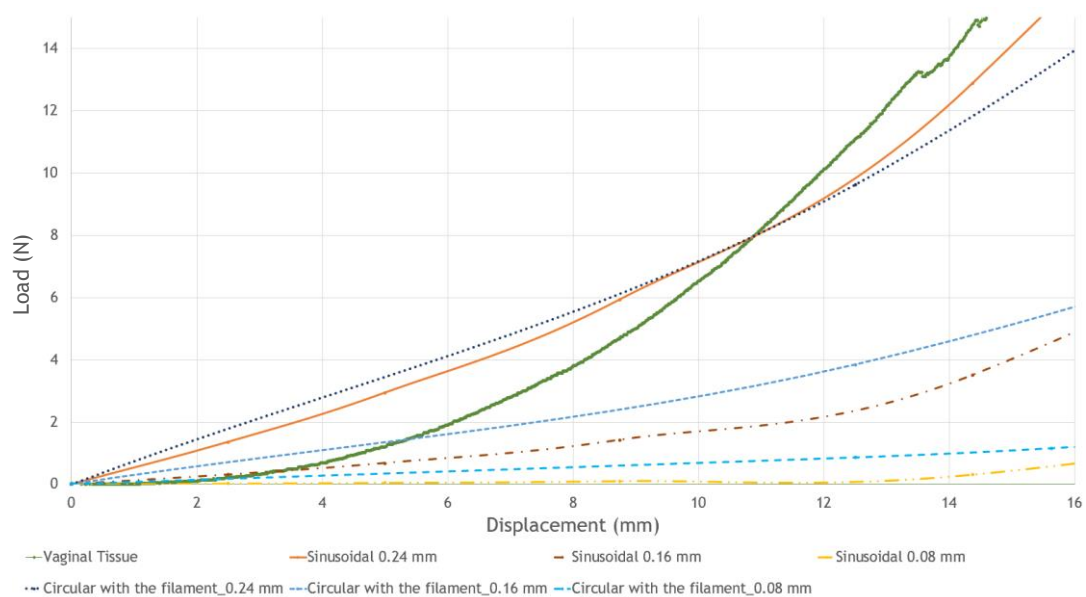


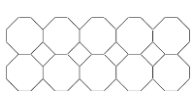
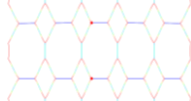
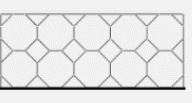
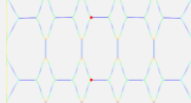
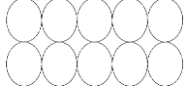
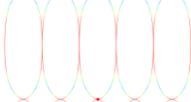
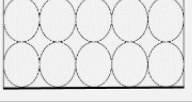
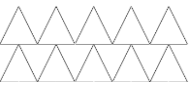
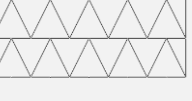
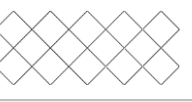
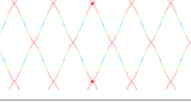
Figure 4.10 Load-displacement curves of the sinusoidal meshes and the circular meshes with a pore diameter of 2.00 mm and a filament around it.

As anticipated, reducing the thickness of the filaments corresponds to lower load-displacement values. As illustrated, the meshes delivering the most favourable outcomes are the ones that have filaments with 0.24 mm of diameter. These results are in line with the results obtained previously—the sinusoidal mesh and the circular mesh with a filament around it, featuring a pore diameter of 2.00 mm.

The results for the remaining Meshes have been consolidated in Table 2, and corresponds to the values obtained in the comfort zone.

Table 2 Values of pore deformation and maximum values of load in the comfort zone for all the meshes created.

Type of Mesh	Filament Thickness (mm)	Pore deformation (%)	Load (N)
Sinusoidal	0.08	21.06%	0.10
	0.16	21.06%	1.43
	0.24	21.06%	5.94
Square	0.08	22.22%	14.86
	0.16	22.22%	6.60
	0.24	22.22%	1.65
Circular without the filament around the mesh, and with 2.00 mm pore diameter	0.08	24.87%	0.02
	0.16	24.65%	0.22
	0.24	24.39%	1.01
Circular with the filament around the mesh, and with 2.00 mm pore diameter	0.08	24.66%	0.53
	0.16	24.58%	2.30
	0.24	24.15%	5.69
Circular without the filament around the mesh, and 2.50 mm pore diameter	0.08	25.65%	0.01
	0.16	25.49%	0.12
	0.24	25.28%	0.58
Circular with the filament around the mesh, and 2.50 mm pore diameter	0.08	24.62%	0.53
	0.16	24.98%	2.23
	0.24	24.80%	5.33
Circular without the filament around the mesh, and 1.50 mm pore diameter	0.08	23.94%	0.03
	0.16	23.61%	0.49
	0.24	23.24%	2.12
Circular with the filament around the mesh, and 1.50 mm pore diameter	0.08	24.29%	0.54
	0.16	23.67%	2.52
	0.24	23.09%	6.66
Diagonal	0.08	23.62%	1.61
	0.16	22.77%	6.55
	0.24	22.20%	14.81

Octagon without the filament around the mesh			0.08	25.89%	0.10
			0.16	22.99% *	0.49
			0.24	18.64% *	1.23
Octagon with the filament around the mesh			0.08	26.20%	0.74
			0.16	25.24%	3.47
			0.24	24.32%	8.93
Oval			0.08	27.11%	0.03
			0.16	27.35%	0.24
			0.24	27.07%	0.86
Oval with the filament around the mesh			0.08	25.93%	0.60
			0.16	26.02%	2.73
			0.24	25.78%	6.94
Triangle			0.08	24.25%	0.02
			0.16	23.68%	0.35
			0.24	23.24%	1.54
Triangle with the filament around the mesh			0.08	22.80%	0.56
			0.16	23.05%	2.50
			0.24	23.13%	6.42
Diamond			0.08	26.91%	0.03
			0.16	26.84%	0.25
			0.24	27.13%	0.84
Diamond with the filament around the mesh			0.08	25.38%	0.59
			0.16	24.92%	2.58
			0.24	24.49%	6.43

* Simulations that aborted.

As indicated in Table 2, meshes with the lowest percentage of pore deformation include the sinusoidal, square, and diagonal ones. However, among these meshes, only the sinusoidal exhibits a mechanical behaviour similar to the vaginal tissue.

There are also octagonal meshes without the filament around them that seem to have minimal pore deformation. Nonetheless, it is worth noting that the simulations for these meshes were aborted, resulting in different displacement conditions compared to other models. Consequently, the observed pore deformation does not correspond to what would be expected with the total displacement within the comfort zone.

Another noteworthy mention goes to the triangular mesh with a filament around it, which also demonstrates one of the lowest pore deformation values. However, this mesh exhibits a notably low maximum load value, differing from the behaviour of vaginal tissue.

In this study, three key attributes of the meshes were varied: pore geometry, the presence or absence of a filament around the mesh, and filament thickness. Based on the findings, it was determined that the sinusoidal mesh with a 1.58 mm pore size and filaments with 0.24 mm diameter, along with the circular mesh featuring 1.50 mm and 2.00 mm diameter pores, filaments with 0.24 mm diameter, and a filament around the mesh, exhibit behaviour most closely resembling the vaginal tissue. However, in the pursuit of enhancing the results and creating

meshes capable of repairing prolapse, a novel concept emerged. This involved designing meshes with filaments present only in specific regions and varying filament thickness throughout the mesh, in contrast to the uniform thickness present in the other developed models. In terms of geometry and pore size, these new meshes feature circular pores with diameters of 1.50 mm, 2.00 mm, and 2.50 mm, as depicted in Figure 4.11.

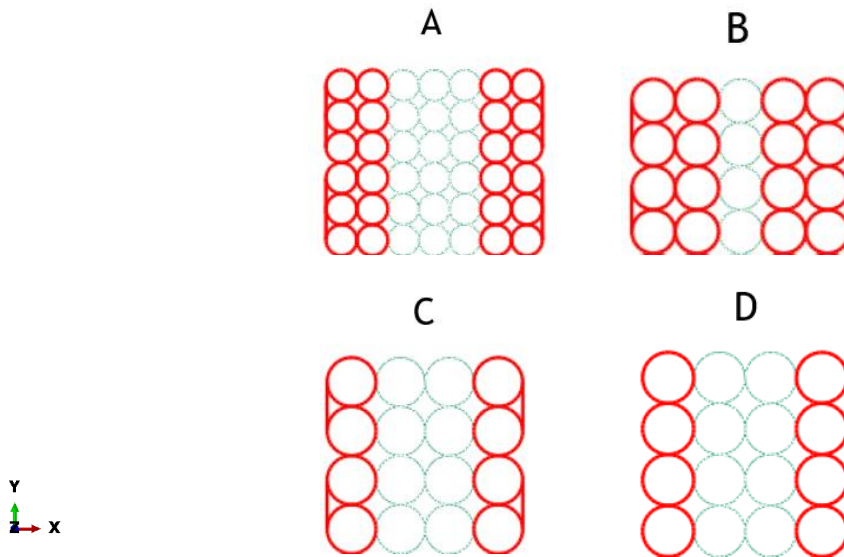


Figure 4.11 Distribution of filament thickness in the circular meshes. A - Mesh with 1.50 mm pore diameter, B - Mesh with 2.00 mm pore diameter, C - Mesh with 2.50 mm pore diameter, D - Mesh with 2.50 mm pore diameter. The red columns represent the filaments with a diameter of 0.08 mm or 0.16 mm, both cases were simulated, and the remaining columns have 0.24 mm of thickness.

This innovative approach also arises due to the fact that the mesh's primary objective is to replace damaged ligaments, muscles, or connective tissues that can no longer adequately support the tissues. Consequently, it is crucial to consider that the mesh, when attached to structures like bone (e.g., the sacrum), exhibits a more rigid behaviour and undergoes property changes as it approaches the uterus. Thus, by incorporating filaments of varying thicknesses across different regions of the mesh, the ability to withstand the force exerted will be different depending on the thickness of the filament. In this case, the central part of the mesh will be able to withstand higher values of force, as it has filaments with a diameter of 0.24 mm.

In the next section, section 4.3., the meshes that present the best results will be compared to the load-displacement values of the uterosacral ligament.

The graphic below (Figure 4.12) illustrates the results obtained from the simulations conducted on these new meshes.

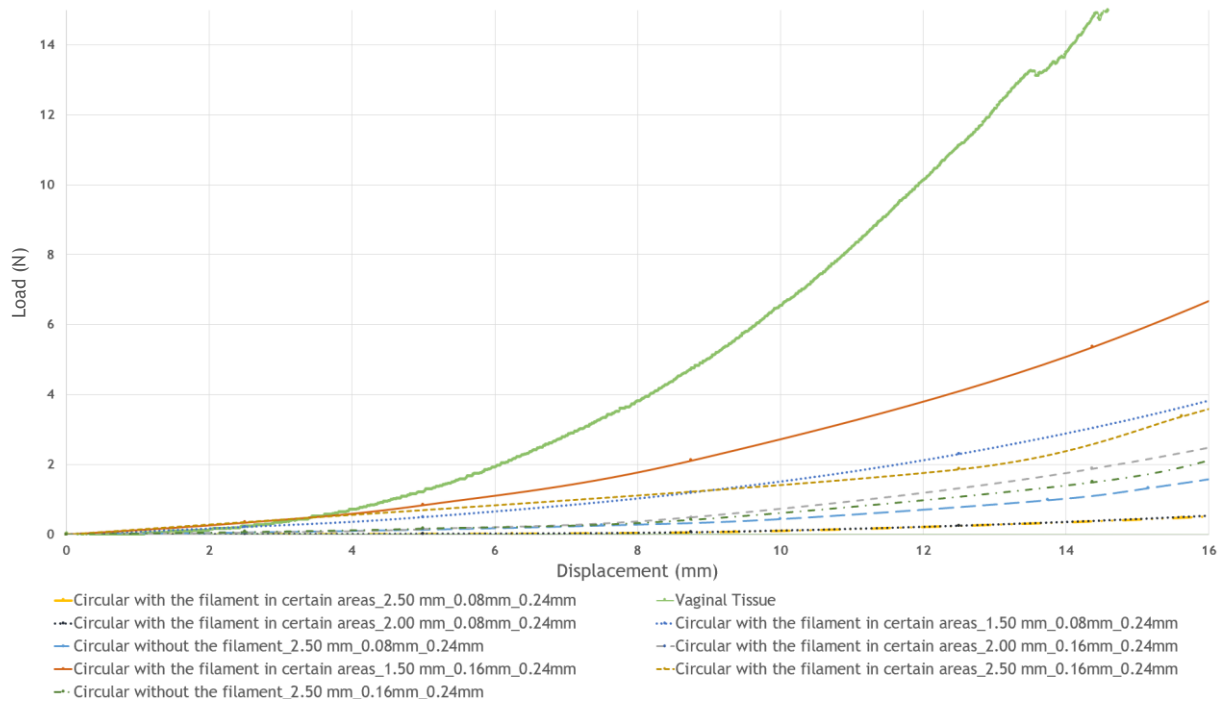


Figure 4.12 Force-displacement curves of the circular meshes with and without a filament around it in certain areas, and with the different filament thickness.

As evident from the graphic, the mesh that exhibits a more similar behaviour to the vaginal tissue features a pore diameter of 1.50 mm, along with filaments around specific areas, and incorporates filaments with 0.16 mm of diameter in the end columns and filaments with 0.24 mm diameter in the central columns.

As done previously, the deformation of the mesh pore that closely mimics the behaviour of vaginal tissue was analysed (Figure 4.13).

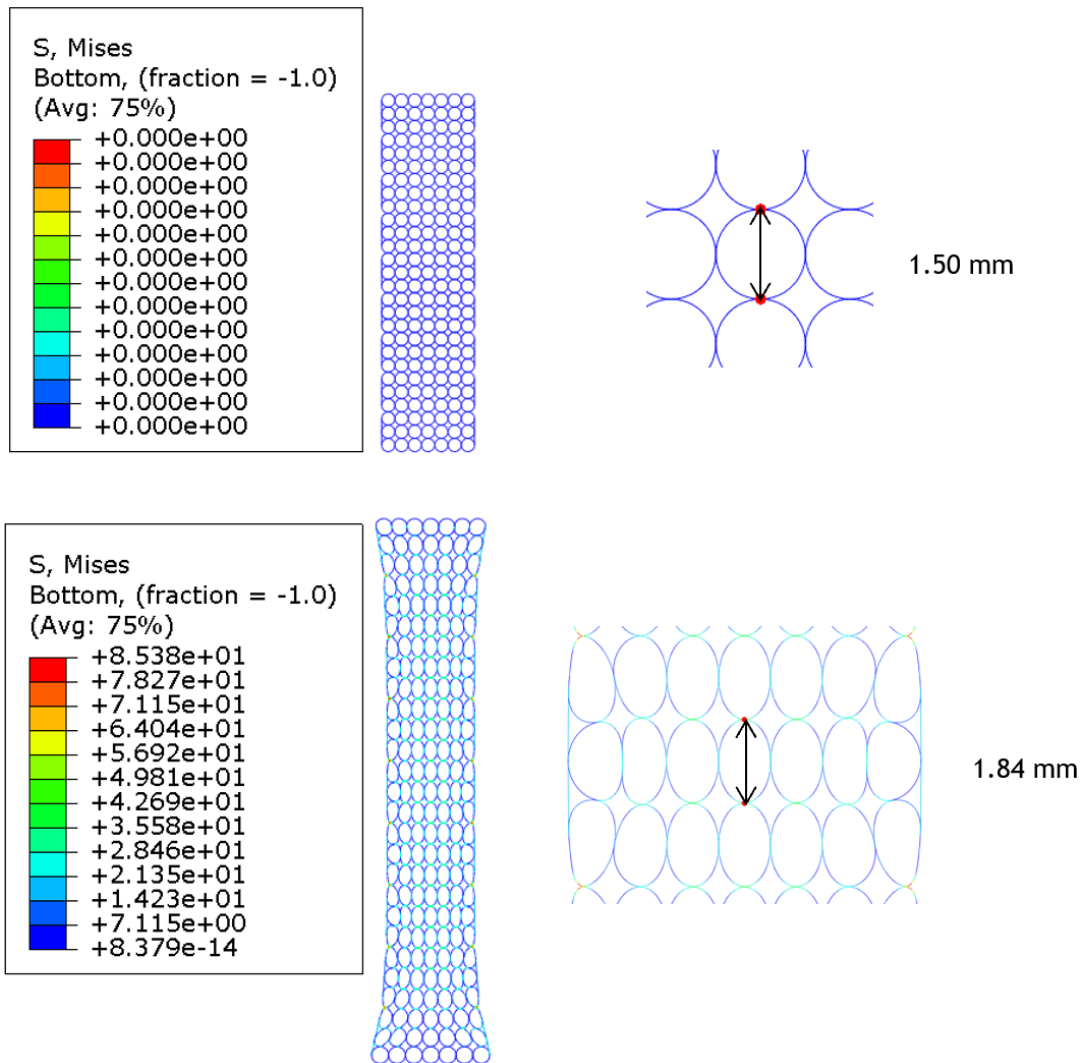
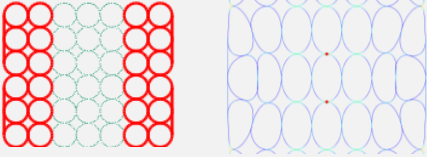
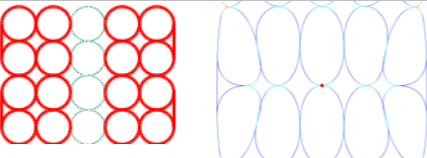
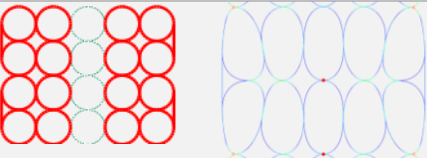
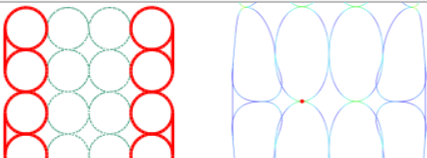
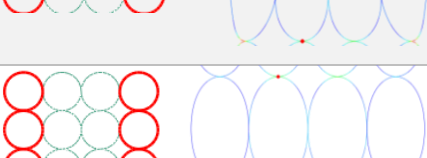
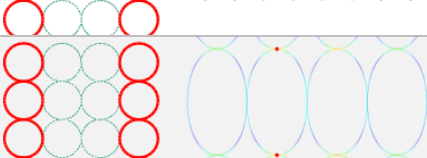


Figure 4.13 Difference between the pores of the circular mesh with a filament around it in certain areas, and with the different filament thickness before and after the simulation.

From Figure 4.13, it is possible to conclude that the recent modifications applied to the meshes result in reduced pore deformation of 22.89% for a maximum load value of 1.75 N in the comfort zone, bringing the outcomes even closer to replicating the behaviour of the vaginal tissue.

Table 3 displays the values of the pore deformation and the maximum load achieved within the comfort zone.

Table 3 Values of pore deformation and maximum values of load in the comfort zone for the circular pore meshes with different filament thickness.

Type of Mesh	Pore	Pore deformation (%)	Load (N)
Circular with the filament in certain areas_1.50 mm_0.08mm_0.24mm		22.50%	0.99
Circular with the filament in certain areas_2.00 mm_0.08mm_0.24mm		24.96%	0.04
Circular with the filament in certain areas_2.00 mm_0.16mm_0.24mm		24.63%	0.39
Circular with the filament in certain areas_2.50 mm_0.08mm_0.24mm		25.60%	0.32
Circular with the filament in certain areas_2.50 mm_0.16mm_0.24mm		25.19%	0.57
Circular without the filament_2.50 mm_0.08mm_0.24mm		24.94%	0.29
Circular without the filament_2.50 mm_0.16mm_0.24mm		25.42%	0.36

As is apparent from the data showcased in Table 3, as the pore size increases, there is a corresponding increase in pore deformation, accompanied by a decrease in the maximum load achieved within the comfort zone.

4.3 Final Remarks Regarding the Computational Models

Taking into consideration the results obtained, the following graphic (Figure 4.14) represents the values of load-displacement of the meshes that demonstrated the best results in the comfort zone, alongside the behaviour of the vaginal tissue, the uterosacral ligament, and the Restorelle® mesh [65][2].

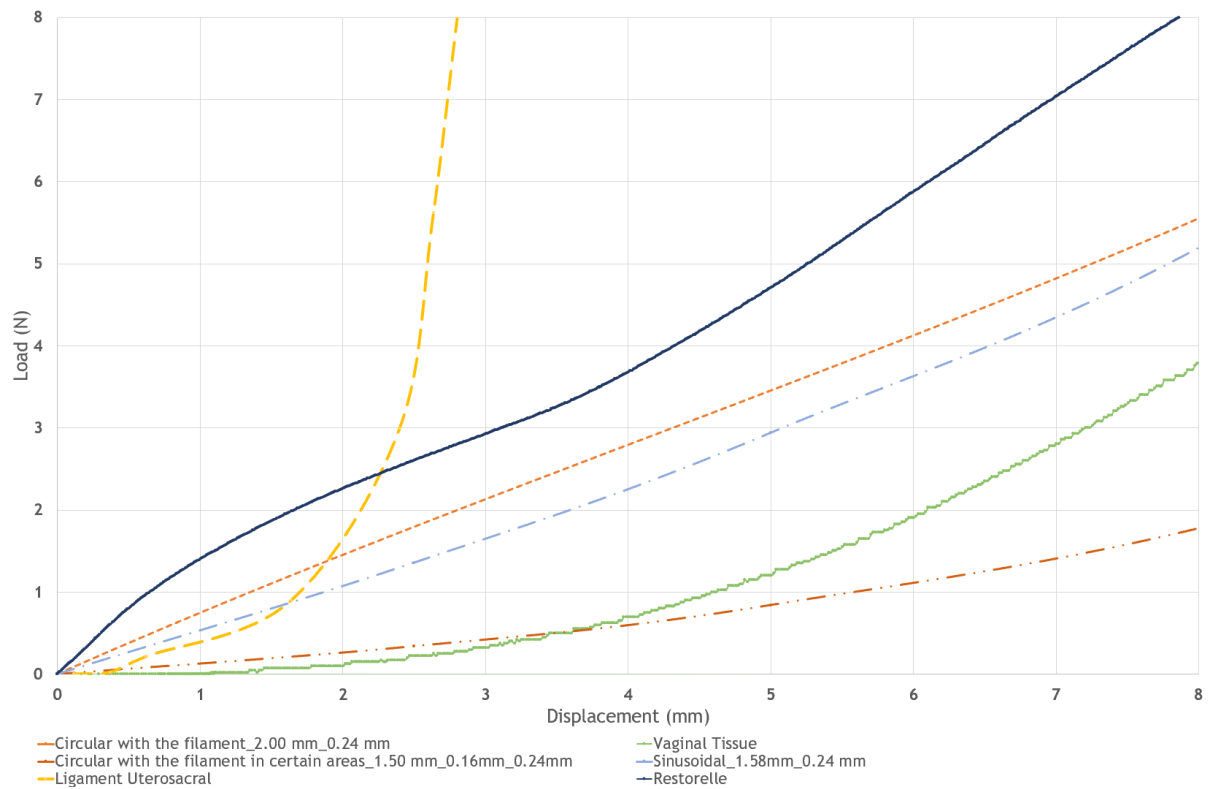


Figure 4.14 Load-displacement curves of the best mesh results obtained, the vaginal tissue, the ligament uterosacral, and the Restorelle® mesh.

As observed in the graphic (Figure 4.14), the mesh that closely emulates the behaviour of the vaginal tissue features a pore diameter of 1.50 mm, filaments positioned in certain areas around the mesh, and filaments with 0.16 mm of diameter in the end columns and filaments with 0.24 mm of diameter in the central columns.

Nonetheless, considering the good results achieved by the other two meshes, the sinusoidal and the circular mesh with a 2.00 mm diameter and 0.24 mm filament thickness, it would be interesting to design meshes that amalgamate the sinusoidal pattern with a circular pore. These new meshes would also incorporate 0.16 mm thick filaments in the end columns and 0.24 mm thick filaments in the central columns while maintaining a pore diameter of 1.50 mm. It is likely that these meshes will yield even more closely aligned load-displacement values with the vaginal tissue. Moreover, the pore deformations in these meshes are expected to be minimal, considering that the sinusoidal pores exhibited the least distortion during the uniaxial tensile test.

The results were also compared to the load-displacement values of the uterosacral ligament. This comparison aims to determine if the developed meshes exhibit a behaviour similar to the ligament or not.

Given that the ligament possesses a more rigid behaviour compared to the vaginal tissue, it is expected that the selected meshes will not behave similarly to the ligament. Nevertheless, a slight resemblance can be observed between the load-displacement values of the sinusoidal mesh and the circular mesh with filaments in specific areas, particularly at the onset of the graphic, resembling the ligament's behaviour to some extent. So, as a future endeavour, it would be important to investigate the type of mesh capable of embodying both the properties of the ligament and the tissue.

Finally, concerning the Restorelle® mesh, it is obvious that this mesh does not have a behaviour akin to that of the vaginal tissue or the uterosacral ligament. Its dissimilarity to both vaginal tissue and the uterosacral ligament is, most likely, one of the main reasons as to why its implementation in patients often leads to issues and tissue damage.

4.4 Main Conclusions

The key conclusions drawn from all the conducted work:

- The outcomes demonstrate an extremely close match between the experimental and computational tests, meaning that the values obtained in the simulations can be relied upon as accurate representations of the meshes' behaviour.
- Meshes without the filament around them exhibit low load values for equivalent displacement values when compared to the vaginal tissue, except for the sinusoidal mesh.
- As vital as it is to pay attention to load and displacement values, it is also important to consider the deformation of each mesh after experiencing a specific level of force, which can result in an unusable mesh due to its degree of distortion. Generally, meshes with a filament around them should experience less deformation in their pores.
- There is a direct relationship between the mesh's pore size and the resulting load values. As a result, the mesh with the smallest pore diameter, 1.50 mm, demonstrates higher load values than the other meshes. This experiment leads to the conclusion that when the mesh pore size decreases, the number of mesh columns increases, and consequently, the mesh's resistance to the applied force rises, resulting in higher load-displacement values.
- Decreasing filament thickness correlates with diminished load-displacement values.
- From the last meshes developed, the mesh that best mimics the behaviour of the vaginal tissue features a pore diameter of 1.50 mm, along with filaments around specific areas, and filaments with 0.16 mm of diameter in the end columns and 0.24 mm of diameter in the central columns.

- Meshes that integrate both the sinusoidal pattern and a circular pore, filaments with 0.16 mm and 0.24 mm of diameter, while maintaining a pore diameter of 1.50 mm, appears to be a viable option. These meshes are likely to display even closer load-displacement values resembling vaginal tissue. Moreover, considering that the sinusoidal pores demonstrated the least deformation during the uniaxial tensile test, it is probable that these meshes will experience minimal pore distortion.
- It is important to explore the possibility of designing a mesh that can incorporate the characteristics of both the ligament and the vaginal tissue.
- Lastly, the Restorelle® mesh does not behave similarly to the vaginal tissue or the uterosacral ligament, indicating that it is not the ideal choice for prolapse repair.

Chapter 5

Conclusions and Future Works

5.1 Conclusions

POP profoundly impacts the daily lives of numerous individuals worldwide, underscoring the growing necessity to allocate resources and efforts towards developing products, techniques, and processes that ameliorate these issues and significantly enhance people's quality of life.

Currently, recommended solutions exist for POP repair. In its initial stages, mild cases of POP can be managed with minimally invasive approaches such as pessaries, physiotherapy, muscle strengthening exercises, biofeedback therapy, and electrical stimulation therapy. These methods are effective and have minimal invasiveness. In cases where they prove ineffective, more invasive treatments can be considered for severe POP cases, typically involving surgery with synthetic mesh for definitive correction. However, the FDA has prohibited the sale and distribution of such meshes for transvaginal prolapse treatment due to associated high risks, creating a significant challenge in this treatment avenue. This situation has prompted the development of biodegradable meshes, offering advantages like flexibility, malleability, biocompatibility, and the promotion of cell growth.

In essence, the introduction of biodegradable meshes into prolapse treatment emerges as a highly recommended option, promising improved outcomes while avoiding the risks and drawbacks associated with synthetic mesh use.

In this context, there were developed several computational models of meshes with different pore geometries, pore sizes, filament thickness, and with filaments around the meshes in certain areas. The models produced promising results, as well as similarities to the load-displacement values of the vaginal tissue. However, it is necessary to improve these computational models to better the results and ultimately achieve the best meshes possible and thus, repair the prolapse.

For this, new concepts have emerged to advance this work further to reach a similar behaviour of the vaginal tissue and ligaments.

5.2 Future Works

Due to the promising results obtained in the simulations carried out on the computational models, for future works, it would be interesting to execute the following ideas/suggestions:

- Develop meshes that incorporate both the sinusoidal pattern and circular pores.
- Test new meshes with pore sizes of approximately 1.50 mm for various geometries.
- Develop computational models by varying the filament thickness throughout the meshes.
- Evaluate the meshes performance using a pelvic cavity model.
- Develop computational models of meshes by using their g-codes. A python code has been developed for this purpose, becoming feasible to create sketches of the meshes through their g-code coordinates, and thus, conduct multiple simulations on the meshes (consult appendix for the python code).
- Perform fatigue tests on the meshes.
- Incorporate substances compatible with the medical-grade PCL and the biological system, to investigate the possibility of enhancing mesh properties and characteristics, as well as comprehending the impact on the results of the mechanical tests.
 - According to a recent study made by Ren et al, in 2022, this could be a feasible option. The composite meshes produced through MEW, incorporating PCL and PEG, offer the advantage of controlling degradation rates by adjusting PEG content. These meshes also exhibit improved mechanical properties, including maximal forces, compared to PCL alone, approaching clinically observed forces. The incorporation of antibacterial properties with controlled release was successfully achieved, although further refinement of the antibacterial agent concentration is required. Nevertheless, it appears possible to manufacture a compliant and antibacterial biodegradable mesh using a form of 3D printing (MEW) [66].

References

- [1] L. H. NYU, “Diagnosing Pelvic Organ Prolapse | NYU Langone Health.” <https://nyulangone.org/conditions/pelvic-organ-prolapse-in-adults/diagnosis> (accessed Jun. 15, 2022).
- [2] M. N. B. da Cunha, R. Rynkevic, M. E. T. da Silva, A. F. Moreira da Silva Brandão, J. L. Alves, and A. A. Fernandes, “Melt Electrospinning Writing of Mesh Implants for Pelvic Organ Prolapse Repair,” *3D Print. Addit. Manuf.*, vol. 00, no. 00, pp. 1-10, 2021, doi: 10.1089/3dp.2021.0010.
- [3] “Biomecânica: Combinar engenharia e experiência clínica para melhorar o tratamento do prolapso de órg - INEGI.” <https://www.inegi.pt/pt/noticias/biomecanica-combinar-engenharia-e-experiencia-clinica-para-melhorar-o-tratamento-do-prolapso-de-orgaos-pelvicos-femininos/> (accessed Nov. 20, 2022).
- [4] “Urinary incontinence and pelvic organ prolapse in women: management NICE guideline Your responsibility,” 2019, Accessed: Nov. 20, 2022. [Online]. Available: www.nice.org.uk/guidance/ng123
- [5] D. Glass, “Demystifying pelvic organ prolapse - UChicago Medicine,” Jan. 30, 2019. <https://www.uchicagomedicine.org/forefront/womens-health-articles/demystifying-pelvic-organ-prolapses> (accessed Jun. 15, 2022).
- [6] “Pelvic Organ Prolapse > Fact Sheets > Yale Medicine.” <https://www.yalemedicine.org/conditions/pelvic-organ-prolapse> (accessed Jun. 13, 2022).
- [7] N. Ng-Stollmann, C. Fünfgeld, B. Gabriel, and A. Niesel, “The international discussion and the new regulations concerning transvaginal mesh implants in pelvic organ prolapse surgery,” *Int. Urogynecol. J.*, vol. 31, no. 10, pp. 1997-2002, 2020, doi: 10.1007/s00192-020-04407-0.
- [8] A. Rita and M. Gomes Da Silva, “Estudo Biomecânico da Cavidade Pélvica da Mulher,” 2012.
- [9] Shazia R. Chaudhry; Ahmed Nahian; Khalid Chaudhry, *Anatomy, Abdomen and Pelvis, Pelvis*. StatPearls Publishing, 2023.
- [10] R. F. Ferreira, “FACULDADE DE ENGENHARIA DA UNIVERSIDADE DO PORTO Development of a Virtual Model of the Pelvic Cavity,” 2020.
- [11] M. Inoue, *Female urology*, vol. 75, no. 6. 2022. doi: 10.5005/jp/books/12162_14.
- [12] M. Frank H. Netter, *Atlas of human anatomy*, 6th ed. 2014.
- [13] Keith L. Moore, Arthur F. Dalley, Anne M.R. Agur, *Clinically Oriented ANATOMY*, 7th ed. MOORE.
- [14] Mayo Clinic, “Female pelvic floor muscles,” 2023. <https://www.mayoclinic.org/healthy-lifestyle/womens-health/multimedia/female-pelvic-floor-muscles/img-20006566> (accessed May 18, 2023).
- [15] K. Hosseinzadeh, M. T. Heller, and G. Houshmand, “Imaging of the female perineum in adults,” *Radiographics*, vol. 32, no. 4, Jul. 2012, doi: 10.1148/rg.324115134.
- [16] V. Raizada and R. K. Mittal, “Pelvic Floor Anatomy and Applied Physiology,” *Gastroenterol. Clin. North Am.*, vol. 37, no. 3, pp. 493-509, 2008, doi: 10.1016/j.gtc.2008.06.003.
- [17] D. Vilas and B. Rodrigues, “Structure Design Optimisation Of Biodegradable Implants For Melt Electrowriting,” 2022.
- [18] J. Eric Jelovsek, C. Maher, M. D. Barber, J. E. Jelovsek, and M. D. Barber, “Pelvic organ

- prolapse,” 2007. [Online]. Available: www.thelancet.com
- [19] M. Thesis, M. Engineering, H. Borges, and C. Esp, “Master Thesis in Mechanical Engineering Development of 3D computational models of biodegradable meshes,” 2022.
- [20] S. E. Swift, S. B. Tate, and J. Nicholas, “Correlation of symptoms with degree of pelvic organ support in a general population of women: what is pelvic organ prolapse?,” *Am. J. Obstet. Gynecol.*, vol. 189, no. 2, 2003, doi: 10.1067/S0002-9378(03)00698-7.
- [21] R. C. Bump *et al.*, “The standardization of terminology of female pelvic organ prolapse and pelvic floor dysfunction,” *Am. J. Obstet. Gynecol.*, vol. 175, no. 1, pp. 10-17, 1996, doi: 10.1016/S0002-9378(96)70243-0.
- [22] A. Arian *et al.*, “Agreement of manual exam (POP-Q) with pelvic MRI in assessment of anterior pelvic organ prolapse,” *Iran. J. Radiol.*, vol. 14, no. 4, Oct. 2017, doi: 10.5812/iranjradiol.38542.
- [23] C. Persu, C. R. Chapple, V. Cauni, S. Gutue, and P. Geavlete, “Pelvic Organ Prolapse Quantification System (POP-Q) - a new era in pelvic prolapse staging.,” *J. Med. Life*, vol. 4, no. 1, pp. 75-81, 2011.
- [24] “Uterine prolapse - Diagnosis and treatment - Mayo Clinic.” <https://www.mayoclinic.org/diseases-conditions/uterine-prolapse/diagnosis-treatment/drc-20353464> (accessed Jun. 13, 2022).
- [25] S. Paramasivam, A. Proietto, and M. Puvaneswary, “Pelvic anatomy and MRI,” *Best Pract. Res. Clin. Obstet. Gynaecol.*, vol. 20, no. 1, pp. 3-22, 2006, doi: 10.1016/j.bpobgyn.2005.09.001.
- [26] N. Yoon, I; Gupta, *Pelvic Prolapse Imaging*. StatPearls Publishing, 2019.
- [27] R. Specialists, “Pelvic Organ Prolapse How is pelvic organ prolapse diagnosed?”.
- [28] F. Khorasani *et al.*, “Physiotherapy and pelvic floor muscle exercises for the prevention and treatment of pregnancy-related pelvic floor dysfunctions: A systematic review and meta-analysis,” *Int. J. Women’s Heal. Reprod. Sci.*, vol. 8, no. 2, pp. 125-132, 2020, doi: 10.15296/ijwhr.2020.20.
- [29] J. Xu and F. Huang, “A study of efficacy of traditional Chinese medicine combined with biofeedback electrical stimulation on postpartum pelvic organ prolapse,” *Int. J. Clin. Exp. Med.*, vol. 13, no. 12, pp. 10031-10038, 2020, [Online]. Available: <https://www.embase.com/search/results?subaction=viewrecord&id=L2005768579&from=export>
- [30] “What is a Pessary: Pessary Device 101 | Penn Medicine.” <https://www.pennmedicine.org/updates/blogs/womens-health/2016/may/what-is-a-pessary> (accessed Nov. 18, 2022).
- [31] “Pelvic Organ Prolapse (POP): Surgical Mesh Considerations and Recommendations | FDA.” <https://www.fda.gov/medical-devices/urogynecologic-surgical-mesh-implants/pelvic-organ-prolapse-pop-surgical-mesh-considerations-and-recommendations> (accessed Jun. 13, 2022).
- [32] M. K. Ammembal and S. C. Radley, “Complications of polypropylene mesh in prolapse surgery,” *Obstet. Gynaecol. Reprod. Med.*, vol. 20, no. 12, pp. 359-363, 2010, doi: 10.1016/j.ogrm.2010.09.006.
- [33] C. Maher, B. Feiner, K. Baessler, C. Christmann-Schmid, N. Haya, and J. Marjoribanks, “Transvaginal mesh or grafts compared with native tissue repair for vaginal prolapse,” *Cochrane Database Syst. Rev.*, vol. 2016, no. 2, Feb. 2016, doi: 10.1002/14651858.CD012079.
- [34] B. Chughtai, J. Mao, T. S. Asfaw, C. Heneghan, C. R. Rardin, and A. Sedrakyan, “Long-term Device Outcomes of Mesh Implants in Pelvic Organ Prolapse Repairs,” *Obstet. Gynecol.*, vol. 135, no. 3, pp. 591-598, 2020, doi: 10.1097/AOG.0000000000003689.
- [35] IEEE, “How the Finite Element Method (FEM) and Finite Element Analysis (FEA) Work Together,” 2023. <https://innovationatwork.ieee.org/how-the-finite-element-method-fem-and-finite-element-analysis-fea-work-together/>
- [36] V. Jagota, A. P. S. Sethi, and K. Kumar, “Finite element method: An overview,” *Walailak J. Sci. Technol.*, vol. 10, no. 1, pp. 1-8, 2013.
- [37] SAE International, Ed., *Finite Element Analysis for Design Engineers*, Third. Sherry Dickinson Nigam, 2022.
- [38] “Finite Element Analysis Software | Autodesk.” <https://www.autodesk.com/solutions/finite-element-analysis> (accessed Jun. 13, 2022).
- [39] “Abaqus - Non-Linear Finite Element Analysis Software | TECHNIA.”

- <https://www.technia.com/software/simulia/abaqus/> (accessed Jun. 13, 2022).
- [40] SIMULIA, “ABAQUS Basics.” <https://classes.engineering.wustl.edu/2009/spring/mase5513/abaqus/docs/v6.6/books/gss/default.htm?startat=ch06s01.html> (accessed May 3, 2023).
- [41] M. E. T. Silva, J. N. M. Bessa, M. P. L. Parente, T. Mascarenhas, R. M. Natal Jorge, and A. A. Fernandes, “Effect of mesh anchoring technique in uterine prolapse repair surgery: A finite element analysis,” *J. Biomech.*, vol. 127, no. July, p. 110649, 2021, doi: 10.1016/j.jbiomech.2021.110649.
- [42] W. R. Barone, K. M. Knight, P. A. Moalli, and S. D. Abramowitch, “Deformation of Transvaginal Mesh in Response to Multiaxial Loading,” *J. Biomech. Eng.*, vol. 141, no. 2, pp. 1-8, 2019, doi: 10.1115/1.4041743.
- [43] R. Rynkevic, M. E. T. Silva, P. Martins, T. Mascarenhas, J. L. Alves, and A. A. Fernandes, “Characterisation of Polycaprolactone Scaffolds Made by Melt Electrospinning Writing for Pelvic Organ Prolapse Correction- a Pilot Study,” *SSRN Electron. J.*, 2022, doi: 10.2139/ssrn.4036396.
- [44] R. Dwivedi *et al.*, “Polycaprolactone as biomaterial for bone scaffolds: Review of literature,” *J. Oral Biol. Craniofacial Res.*, vol. 10, no. 1, pp. 381-388, 2020, doi: 10.1016/j.jobcr.2019.10.003.
- [45] J. C. Kade and P. D. Dalton, “Polymers for Melt Electrowriting,” *Adv. Healthc. Mater.*, vol. 10, no. 1, 2021, doi: 10.1002/adhm.202001232.
- [46] M. Isabel and A. Pinto, “Melt electrowriting prototype optimization for medical-grade polycaprolactone mesh printing Melt electrowriting prototype optimization for medical-grade polycaprolactone mesh printing,” no. september, 2022.
- [47] J. K. Lunney, A. Van Goor, K. E. Walker, T. Hailstock, J. Franklin, and C. Dai, “Importance of the pig as a human biomedical model,” *Sci. Transl. Med.*, vol. 13, no. 621, pp. 1-20, 2021, doi: 10.1126/scitranslmed.abd5758.
- [48] C. Soares, P. Martins, E. Silva, L. Hymanova, and R. Rynkevic, “Cog Threads for Transvaginal Prolapse Repair: Ex-Vivo Studies of a Novel Concept,” *Surgeries (Switzerland)*, vol. 3, no. 2, pp. 101-110, 2022, doi: 10.3390/surgeries3020012.
- [49] U. of P. Perelman School of Medicine, “Uniaxial Testing.” <https://www.med.upenn.edu/pcmd/uniaxial-testing.html> (accessed Jun. 04, 2023).
- [50] E. Britannica, ““micrometer.”” <https://www.britannica.com/technology/micrometer> (accessed Sep. 21, 2023).
- [51] M. N. B. Cunha, “Optimisation of a MEW prototype for mesh implants fabrication,” 2020.
- [52] K. M. Knight, P. A. Moalli, and S. D. Abramowitch, “Preventing Mesh Pore Collapse by Designing Mesh Pores with Auxetic Geometries: A Comprehensive Evaluation Via Computational Modeling,” *J. Biomech. Eng.*, vol. 140, no. 5, pp. 1-8, 2018, doi: 10.1115/1.4039058.
- [53] K. Baylón, P. Rodríguez-Camarillo, A. Elías-Zúñiga, J. A. Díaz-Elizondo, R. Gilkerson, and K. Lozano, “Past, present and future of surgical meshes: A review,” *Membranes (Basel)*, vol. 7, no. 3, pp. 1-23, 2017, doi: 10.3390/membranes7030047.
- [54] H. Elsaghir, “R Econstructive S Urgery of the T Horacolumbar,” *Neurosurgery*, vol. 51, no. November, pp. 118-122, 2002.
- [55] Coloplast, ““Restorelle Flat Mesh.”” <https://products.coloplast.us/coloplast/implantable-devices/womens-health-wh/pelvic-floor-repair/restorelle/restorelle-flat-mesh/> (accessed Jul. 23, 2023).
- [56] “Physics - Young’s modulus - University of Birmingham.” <https://www.birmingham.ac.uk/teachers/study-resources/stem/Physics/youngs-modulus.aspx> (accessed Jun. 13, 2022).
- [57] S. Eshraghi and S. Das, “Mechanical and microstructural properties of polycaprolactone scaffolds with one-dimensional, two-dimensional, and three-dimensional orthogonally oriented porous architectures produced by selective laser sintering,” *Acta Biomater.*, vol. 6, no. 7, pp. 2467-2476, 2010, doi: 10.1016/j.actbio.2010.02.002.
- [58] Corbion, “Purasorb® DL - Product Specification Data Sheet,” no. September. pp. 1-2, 2019. [Online]. Available: <https://www.corbion.com/static/downloads/datasheets/20d/purasorb-dl.pdf>
- [59] G. N. Greaves, A. L. Greer, R. S. Lakes, and T. Rouxel, “Poisson’s ratio and modern

- materials,” *Nat. Mater.* 2011 1011, vol. 10, no. 11, pp. 823-837, Oct. 2011, doi: 10.1038/nmat3134.
- [60] H. Marsh and F. Rodríguez-Reinoso, “Activated Carbon (Origins),” *Act. Carbon*, pp. 13-86, 2006, doi: 10.1016/B978-008044463-5/50016-9.
- [61] E. Characterization and F. Element, “applied sciences Experimental Characterization and Finite Element Modeling of the Effects of 3D Bioplotting Process Parameters on Structural and Tensile Properties of Polycaprolactone (PCL) Scaffolds”.
- [62] U. Klinge, J. Otto, and T. Mühl, “High structural stability of textile implants prevents pore collapse and preserves effective porosity at strain,” *Biomed Res. Int.*, vol. 2015, 2015, doi: 10.1155/2015/953209.
- [63] S. Sterk, E. Silva, and A. A. Fernandes, “Development of New Surgical Mesh Geometries with Different Mechanical Properties Using the Design Freedom of 3D Printing,” *2023 IEEE 7th Port. Meet. Bioeng. ENBENG 2023*, pp. 144-147, 2023, doi: 10.1109/ENBENG58165.2023.10175368.
- [64] Z. Mardina, J. Venezuela, C. Maher, Z. Shi, M. S. Dargusch, and A. Atrens, “Design, mechanical and degradation requirements of biodegradable metal mesh for pelvic floor reconstruction,” *Biomater. Sci.*, vol. 10, no. 13, pp. 3371-3392, 2022, doi: 10.1039/d2bm00179a.
- [65] P. Martins, “Experimental and Numerical Studies of Soft Biological Tissues,” vol. I, no. 1577, pp. 333-339, 2010.
- [66] J. Ren *et al.*, “Development of 3D Printed Biodegradable Mesh with Antimicrobial Properties for Pelvic Organ Prolapse,” *Polymers (Basel)*, vol. 14, no. 4, 2022, doi: 10.3390/polym14040763.

Appendix

```

from abaqus import *
from abaqusConstants import *
import regionToolset
import __main__
import section
import regionToolset
import part
import material
import assembly
import step
import interaction
import load
import mesh
import job
import sketch
import visualization
import xyPlot
import connectorBehavior
import odbAccess
from operator import add
import numpy as np

s1 = mdb.models['Model-1'].ConstrainedSketch(name='Sketch-1',
      sheetSize=200.0)
g, v, d, c = s1.geometry, s1.vertices, s1.dimensions, s1.constraints
s1.setPrimaryObject(option=STANDALONE)

n_points=29403

Input_txt=np.loadtxt('FicheiroComCoordenadas.txt')

myLenght_list = []
myLenght_list = Input_txt[:,0]
print >> sys.__stdout__, str(myLenght_list)

myThickness_list = []
myThickness_list = Input_txt[:,1]
print >> sys.__stdout__, str(myThickness_list)

myPart = "Malha"

for i in range(n_points-1):
    s1.Line(point1=(myLenght_list[i], myThickness_list[i]), point2=(myLenght_list[i+1], myThickness_list[i+1]))

s1.unsetPrimaryObject() # Close the sketch

mdb.models['Model-1'].Part(dimensionality=TWO_D_PLANAR, name='Part-1', type=
    DEFORMABLE_BODY)
mdb.models['Model-1'].parts['Part-1'].BaseWire(sketch=
    mdb.models['Model-1'].sketches['Sketch-1'])

```

Development of 3D computational models of biodegradable meshes

Francisca Vaz
LAETA, INEGI, Faculdade de
Engenharia, Universidade do
Porto
Porto, Portugal
kika.vaz2000@gmail.com

Maria Elisabete Silva
LAETA, INEGI, Faculdade de
Engenharia, Universidade do
Porto
Porto, Portugal
mesilva@inegi.up.pt

António Augusto Fernandes
LAETA, INEGI, Faculdade de
Engenharia, Universidade do
Porto
Porto, Portugal
aaf@fe.up.pt

Marco Parente
LAETA, INEGI, Faculdade de
Engenharia, Universidade do
Porto
Porto, Portugal
mparente@fe.up.pt

Abstract— The number of pelvic organ prolapse (POP) cases has been increasing over the years, affecting the lives of countless people around the world. To try to solve this problem, synthetic meshes were introduced until the FDA banned the commercialization of some of these meshes, and therefore new approaches are urgently needed [1]. Thus, the possibility of developing biodegradable meshes arises to overcome the problems encountered so far with the use of synthetic meshes, mainly due to their biocompatibility and biomechanical properties. Besides its main functionality of guaranteeing organ support, it presents good characteristics regarding its flexibility and resistance, thus guaranteeing a better reinforcement of the intervened region, avoiding eventual tissue injuries. This abstract focuses on the development of computational models of biodegradable meshes that, in the future, can be used to treat the POP.

Keywords— Pelvic organ prolapse, biodegradable mesh, computational models.

I. INTRODUCTION

A. Pelvic Organ Prolapse

Pelvic organ prolapse (POP) is the descent of the pelvic organs such as the bladder, urethra, rectum, uterus, and vagina. The prolapse of these organs is caused by lesions in the muscles, ligaments, and connective tissue, being one of their main functions to support the tissues [2].

POP structures may cause a sensation of pressure in the pelvic area or, for women, the sensation that something is descending towards the vagina, and in some cases, a protuberance may appear in the area in question. In addition to these symptoms, this condition may be associated with urinary and fecal incontinence, incomplete defecation, and sexual dysfunction. Other symptoms include pain during sexual intercourse, irregular vaginal bleeding, and back pain. It is important to note that not all patients experience these symptoms, and they vary depending on the organ [2].

Usually, it is a combination of several factors that lead to organ prolapses, such as vaginal delivery, obesity, injury to any of the pelvic organs due to surgery, aging, and activities that significantly increase the pressure exerted on the abdomen/pelvic area, such as lifting heavy objects [2].

XXX-X-XXXX-XXXX-X/XX/\$XX.00 ©20XX IEEE

There are different types of POP, the prolapse of the rectum, called rectocele, of the small intestine, also known as enterocele, the prolapse of the bladder, named cystocele, prolapse of the urethra or urethrocele, vaginal dome prolapse, and uterine prolapse. (Fig.1) [2].

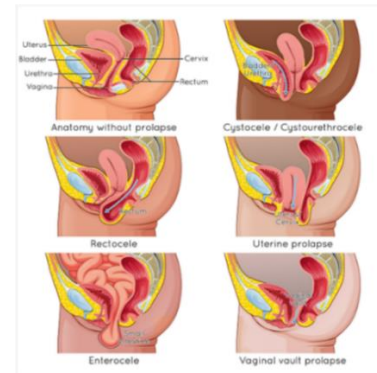


Fig. 1. Types of pelvic organ prolapse [3].

B. Impact of pelvic organ prolapse

Pelvic organ prolapse limits people's quality of life, and it is quite common in women, especially with advancing age, and this condition predominantly affects women between 40 and 60 years old [4].

Pelvic organ prolapse affects 41% of women over the age of 60, with one in four cases being symptomatic. It is estimated that 2.9% to 8% of the female population suffers from this condition, and there is a 12.6% lifetime risk that women will require surgery to correct prolapse [1].

In the United States, about one-third of women in their lifetimes will experience vaginal prolapse, and almost half of the women between 50 and 79 years of age will eventually experience pelvic organ prolapse, and the severity of prolapse varies from patient to patient. About 50% of women who have a vaginal delivery end up during their lives experiencing pelvic organ prolapse. This leads to the belief that, by 2050, around 50 million women in the US will have pelvic organ prolapse. [5] [6].

In Portugal, female pelvic organ prolapse affects the lives of about 7,000 women annually and has been increasing over the years, and in the UK, in 2019, in primary care, 8.4% of

women had vaginal lumps or nodules, and after examination, prolapse was seen in 50% of patients [7][8].

Thus, it is important to note that due to the aging population, the number of surgeries to treat prolapse is expected to increase.

Therefore, from the information and data presented, pelvic organ prolapse has a significant negative impact on the world population, and the number of cases will increase over the years. In addition, this condition influences people's daily lives, ultimately reducing their quality of life.

C. Treatment methods

There are some non-invasive treatments for this condition, such as physiotherapy exercises and muscle strengthening exercises in the pelvic area, biofeedback therapy, electrical stimulation therapy, the use of a pessary, and surgery. To make the least invasive treatment possible, doctors resort to surgery only as a last option, i.e. if the prolapse is severe.

Regarding physical therapy exercises, Kegel exercises are the most used in the initial phase, from the moment the prolapse is detected since they aim to tighten and relax the pelvic muscles to increase their strength [9].

Biofeedback therapy helps to localize and strengthen the muscles in the pelvic area. For this, a sensor is placed in the vagina or rectum, and a second sensor in the abdomen. As the patient contracts and relaxes the pelvic muscles, their electrical signals are recorded in a computer, to understand whether the muscles can contract [10].

Electrical stimulation therapy is often used in conjunction with biofeedback therapy. In this treatment, the pelvic area muscles contract through stimuli caused by electrical currents. However, the patient should do physiotherapy exercises at home to complement the treatment [10].

Another solution for the correction of POP is the use of a pessary. A pessary is a small silicone in various sizes and shapes. It is inserted into the vagina and holds the bladder, uterus, or rectum in the appropriate place. Pessaries are often recommended as a low-invasive, low-maintenance, and less expensive form of treatment than surgery. It can be used for months, however, needs to be removed at least once every 3 months, to be cleaned, as well as to assess the vagina for possible signs of erosion caused by the pessary.

Although this solution is useful at an early stage of the problem, many women do experience vaginal irritation due to the use of this device, as well as excessive vaginal discharge. In addition to these disadvantages, the size of the pessary can also be a problem, as it may be too small, and fall out. In other words, it is not always possible to find a pessary that fits every patient perfectly [11].

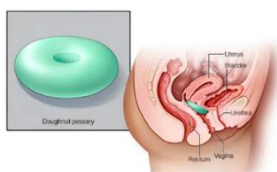


Fig. 2. An example of a pessary [12].

All these solutions, despite being practically non-invasive, are only useful at an early stage of the problem. However, if the prolapse is detected in a severe stage is necessary, to resort to surgery using native tissue or meshes.

Surgical intervention, although an invasive solution, is the only one that can correct the prolapse in more severe cases.

Surgical intervention using native tissue can also be used to POP repair. However, this alternative is not very feasible, because has high failure rates in the correction of prolapse. In a 2016 study conducted on 4023 women, it was concluded that after surgery, using native tissue, 38% of the women may experience prolapse again. In addition, 5% of women who have used native tissue will end up needing another surgery [13].

The synthetic meshes are used to repair the prolapse. However, in 2019, in the United States, the FDA (Food and Drug Administration) banned the sale and distribution of these meshes for the treatment of transvaginal prolapse due to the high risks associated with this product [14].

The use of these meshes can lead to infections, pain, scarring, incontinence, bowel problems, vaginal problems, excessive vaginal discharge, and muscle problems, among others. These problems normally require additional medical intervention and, could require another surgery [14].

Around 11% to 20% of patients who resort to a synthetic mesh, may suffer from prolapse again, and 7% to 18% of the patients who used the mesh will require a new intervention [13].

Thus, although the transvaginal mesh is no longer being used, the possibility of complications has not decreased over time, and women who still have these meshes need regular follow-ups, i.e., it is essential to monitor the mesh to ensure the safety and well-being of patients who still have them [15].

The high rate of complications may be due to low biocompatibility, inadequate biomechanical properties, and other factors, such as the person's age, general health, previous surgeries, the severity of the prolapse, as well as the surgeon's experience [1].

II. METHODS

This project is intended to simulate, using the Abaqus software, the biodegradable meshes, printed through PCL (polycaprolactone), and analyze their stress-strain response. In the process, it is important to ensure that they have the strength and elasticity to correct the POP without injuring the patient's tissues and muscles. Some mechanical characteristics are important, including filament diameter and pore size. Ideally, the thickness of the mesh diameter would vary between 80, 160, and 240 micrometers. The pores of the mesh would be approximately 2 mm in diameter to favor cell growth, thus correcting the prolapse.[1] Several meshes with different geometries and dimensions were developed to better understand which one best resembles the stress-strain values of the sheep vaginal tissue.

PCL is an FDA-approved material, that has been used in humans and is commonly applied in electrospinning processes

[16]. This material is an aliphatic semicrystalline polymer and has a melting temperature that varies between 59°C and 64°C. Thus, at normal body temperature, this material has enhanced mechanical properties, such as high strength and elasticity. PCL is a non-toxic material and has great tissue compatibility, being frequently used for resorbable sutures, drug delivery applications and as a support in regenerative therapies. Another advantage of this biodegradable polymer is the fact that it has a long degradation period, being one of the polymers with the lowest rate of erosion, which can vary between two and three years [17].

Firstly, it was developed a PCL medical grade mesh (Fig.3), with rectangular pores, 40 mm of length, 10 mm width, 0.16 mm diameter filaments, and using a beam element “B23”.

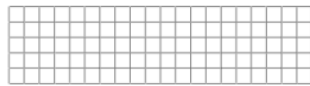


Fig. 3. Computational model of the biodegradable mesh.

After the development of several models, the ones that presented the best results were those with circular pores. There are four, and three of them had a filament around the mesh in certain parts to try to restrict the deformation of the mesh, and the other one did not have the filament.

These meshes were developed in the same way as the rectangular mesh mentioned previously. However, these meshes were built with three different pore sizes, 1.50 mm, 2.00 mm, and two of the four meshes, had pores of 2.50 mm (Fig.4).

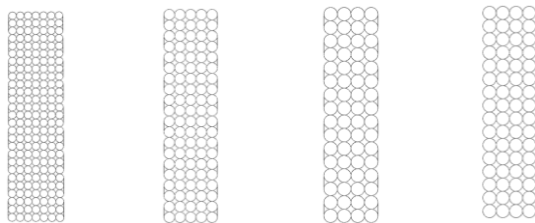


Fig. 4. Computational models of the meshes with 1.50 mm, 2.00 mm, and the last two with 2.50 mm pore diameter, respectively.

Another difference from the rectangular mesh is the filament thickness, for these meshes were used filaments with 80 and 240 micrometers. For the columns in the extremities of the mesh were used filaments with a diameter of 80 micrometers and in the remaining columns 240 micrometers (Fig.5).

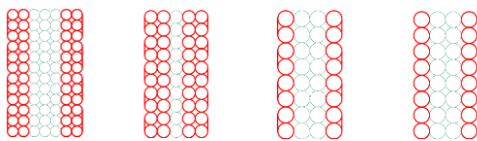


Fig. 5. Distribution of filament thickness in the meshes. The red columns represent the filaments with a diameter of 80 micrometers.

To simulate the uniaxial tensile test, it was defined the boundary conditions. At the lower end of the mesh, the nodes were considered fixed and at the top edge of the mesh, it was applied a displacement (Fig.6).

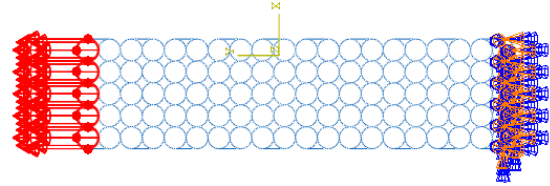


Fig. 6. Definition of the boundary conditions of the mesh with 2.00 mm of pore diameter.

III. RESULTS AND DISCUSSION

Initially, in order to confirm that the results obtained in the simulation performed in Abaqus are similar to the experimental results, the values of strain and stress obtained in both cases were compared.

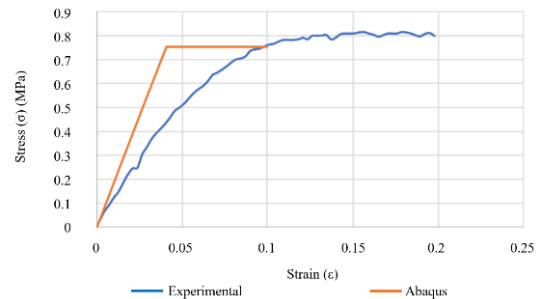


Fig. 7. Stress and strain values obtained from the developed model and the experimental mesh.

As can be seen in the obtained graphic of the magnitude of the values is the same and the lines exhibit a similar behavior, also, as expected, the behavior of the developed model tends to be stiffer than the experimental model. These values are the result of simulations and tests performed with a rectangular pore mesh (Fig.3). It is important to mention that, depending on the geometry and characteristics of the mesh, the results may vary. The computational model was built and simulated based on the experimental results. An experimental mesh was printed by melt electrowriting spinning, using PCL medical grade. The results show an approximation between the experimental and computational tests. The maximum stress value obtained was approximately 0.80 MPa for the experimental mesh and 0.75 MPa for the computational model.

For the circular pore meshes shown previously, a graphic of the stress-strain curves was presented to compare with the behavior of the vaginal tissue (Fig.8).

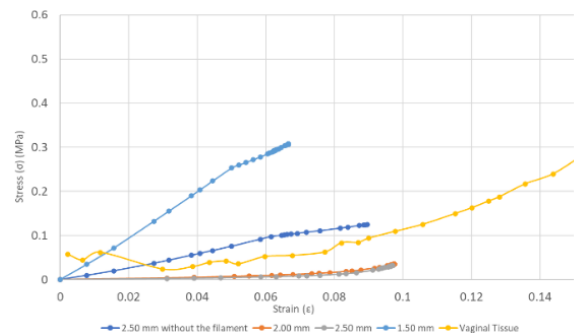


Fig. 8. Stress-strain curve of models developed with circular pores.

These meshes tend to have similar behavior to the vaginal tissue stress-strain curve, except for the mesh with a pore diameter of 1.50 mm that in general, shows higher stress values for the same strain values as the vaginal tissue. The meshes with 2.00 mm and 2.50 mm pore size are quite similar and show lower stress values than the vaginal tissue. Finally, it can be seen from the graphic (Fig. 8) that the stress and strain values of the 2.50 mm pore size without a filament around certain areas of the mesh are the closest to the stress and strain values of the vaginal tissue.

In addition to these results, it is critical to pay attention to the deformation that the meshes exhibit in the simulations performed (Fig. 9).

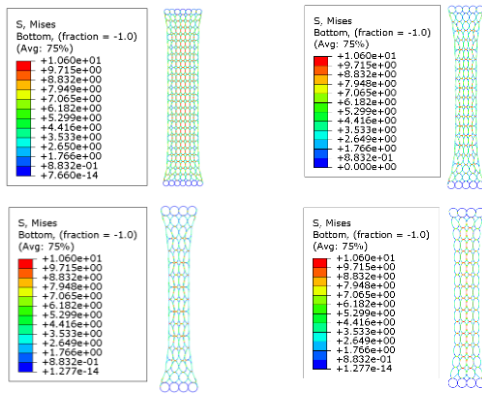


Fig. 9. The deformation of each mesh.

Although the last mesh shows good results, its geometry and shape deform, losing its original shape. So, as important as it is, to pay attention to the values of stress and strain, it is also relevant to have into consideration the deformation of each mesh after suffering a certain level of stress, which can result in an unusable mesh due to its degree of deformation.

IV. CONCLUSION

In this context, the opportunity arises to develop new meshes made of a biodegradable material that has excellent characteristics, such as flexibility, malleability, biocompatibility, and the possibility of promoting cell growth. The simulations performed show promising results, as well as similarity to the values of stress-strain of the vaginal tissue. However, it is necessary to improve these computational models to better the results and ultimately achieve the best meshes possible and thus, repair the prolapse. For this, new models are being developed to reach a similar behavior of the vaginal tissue. Therefore, it is recommended to deepen the level of assertiveness in the choice of meshes, namely the type of geometry and dimensions.

ACKNOWLEDGMENT

The authors thank the Emprego Científico 2021.00077.CEECIND, Funded by FCT. This work was supported by FCT, through INEGI, in the scope of LAETA, project UIDB/50022/2020 and UIDP/50022/2020.

REFERENCE

[1] M. N. B. da Cunha, R. Rynkevici, M. E. T. da Silva, A. F. Moreira da Silva Brandão, J. L. Alves, and A. A. Fernandes, "Melt Electrospinning

Writing of Mesh Implants for Pelvic Organ Prolapse Repair," 3D Print. Addit. Manuf., vol. 00, no. 00, pp. 1–10, 2021, doi: 10.1089/3dp.2021.0010.

[2] D. Vilas and B. Rodrigues, "Structure Design Optimisation Of Biodegradable Implants For Melt Electrospinning," 2022.

[3] M. Thesis, M. Engineering, H. Borges, and C. Esp, "Master Thesis in Mechanical Engineering Development of 3D computational models of biodegradable meshes," 2022.

[4] "Diagnosing Pelvic Organ Prolapse | NYU Langone Health." <https://nyulangone.org/conditions/pelvic-organ-prolapse-in-adults/diagnosis> (accessed Jun. 15, 2022).

[5] D. Glass, "Demystifying pelvic organ prolapse - UChicago Medicine," Jan. 30, 2019. <https://www.uchicagomedicine.org/forefront/womens-health/articles/demystifying-pelvic-organ-prolapses> (accessed Jun. 15, 2022).

[6] N. Ng-Stollmann, C. Fünfgeld, B. Gabriel, and A. Niesel, "The international discussion and the new regulations concerning transvaginal mesh implants in pelvic organ prolapse surgery," Int. Urogynecol. J., vol. 31, no. 10, pp. 1997–2002, 2020, doi: 10.1007/s00192-020-04407-0.

[7] "Biomecânica: Combinar engenharia e experiência clínica para melhorar o tratamento do prolapso de órg - INEGI." <https://www.inegi.pt/pt/noticias/biomecânica-combinar-engenharia-e-experiência-clínica-para-melhorar-o-tratamento-do-prolapso-de-orgaos-pelvicos-femininos/> (accessed Nov. 20, 2022).

[8] "Urinary incontinence and pelvic organ prolapse in women: management NICE guideline Your responsibility," 2019, Accessed: Nov. 20, 2022. [Online]. Available: www.nice.org.uk/guidance/ng123

[9] F. Khorasani et al., "Physiotherapy and pelvic floor muscle exercises for the prevention and treatment of pregnancy-related pelvic floor dysfunctions: A systematic review and meta-analysis," Int. J. Women's Heal. Reprod. Sci., vol. 8, no. 2, pp. 125–132, 2020, doi: 10.15296/ijwhr.2020.20.

[10] J. Xu and F. Huang, "A study of efficacy of traditional Chinese medicine combined with biofeedback electrical stimulation on postpartum pelvic organ prolapse," Int. J. Clin. Exp. Med., vol. 13, no. 12, pp. 10031–10038, 2020, [Online]. Available: <https://www.embase.com/search/results?subaction=viewrecord&id=L2005768579&from=export>

[11] "What is a Pessary: Pessary Device 101 | Penn Medicine." <https://www.pennmedicine.org/updates/blogs/womens-health/2016/may/what-is-a-pessary> (accessed Nov. 18, 2022).

[12] "Uterine prolapse - Diagnosis and treatment - Mayo Clinic." <https://www.mayoclinic.org/diseases-conditions/uterine-prolapse/diagnosis-treatment/drc-20353464> (accessed Jun. 13, 2022).

[13] C. Maher, B. Feiner, K. Baessler, C. Christmann-Schmid, N. Haya, and J. Marjoribanks, "Transvaginal mesh or grafts compared with native tissue repair for vaginal prolapse," Cochrane Database Syst. Rev., vol. 2016, no. 2, Feb. 2016, doi: 10.1002/14651858.CD012079.

[14] "Pelvic Organ Prolapse (POP): Surgical Mesh Considerations and Recommendations | FDA." <https://www.fda.gov/medical-devices/urogynecologic-surgical-mesh-implants/pelvic-organ-prolapse-pop-surgical-mesh-considerations-and-recommendations> (accessed Jun. 13, 2022).

[15] B. Chughtai, J. Mao, T. S. Asfaw, C. Heneghan, C. R. Rardin, and A. Sedrakyan, "Long-term Device Outcomes of Mesh Implants in Pelvic Organ Prolapse Repairs," Obstet. Gynecol., vol. 135, no. 3, pp. 591–598, 2020, doi: 10.1097/AOG.0000000000003689.

[16] R. Rynkevici, M. E. T. Silva, P. Martins, T. Mascarenhas, J. L. Alves, and A. A. Fernandes, "Characterisation of Polycaprolactone Scaffolds Made by Melt Electrospinning Writing for Pelvic Organ Prolapse Correction- a Pilot Study," SSRN Electron. J., 2022, doi: 10.2139/ssrn.4036396.

[17] R. Dwivedi et al., "Polycaprolactone as biomaterial for bone scaffolds: Review of literature," J. Oral Biol. Craniofacial Res., vol. 10, no. 1, pp. 381–388, 2020, doi: 10.1016/j.jobcr.2019.10.003.

Development of 3D computational models of biodegradable meshes

Francisca Vaz¹[0009-0004-9793-4076], Maria Elisabete Silva²[0000-0003-2889-4969], Marco Parente³[0000-0002-3326-6345] and António Augusto Fernandes⁴[0000-0002-7146-9944]

¹ LAETA, INEGI, Faculty of Engineering, University of Porto, Porto, Portugal;

² LAETA, INEGI, Porto, Portugal; mesilva@inegi.up.pt

³ LAETA, INEGI, Faculty of Engineering, University of Porto, Porto, Portugal; mparente@fe.up.pt

⁴ LAETA, INEGI, Faculty of Engineering, University of Porto, Porto, Portugal; aaf@fe.up.pt
kika.vaz2000@gmail.com

Abstract. Over time, there has been a noticeable increase in the incidence of pelvic organ prolapse (POP), impacting individuals worldwide in significant ways. Efforts were made to mitigate this concern by creating synthetic meshes. However, certain types of these meshes faced FDA restrictions, prompting the need for innovative approaches. Consequently, the idea of crafting biodegradable meshes has arisen as a potential remedy to tackle the issues associated with the utilization of synthetic meshes. This primarily pertains to their compatibility with the body and their mechanical characteristics. Beyond their fundamental role of providing support to organs, these biodegradable meshes also possess favorable attributes in terms of flexibility and resilience. These qualities contribute to a more effective reinforcement of the treated area, thereby reducing the risk of potential harm to tissues. The central focus of this abstract lies in the development of computational models for these biodegradable meshes, which hold promise for future applications in the treatment of pelvic organ prolapse.

Keywords: Computational models, biodegradable mesh, pelvic organ prolapse.

1 Introduction

This chapter is intended to explore in more detail the pelvic organ prolapse, as well as the symptoms that appear and the impact it has on people's quality of life.

1.1 Pelvic Organ Prolapse

POP is the downward displacement of pelvic structures, such as the vagina, bladder, rectum, urethra, and uterus. This occurs due to weaknesses in muscles, ligaments, and connective tissue, which normally offer support to these organs [1].

In cases of POP, individuals might experience sensations of pressure in the pelvic region, especially women who might perceive a sensation of something descending towards the vaginal area. In certain instances, a bulge could become evident in the affected region. This condition can also lead to issues like fecal and urinary incontinence, sexual dysfunction, and difficulty with complete defecation. Additional symptoms

encompass unusual vaginal bleeding, and discomfort during sexual intercourse. Importantly, it is crucial to emphasize that these symptoms are not identical across all individuals and can differ based on the specific organ affected [1].

The onset of organ prolapses typically results from a combination of factors, including vaginal childbirth, obesity, surgical trauma to pelvic organs, the natural aging process, and activities that exert significant pressure on the abdominal or pelvic regions, such as lifting heavy objects [1].

Various types of POP exist, including rectocele, enterocele, cystocele, vaginal dome prolapse, urethrocele, and uterine prolapse (depicted in Figure 1) [1].

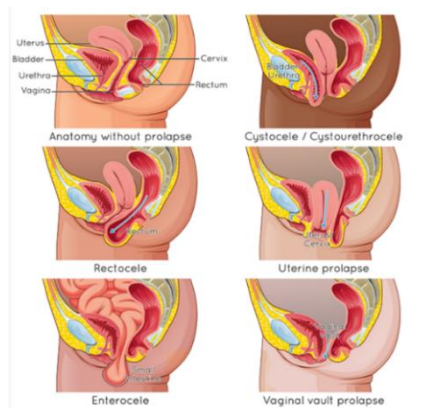


Fig. 1. Varieties of POP [2].

1.2 Impact of pelvic organ prolapse

POP has a considerable impact on individuals' quality of life and is notably prevalent among women, particularly as they age. This condition predominantly impacts women within the age range of 40 and 60 [3].

Among women aged 60 and above, around 41% experience pelvic organ prolapse, with one in every four cases resulting in symptomatic issues. The likelihood of women requiring corrective surgery for prolapse is estimated at a lifetime risk of 12.6% [4].

In the United States, approximately a third of women will encounter vaginal prolapse during their lifetimes. Moreover, nearly half of women between the ages of 50 and 79 are expected to face pelvic organ prolapse at some point. The severity of prolapse varies between individuals, and about 50% of women who have undergone vaginal deliveries will experience pelvic organ prolapse at some stage. These statistics suggest that by the year 2050, approximately 50 million women in the US could be affected by pelvic organ prolapse [5][6].

In Portugal, around 7,000 women annually are affected by female pelvic organ prolapse, a number that has been increasing over time. Similarly, in the UK, statistics from 2019 indicate that 8.4% of women reported experiencing vaginal nodules or lumps, with prolapse observed in half of patients upon examination [7][8].

Consequently, it is important to underscore that the number of procedures aimed at addressing prolapse is anticipated to rise in correlation with the aging population.

Given the provided facts and data, it is evident that POP has a substantial adverse effect on the global population, and the prevalence of cases is expected to rise over time. This dysfunction significantly influences the daily lives of affected women, ultimately diminishing their overall quality of life.

1.3 Treatment methods

Non-invasive approaches encompass physiotherapy exercises and exercises that strengthen pelvic muscles, biofeedback therapy, electrical stimulation therapy, the utilization of a pessary, and surgical intervention as a last resort for severe cases. Surgeons opt for surgery only when the prolapse reaches a severe stage.

At the outset of management, Kegel exercises are the most widely employed physical therapy exercises. They are initiated upon detecting the prolapse and involve contracting and relaxing pelvic muscles to enhance their strength [9].

Biofeedback therapy aids in pinpointing and reinforcing pelvic muscles. This technique involves placing a sensor in the rectum or vagina, along with another sensor on the abdomen. The computer records the electrical signals produced when the patient contracts and relaxes their pelvic muscles, determining their contractile capability [10].

Complementary to biofeedback therapy, electrical stimulation therapy is commonly employed. In this approach, electrical currents prompt contractions of the pelvic muscles. It is recommended for patients to engage in at-home physiotherapy exercises to complement this treatment [10].

An alternative for correcting POP is the usage of a pessary. A pessary, a silicone device of different shapes and sizes, is introduced into the vagina to support the uterus, rectum, or bladder. Pessaries are often advocated as a less invasive, cost-effective option compared to surgery. They can be worn for several months, but removal every three months is essential for cleaning and to assess potential pessary-related erosion.

While effective in early-stage cases, some women report vaginal irritation and excessive vaginal discharge due to pessary use. Moreover, size-related issues may arise, leading to potential dislodgement. In essence, finding a pessary that completely matches the requirements of every patient is not always achievable. [11].

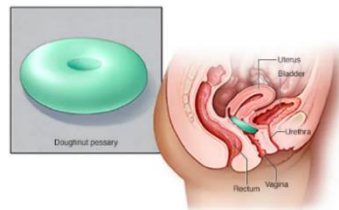


Fig. 2. An illustration of a pessary [12].

Although these solutions are minimally invasive, they primarily offer effective results in the early stages of the issue. However, if the prolapse is identified at an advanced stage, surgical intervention involving native tissue or meshes becomes necessary.

In cases of severe prolapse, surgery remains the sole option for rectification, despite its invasive nature. Surgical correction using native tissue is also a potential approach for POP repair. Nevertheless, this method is not particularly practical due to its notable failure rates in prolapse correction. A study conducted in 2016, involving 4023 women, indicated that 38% of them might experience recurrent prolapse following surgery with native tissue. Moreover, 5% of women who underwent native tissue surgery required further surgical intervention [13].

Synthetic meshes are employed for prolapse repair; however, these products carry considerable risks. In 2019, the FDA in the United States prohibited the sale and distribution of these meshes for transvaginal prolapse treatment due to significant dangers [14]. Potential side effects associated with mesh use include infections, discomfort, scarring, incontinence, gastrointestinal issues, vaginal problems, excessive vaginal discharge, and muscular complications. Addressing these issues often necessitates additional medical attention and might lead to the need for further surgery [14].

Approximately 11% to 20% of patients utilizing synthetic mesh may experience recurrent prolapse, with 7% to 18% requiring subsequent intervention [13].

Therefore, even though transvaginal mesh is not used anymore, the risk of complications has not reduced over time. Women with existing meshes still require regular follow-ups to ensure their safety and well-being [15].

Aspects such as limited biocompatibility, insufficient biomechanical characteristics, and individual factors including age, overall health, previous surgeries, prolapse severity, and surgeon's skill collectively contribute to a heightened probability of complications [4].

2 Methods

The primary objective of this project is to create simulations and analyze the stress-strain behavior of biodegradable meshes fabricated using PCL (polycaprolactone) through the utilization of Abaqus[®] Software (developed by Mathematical Computing Software, Natick, Massachusetts, USA). The paramount concern is that these meshes possess the necessary strength and elasticity to effectively address POP (pelvic organ prolapse) while ensuring no harm to the patient's muscles and tissues. Key mechanical properties, such as filament diameter and pore size, play a crucial role. The optimal thickness of the mesh diameter should fall within the range of 80, 160, and 240 micrometers. Meanwhile, the mesh's pores should have a diameter of about 2 mm to facilitate cell growth and thereby rectify the prolapse [4]. A comprehensive exploration of meshes with diverse dimensions and geometries was conducted to ascertain which mesh configuration best replicates the stress and strain characteristics of sheep vaginal tissue.

PCL, an FDA-approved substance, has a history of human use and is frequently employed in electrospinning procedures [16]. This aliphatic semicrystalline polymer possesses a melting temperature ranging from 59°C to 64°C. Consequently, the material displays favorable mechanical properties like high strength and flexibility at room temperature. PCL stands out as a non-toxic polymer with notable tissue compatibility. It

finds common application in absorbable sutures, as a scaffold in regenerative therapies, and drug delivery methods. An added advantage of this biodegradable polymer is its extended degradation period, making it one of the polymers with the slowest erosion rate, typically spanning between two to three years [17].

To commence, a PCL mesh of medical grade (as depicted in Fig. 3) was fashioned, characterized by rectangular pores, a length of 40 mm, width of 10 mm, filament diameter of 0.16 mm, and implemented with a "B23" beam element.

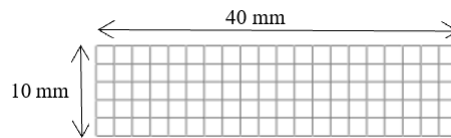


Fig. 3. Computational representation of the biodegradable mesh.

The diagram in Figure 4 depicts the mean of the experimental data acquired from tests conducted on a medical-grade PCL filament. To replicate the material's performance in Abaqus®, it is essential to ascertain its Young's modulus and yield stress. The parameters employed in the simulations were 229.98 MPa for Young's modulus and 10.59 MPa for yield stress, which signifies the transition from elastic to plastic behavior in the material.

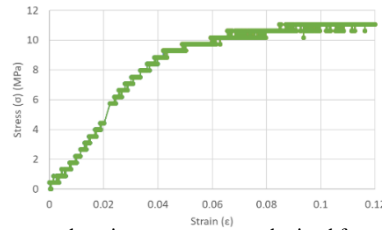


Fig. 4. Stress and strain measurements obtained from filament tests.

Numerous mesh configurations were designed with the aim of producing a mesh that exhibits stress-strain characteristics akin to those of vaginal tissue.

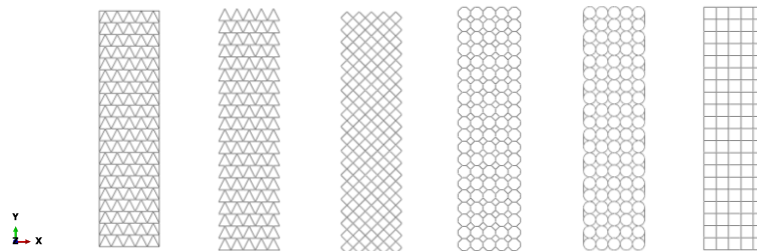


Fig. 5. Some examples of the different developed meshes.

Following the creation of numerous models, significant results were achieved with meshes featuring circular pores. Among these, there were four configurations, with three of them incorporating filament wrapping around specific areas of the mesh to mitigate deformation, while the fourth did not adopt this approach.

The development process for these meshes was analogous to that of the previously mentioned rectangular mesh. Similar to the rectangle mesh, these configurations

encompassed three varying pore diameters: 1.50 mm, 2.00 mm, and two of the four meshes featured pores measuring 2.50 mm (as illustrated in Figure 6).

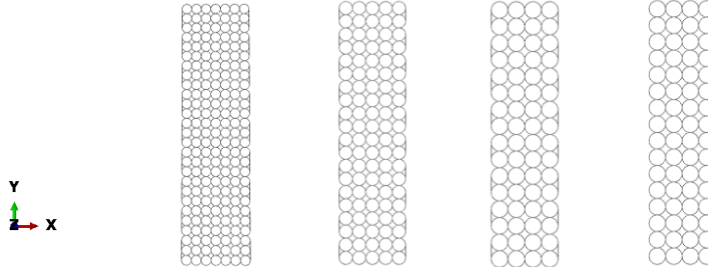


Fig. 6. Computational representations of meshes featuring pore diameters of 1.50 mm, 2.00 mm, and the remaining two with a pore diameter of 2.50 mm, respectively.

Another differentiation between these meshes and the rectangular meshes lies in the filament thickness. In the case of these meshes, filaments of 80 and 240 micrometers were employed. Filaments measuring 80 micrometers in diameter were affixed to the mesh's edges, whereas filaments with a diameter of 240 micrometers were employed for the remaining sections (as represented in Figure 7).

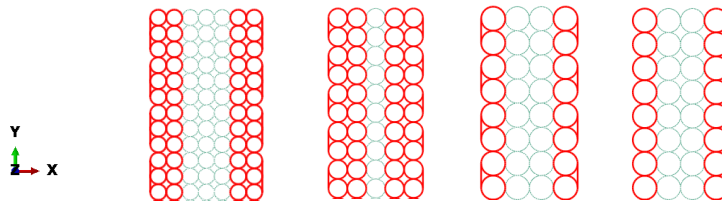


Fig. 7. Arrangement of filament thickness within the meshes. The red columns symbolize the filaments measuring 80 micrometers in diameter.

In order to replicate the uniaxial tensile test, boundary conditions were established. Nodes at the lower end of the mesh were designated as fixed, while at the upper edge of the mesh, a displacement was imposed (as illustrated in Figure 8).

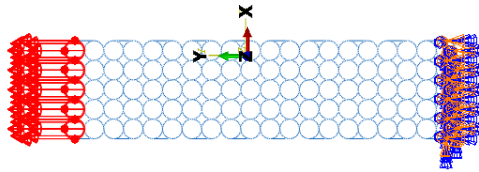


Fig. 8. Establishment of the boundary conditions for the mesh with a pore diameter of 2.00 mm.

3 Results and Discussion

At the outset, a comparison was conducted between the strain and stress values obtained from both the Abaqus[®] simulation and the corresponding experimental results. This verification aimed to establish the similarity between the outcomes derived from these two approaches.

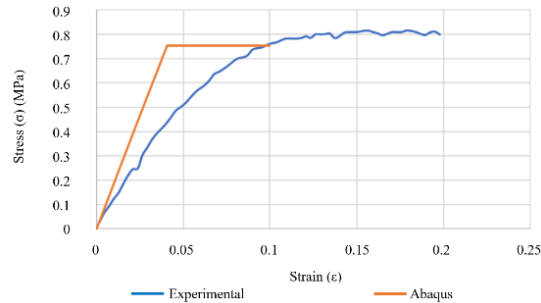


Fig. 9. Stress-strain values obtained from the computational model and the experimental mesh [18].

As evident from the depicted graphic (Fig. 9), the magnitudes of the values align, and the lines manifest a comparable pattern. Additionally, as anticipated, the developed model demonstrates greater stiffness in comparison to the behavior observed in the experimental model. These observations stem from models and trials conducted using a mesh featuring rectangular pores (Fig. 3). It is noteworthy that the outcomes could fluctuate based on the specific geometry and attributes of the mesh under consideration. The computational model was constructed and simulated using insights from the experimental findings. An experimental mesh was generated through melt electrospinning with the utilization of PCL medical grade. The outcomes underscore a notable correspondence between the experimental and computational assessments. For the experimental mesh, the highest stress value was recorded around 0.80 MPa, while the computational model yielded approximately 0.75 MPa.

The graphic of the Figure 10 shows the stress-strain values obtained for the different mesh models, comparing them with the values of stress and strain of the vaginal tissue.

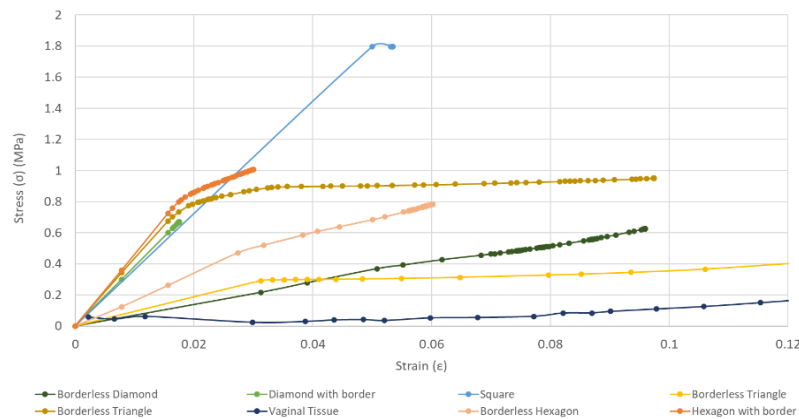


Fig. 10. Stress-strain curve of the computational models with different geometries of pores.

As shown in the graphic, it is possible to conclude that meshes with a filament around them present higher stress values, in comparison with the meshes without the filament around them, meaning that the presence of a filament around the mesh influences the obtained stress values.

As previously mentioned, the models with the best results were the circular pore meshes. The comparison between these meshes and the behavior of the vaginal tissue is represented through the values of stress and strain in the next graphic (Fig.11).

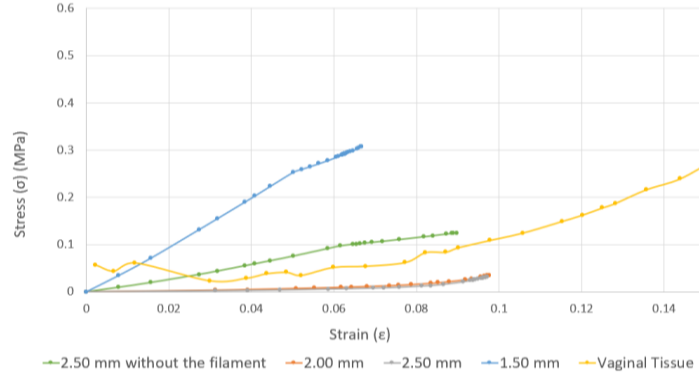


Fig. 11. Stress-strain curve of the computational models created with circular pores.

With the exception of the mesh featuring a pore width of 1.50 mm, which displays elevated stress values for equivalent strain values compared to the tissue, these meshes generally exhibit behavior that is analogous to the stress-strain curve of vaginal tissue. Meshes with pore dimensions of 2.00 mm and 2.50 mm display considerable similarity and present stress values lower than those of vaginal tissue. Ultimately, the graphical representation (Fig. 11) illustrates that the stress-strain values of the 2.50 mm pore size, devoid of filament wrapping around specific mesh portions, align most closely with the stress-strain values exhibited by the tissue.

Furthermore, it is essential to highlight the deformation patterns observed in the simulations for these meshes (Fig. 12).

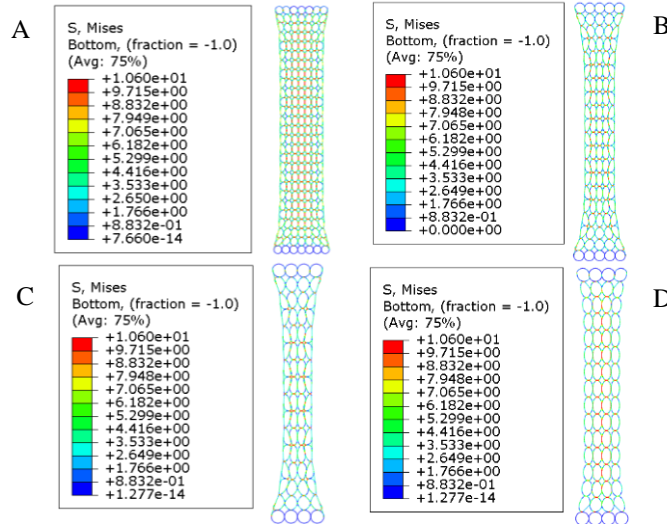


Fig. 12. The deformation of each mesh. A) Mesh with 1.50 mm pore diameter. B) Mesh featuring a pore diameter of 2.00 mm. C) Mesh possessing a pore diameter of 2.50 mm. D) Mesh with a pore diameter of 2.50 mm, lacking filament wrapping around specific sections of the mesh.

While the last mesh yields favorable outcomes, its geometry and form undergo deformation, leading to a departure from its initial shape. As crucial as it is to closely monitor stress and strain values, equal significance should be accorded to evaluating the deformation experienced by each mesh under particular stress levels. Such deformation has the potential to render a mesh unusable, owing to the extent of distortion it undergoes.

4 Conclusion

In this scenario, there exists an opportunity to produce unique meshes using a biodegradable material possessing advantageous traits such as flexibility, adaptability, biocompatibility, and the capacity to facilitate cell growth. The generated models have yielded promising outcomes and demonstrated resemblances to stress-strain characteristics of vaginal tissue. Nevertheless, there remains room for enhancing these computational models to achieve even more favorable results and ultimately optimize the quality of meshes for effective prolapse repair. In pursuit of this, fresh models are being developed with the objective of mimicking the behavior of vaginal tissue. Consequently, it is advisable to enhance the precision when choosing meshes, particularly regarding their dimensions and geometry.

Acknowledgment

The authors express their gratitude to the Emprego Científico 2021.00077.CEECIND, funded by FCT. This research received support from FCT, through INEGI, as part of the LAETA project under the grants UIDB/50022/2020 and UIDP/50022/2020.

References

- [1] D. Vilas and B. Rodrigues, "Structure Design Optimisation Of Biodegradable Implants For Melt Electrowriting," 2022.
- [2] M. Thesis, M. Engineering, H. Borges, and C. Esp, "Master Thesis in Mechanical Engineering Development of 3D computational models of biodegradable meshes," 2022.
- [3] "Diagnosing Pelvic Organ Prolapse | NYU Langone Health." <https://nyulangone.org/conditions/pelvic-organ-prolapse-in-adults/diagnosis> (accessed Jun. 15, 2022).
- [4] M. N. B. da Cunha, R. Rynkevic, M. E. T. da Silva, A. F. Moreira da Silva Brandão, J. L. Alves, and A. A. Fernandes, "Melt Electrospinning Writing of Mesh Implants for Pelvic Organ Prolapse Repair," *3D Print. Addit. Manuf.*, vol. 00, no. 00, pp. 1–10, 2021, doi: 10.1089/3dp.2021.0010.
- [5] D. Glass, "Demystifying pelvic organ prolapse - UChicago Medicine," Jan. 30, 2019. <https://www.uchicagomedicine.org/forefront/womens-health-articles/demystifying-pelvic-organ-prolapses> (accessed Jun. 15, 2022).
- [6] N. Ng-Stollmann, C. Fünfgeld, B. Gabriel, and A. Niesel, "The international discussion and the new regulations concerning transvaginal mesh implants in pelvic organ prolapse surgery," *Int. Urogynecol. J.*, vol. 31, no. 10, pp. 1997–2002, 2020, doi: 10.1007/s00192-020-04407-0.
- [7] "Biomecânica: Combinar engenharia e experiência clínica para melhorar o tratamento do prolapso de órg - INEGI." <https://www.inegi.pt/pt/noticias/biomecanica-combinar-engenharia-e-experiencia-clinica-para-melhorar-o-tratamento-do-prolapso-de-orgaos-pelvicos-femininos/> (accessed Nov. 20, 2022).

- [8] “Urinary incontinence and pelvic organ prolapse in women: management NICE guideline Your responsibility,” 2019, Accessed: Nov. 20, 2022. [Online]. Available: www.nice.org.uk/guidance/ng123
- [9] F. Khorasani et al., “Physiotherapy and pelvic floor muscle exercises for the prevention and treatment of pregnancy-related pelvic floor dysfunctions: A systematic review and meta-analysis,” *Int. J. Women’s Heal. Reprod. Sci.*, vol. 8, no. 2, pp. 125–132, 2020, doi: 10.15296/ijwhr.2020.20.
- [10] J. Xu and F. Huang, “A study of efficacy of traditional Chinese medicine combined with biofeedback electrical stimulation on postpartum pelvic organ prolapse,” *Int. J. Clin. Exp. Med.*, vol. 13, no. 12, pp. 10031–10038, 2020, [Online]. Available: <https://www.embase.com/search/results?subaction=viewrecord&id=L2005768579&from=export>
- [11] “What is a Pessary: Pessary Device 101 | Penn Medicine.” <https://www.pennmedicine.org/updates/blogs/womens-health/2016/may/what-is-a-pessary> (accessed Nov. 18, 2022).
- [12] “Uterine prolapse - Diagnosis and treatment - Mayo Clinic.” <https://www.mayoclinic.org/diseases-conditions/uterine-prolapse/diagnosis-treatment/drc-20353464> (accessed Jun. 13, 2022).
- [13] C. Maher, B. Feiner, K. Baessler, C. Christmann-Schmid, N. Haya, and J. Marjoribanks, “Transvaginal mesh or grafts compared with native tissue repair for vaginal prolapse,” *Cochrane Database Syst. Rev.*, vol. 2016, no. 2, Feb. 2016, doi: 10.1002/14651858.CD012079.
- [14] “Pelvic Organ Prolapse (POP): Surgical Mesh Considerations and Recommendations | FDA.” <https://www.fda.gov/medical-devices/urogynecologic-surgical-mesh-implants/pelvic-organ-prolapse-pop-surgical-mesh-considerations-and-recommendations> (accessed Jun. 13, 2022).
- [15] B. Chughtai, J. Mao, T. S. Asfaw, C. Heneghan, C. R. Rardin, and A. Sedrakyan, “Long-term Device Outcomes of Mesh Implants in Pelvic Organ Prolapse Repairs,” *Obstet. Gynecol.*, vol. 135, no. 3, pp. 591–598, 2020, doi: 10.1097/AOG.0000000000003689.
- [16] R. Rynkevic, M. E. T. Silva, P. Martins, T. Mascarenhas, J. L. Alves, and A. A. Fernandes, “Characterisation of Polycaprolactone Scaffolds Made by Melt Electrospinning Writing for Pelvic Organ Prolapse Correction- a Pilot Study,” *SSRN Electron. J.*, 2022, doi: 10.2139/ssrn.4036396.
- [17] R. Dwivedi et al., “Polycaprolactone as biomaterial for bone scaffolds: Review of literature,” *J. Oral Biol. Craniofacial Res.*, vol. 10, no. 1, pp. 381–388, 2020, doi: 10.1016/j.jobcr.2019.10.003.
- [18] M. Isabel and A. Pinto, “Melt electrowriting prototype optimization for medical-grade polycaprolactone mesh printing,” no. september, 2022.

3D Printing and Development of Computational Models of Biodegradable Meshes

Francisca Vaz ¹, Marco Parente ², Maria Elisabete Silva ³, and António Augusto Fernandes ⁴

¹ LAETA, INEGI, Faculty of Engineering, University of Porto, Porto, Portugal; kika.vaz2000@gmail.pt

² LAETA, INEGI, Faculty of Engineering, University of Porto, Porto, Portugal; mparente@fe.up.pt

³ LAETA, INEGI, Porto, Portugal; mesilva@inegi.up.pt

⁴ LAETA, INEGI, Faculty of Engineering, University of Porto, Porto, Portugal; aaf@fe.up.pt

Abstract

The pelvic region in the human body contains various organs that can experience prolapse due to factors like natural childbirth or heavy lifting, leading to discomfort and pain. This widespread issue significantly impacts people's daily lives, negatively affecting their overall well-being. While there are existing solutions for correcting prolapse, they come with several limitations and drawbacks that necessitate more effective alternatives to enhance treatment outcomes.

One potential solution is the development of specialized meshes designed to address pelvic organ prolapse. Initially, synthetic polypropylene meshes were introduced, showing success in treating abdominal hernias. However, the FDA's ban on certain mesh products prompted the search for new approaches. Biodegradable meshes have emerged as a promising alternative to tackle the issues associated with synthetic meshes.

Biodegradable meshes can be surgically implanted in the patient's body, providing support to the organs while offering advantages such as flexibility and resistance. These qualities contribute to better reinforcement of the treated area, reducing the risk of tissue injuries. Furthermore, biodegradable meshes exhibit biocompatibility and biomechanical properties, making them a potential solution to overcome the drawbacks of synthetic meshes.

A series of tests were conducted to explore this potential, yielding promising results. These tests involved variations in mesh geometry, thickness, and pore diameter, indicating the feasibility of biodegradable meshes as a more effective approach for treating pelvic organ prolapse.

Key words: Pelvic Organ Prolapse; Biodegradable Mesh; Computational Model

1. Introduction

Pelvic organ prolapse (POP) refers to the downward displacement of pelvic organs, including the bladder, urethra, rectum, uterus, and vagina. This condition results from damage to the muscles, ligaments, and connective tissue responsible for supporting these organs [1][2].

Individuals experiencing POP may notice symptoms like pelvic pressure, a sensation of organs descending towards the vagina, and sometimes the appearance of a bulge in the affected area. Additionally, POP can lead to issues such as urinary and fecal incontinence, incomplete bowel movements, and sexual dysfunction. Other symptoms may include pain during sexual intercourse, irregular vaginal bleeding, and back pain. Not all patients will experience these symptoms, and their severity varies depending on the affected organ [1][2].

Pelvic organ prolapse typically results from a combination of factors, including vaginal childbirth, obesity, surgical trauma to pelvic organs, aging, and activities that exert significant pressure on the abdominal and pelvic regions, such as heavy lifting [1][2]. These factors can predispose some women to disruptions, stretching, or dysfunction of the *levator ani* complex, connective tissue attachments of the vagina, or both, ultimately leading to prolapse.

Various types of POP exist, including rectocele (rectal prolapse), enterocele (small intestine prolapse), cystocele (bladder prolapse), urethrocele (urethral prolapse), vaginal dome prolapse, and uterine prolapse [1][2].

If a patient presents symptoms suggestive of prolapse, they should undergo a comprehensive pelvic examination, accompanied by a thorough review of their medical history. This routine examination allows the physician to assess the condition of various pelvic organs, including the uterus, vagina, fallopian tubes, ovaries, bladder, and rectum.

In situations where the symptoms suggest the involvement of multiple organs in prolapse, the physician may recommend additional diagnostic procedures such as ultrasound or MRI scans. These imaging techniques provide visual insights into the pelvic area, aiding in the determination of the prolapse's severity based on the captured images [3][4].

One system used to classify the severity of the prolapse is the "Baden-Walker Halfway Scoring System". The prolapse can be classified in 4 grades; grade 0 - no prolapse, grade 1 - Descent halfway to the hymen, grade 2 - Descent to the hymen, grade 3 - Descent halfway past the hymen, and grade 4 - Maximum descent possible [5].

Treatment options for this condition include non-invasive approaches such as physiotherapy with pelvic muscle strengthening exercises, biofeedback therapy, electrical stimulation therapy, the use of pessaries, and surgical interventions. Surgery is typically considered a last resort, reserved for severe cases of prolapse [6].

In terms of physiotherapy exercises, Kegel exercises are commonly prescribed in the early stages upon detecting prolapse. These exercises aim to strengthen pelvic muscles by contracting and relaxing them, ultimately enhancing their strength. Patients receive instruction on various exercises during physiotherapy sessions and continue practicing them independently at home [7].

Biofeedback therapy assists in locating and strengthening pelvic muscles. It involves placing a sensor in the vagina or rectum and another sensor on the abdomen. As patients contract and relax their pelvic muscles, electrical signals are recorded on a computer to assess muscle functionality [8].

Electrical stimulation therapy is often employed alongside biofeedback therapy. This treatment induces pelvic muscle contractions through electrical current stimulation. It is worth noting that patients are encouraged to complement their treatment with at-home physiotherapy exercises [8][9].

An alternative solution for rectifying pelvic prolapse is the use of a pessary. Comprising mainly silicone, pessaries come in various sizes and shapes. When inserted into the vagina, they provide support for the bladder, uterus, or rectum. Pessaries are frequently recommended as a minimally invasive, cost-effective, and low-maintenance treatment compared to surgery. They can be utilized for several months but require removal and cleaning at least once every three months to prevent potential irritation and assess the vagina for signs of pessary-related erosion.

However, some women may encounter vaginal irritation and increased vaginal discharge due to pessary use. Additionally, selecting the ideal-sized pessary for each patient can be challenging, as a one-size-fits-all approach may not apply [9].

All of these treatments, although minimally invasive, are primarily effective in the early stages of the condition. If the situation worsens, surgical intervention using either meshes or native tissue becomes necessary.

Surgical intervention, while invasive, remains the sole viable option for correcting prolapse in more severe cases. Initially, synthetic polypropylene meshes were introduced for repairs due to their notable success in correcting abdominal hernias. However, in 2019, the FDA (Food and Drug Administration) in the United States prohibited the sale and distribution of these meshes for transvaginal prolapse treatment due to the associated high risks [10].

In the initial post-surgery period, prolapse may appear corrected, but in many cases, after a few months, the mesh deteriorates or tears. In severe instances, surgical procedures are required to remove the damaged portion or the entire mesh. The elevated complication rate may be attributed to poor biocompatibility, inadequate biomechanical properties, as well as various factors such as age, overall health, prior surgeries, prolapse severity, and surgeon expertise, which plays a crucial role [11].

Consequently, mesh usage can result in infections, pain, scarring, incontinence, bowel issues, excessive vaginal discharge, muscle complications, and more. Many of these complications necessitate further medical attention, and occasionally, additional surgical interventions may be required [12].

In addition to synthetic mesh, surgical intervention using native tissue remains an option. However, this alternative also faces challenges, with high failure rates in prolapse correction, mirroring the issues encountered with mesh procedures. For instance, a comprehensive 2016 study involving 4,023 women revealed that following native tissue surgery, 38% of women may experience prolapse recurrence, compared to 11% to 20% for patients who underwent synthetic

mesh procedures. Furthermore, 5% of women relying on native tissue surgery will require a secondary procedure, while 7% to 18% of those who opted for mesh surgery will need further interventions [13].

Another study conducted between 2008 and 2016 aimed to assess the impact of mesh and native tissue procedures on patients' lives when treating pelvic organ prolapse. This research, conducted at a New York hospital, aimed to gauge long-term safety and understand the consequences of secondary interventions involving mesh used for treatment. The study identified 54,194 women requiring prolapse correction, with 11,205 opting for mesh procedures and 41,205 choosing native tissue repair. The average age of the women was 59.8 years, and the average follow-up period was 4.7 years. The findings indicated a higher risk of requiring secondary intervention when mesh was employed for prolapse repair compared to procedures utilizing native tissue. Among patients undergoing mesh surgery, 18.5% required further interventions due to complications associated with the mesh [12].

Consequently, even though transvaginal mesh has been withdrawn from the market, the risk of complications has not diminished over time. Women with existing mesh implants require regular monitoring to ensure their safety and well-being, emphasizing the importance of ongoing mesh surveillance for these patients [12].

To explore innovative treatment approaches, a software such as Abaqus® can be used to visualize and comprehend the behaviour of objects based on their physical characteristics. Therefore, delving into simulations related to POP can yield valuable insights.

One illustrative example of such simulations pertains to the investigation of mesh anchoring techniques in uterine prolapse repair surgery, as demonstrated by Silva et al. in 2021 [14]. This study involved simulating transvaginal reconstructive surgery aimed at addressing the repair of apical ligaments, specifically the uterosacral ligaments (USLs) and cardinal ligaments (CLs). Various scenarios, including different degrees of ligament impairment (90% and 50%) and complete rupture, were modelled. Implants intended to reinforce or replace these ligaments were designed following literature guidelines, and their mechanical properties were derived from uniaxial tensile tests. The primary objective of this study was to simulate the impact of diverse mesh anchoring techniques and assess the extent of pelvic tissue displacement during the Valsalva manoeuvre [14].

This study proposes the development of biodegradable meshes that offers a potential solution to address the primary drawbacks associated with synthetic meshes, owing to the biocompatibility and biomechanical properties inherent to biodegradable meshes. To explore this, computational models were developed, with variations in pore geometry, pore size, filament thickness, and the incorporation of filaments around specific mesh regions. Subsequently, one of these meshes was fabricated to validate the simulation results. Following this, uniaxial tensile tests were conducted on sow's vaginal tissue to enable a comparison with the simulations, with the aim of identifying meshes exhibiting behaviour akin to vaginal tissue. Lastly, the most promising outcomes were juxtaposed with the uterosacral ligament and a commercially available mesh for further evaluation.

2. Materials and Methods

2.1 Vaginal Tissue

Animal models play a pivotal role in advancing the understanding of human development, diseases, and the development of effective therapeutics and vaccines. Among these models, pigs stand out due to their striking similarities with humans in various aspects, including anatomical structure, size, genome, immunology, and physiology. These similarities make pigs a more relevant alternative to rodent models, particularly in translational and clinical research. Pigs offer distinct advantages over primates and other livestock models, including larger litters, shorter generation times, and a genome that can be readily manipulated [15].

The shared anatomical and physiological characteristics between pigs and humans underscore the suitability of pigs as valuable biomedical models for studying human biology. To facilitate the comparison of results obtained in simulations, five samples of porcine vaginal tissue were utilized for uniaxial tensile tests. Soft tissues from the pelvic floor of sows were sourced from Matadouro Carneiro e Salgueirinho Lda slaughterhouse in Trofa, Portugal, for research purposes. All procedures were conducted in strict compliance with the regulations outlined in Regulation (EC) No. 1069/2009 dated 21 October. The obtained animal components included the vaginal canal, rectum, muscles, and adjacent fat, treated as a single unit [15][16].

Subsequently, the vaginal canal was isolated, and specimens were meticulously prepared, as depicted in the Figure 2.1.



Figure 2.1 The samples of the vaginal tissue.

2.2 Melt electrowriting

The melt electrowriting device is utilized for mesh and filament printing, this device was successfully developed as part of the "SPINMESH" project (Figure 2.2). Recently, it has been modified to incorporate a pellet extruder, allowing the printing of meshes using medical-grade PCL, which is available only in pellet form. The printer comprises an aluminium structure with a collector plate featuring X-Y movement for material deposition and a Z-movable print head through which the material flows. This flow is achieved through a heating mechanism that melts the material in a spinneret. These components are connected to an external high voltage power

supply via electrodes. Additionally, instructions are configured through a computer and a translation system, defining the desired direct writing patterns [17].

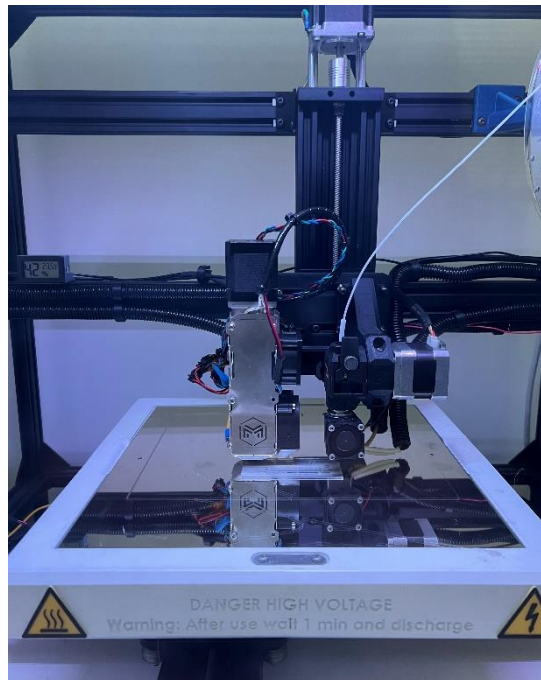


Figure 2.2 Melt electrowriting device.

2.3 Medical-grade PCL

PCL, an FDA-approved material, has a well-established history of human use and finds frequent application in 3D printing, particularly in the context of MEW (Melt Electrowriting spinning). Its suitability for MEW is attributed to its low melting point and rapid solidification. This polymer, aliphatic semicrystalline, presents a melting temperature range of 59°C to 64°C, rendering it mechanically robust and flexible at room temperature. PCL is recognized for its biocompatibility, making it a preferred choice in resorbable sutures, drug delivery systems, and regenerative therapies. Additionally, it boasts an extended degradation period, with erosion rates spanning two to three years [18].

Within the realm of MEW, medical-grade PCL, such as PC12, stands out as the most extensively utilized and researched polymer, as supported by existing literature. Medical-grade PCL offers superior purity and enhanced printing quality compared to its technical-grade counterpart. Opting for medical-grade PCL in MEW processes empowers precise control and accuracy, ultimately leading to superior structural outcomes and designs [19][17].

The meshes under examination were 3D printed using medical-grade PCL from Corbion, bearing the trade name PURASORB PC12. This homopolymer features an intrinsic viscosity falling within the range of 1.0 to 1.3 dl/g and was employed in pellet form [19][17]. It is important to mention that during the printing process, the temperature and humidity were controlled.

2.4 Uniaxial Tensile Test

Uniaxial testing is a method wherein a specimen undergoes the application of force along a single axis until it reaches the point of failure. This force can take the form of either tension or compression. During these tests, the force acting on the sample is continuously monitored concerning the displacement occurring between the grips of the testing machine. Critical properties that can be directly evaluated through a uniaxial test include the ultimate tensile or compressive strength, changes in specimen length, and alterations in cross-sectional area. By utilizing these measurements, it becomes feasible to calculate essential parameters like stress, strain, and Young's Modulus, which represents elasticity, for the given specimen [20].

The dimensions of the meshes and the vaginal tissue samples when subjected to a uniaxial tensile test are illustrated in the accompanying image, as depicted in Figure 2.3. The length (a) varies between the meshes, with a length of 40 mm, and the vaginal tissue, with a length of 50 mm.

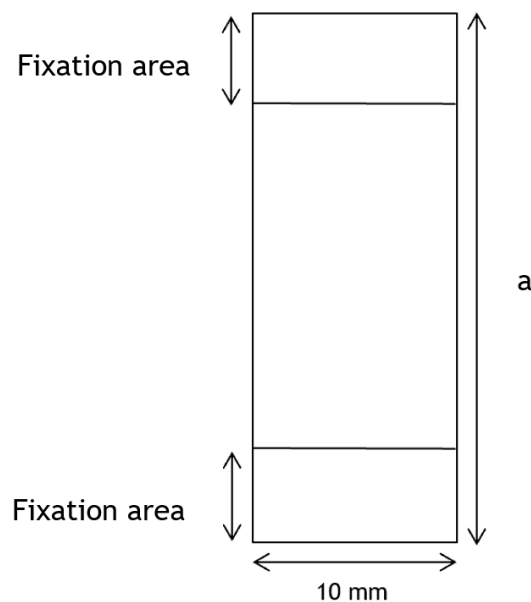


Figure 2.3 Schematization of the samples' dimensions for the uniaxial tensile

2.5 Mesh Prototyping

To gain insight into the desired characteristics of the meshes, it is essential to conduct research on existing meshes and those previously employed in treating various cases of pelvic organ prolapse.

Ideally, the mesh thickness should fall within the range of 0.08 mm to 0.24 mm, considering the dimensions of meshes documented in the literature [21][22]. Additionally, the mesh pores should have a diameter of approximately 2.00 mm to promote cell growth, thus effectively addressing the prolapse issue [11].

It is noteworthy that meshes with small pores, specifically those smaller than one millimetre, and low porosity levels can lead to heightened inflammation and the development of connective

tissue, resulting in patient discomfort. This is not the case with meshes featuring pore sizes exceeding 1.00 mm, which are considered to have large pores and high porosity. Conversely, pore collapse within the mesh, caused by tension forces, is linked to vaginal pain. Problematic areas for patients often coincide with regions where the mesh pores have collapsed. Pore collapse also reduces the potential for cell growth during the initial phase until the mesh degrades. Therefore, it is imperative to control and predict pore behaviour when forces are applied to the mesh, ensuring excellent compatibility between the mesh and the patient's tissues [23].

In contrast to multifilament mesh, monofilament mesh lacks small gaps between its filaments, reducing the chances of bacterial growth and, consequently, lowering the risk of infection. Regarding weight, a lighter mesh typically indicates less tissue involvement, thereby reducing the likelihood of inflammation [24][25].

With this comprehensive information in hand, a thorough analysis of existing products, such as the Restorelle® mesh, was conducted before embarking on the mesh development process. The Restorelle® mesh is an ultra-lightweight polypropylene (PP) mesh with a density of 19g/m², constructed from three knitted monofilaments (each with a diameter of 0.08 mm). It boasts a pore size of approximately 2.00 mm [21]. For visual reference, Figure 2.4 provides an image of the Restorelle® mesh along with its SEM image [11][26].

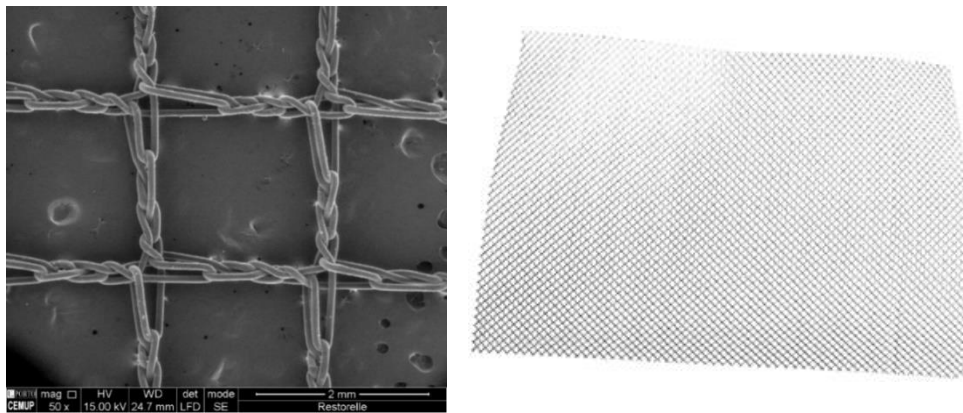


Figure 2.4 A SEM image of the Restorelle® mesh, and an example of the Restorelle® mesh, respectively (adapted from [11][26]).

2.6 Computational Modelling of the Biodegradable Mesh

The graphic in Figure 2.5 illustrates the average experimental values obtained from the uniaxial tensile test conducted on a filament of medical-grade PCL with a diameter of 0.24 mm. The value utilized in the simulations was 251.56 MPa. As per literature, the Young's modulus is expected to be higher, falling within the range of 343.9 MPa to 363.4 MPa [27]. The observed lower Young's modulus value may be attributed to the temperature exposure of the material during the printing process, which, in this case, reached 200°C, potentially altering the properties of the medical-grade PCL.

Another contributing factor to the deviation in Young's modulus values could be the medical-grade PCL may not have received adequate maintenance during the work period, given that all materials and equipment are shared, which can lead to potential errors or oversights in its handling. Ideally, this material should be stored in an inert atmosphere at low temperatures (-15°C). Alternatively, it can be preserved in its original packaging at room temperature, thereby retaining its initial properties for a minimum of one year [28].

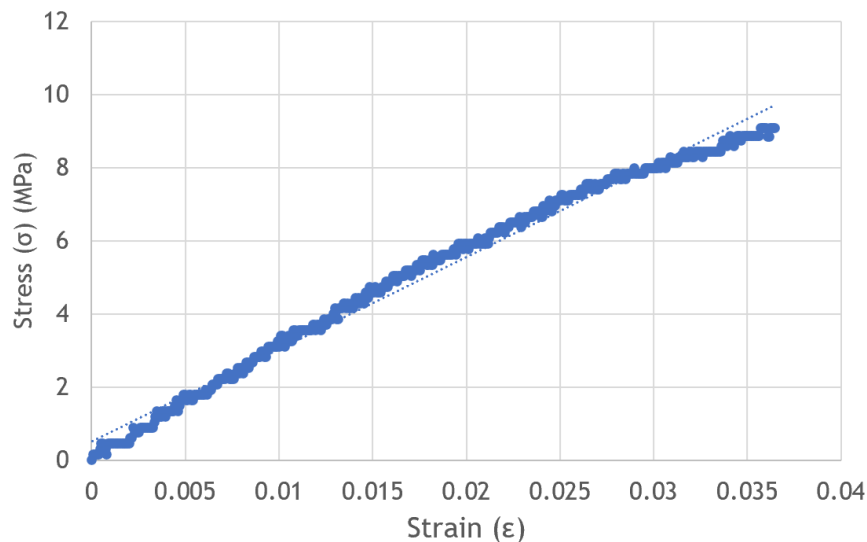


Figure 2.5 Stress and strain values obtained from the uniaxial tensile test done to the filament.

It is important to note that the results represent the average of stress-strain values obtained from three separate uniaxial tensile tests performed on three medical-grade PCL filaments.

In addition to determining the Young's modulus, it is crucial to establish the Poisson's ratio for the simulations. Poisson's ratio characterizes the relationship between a material's change in width and length when subjected to an applied force. Specifically, it is calculated as the ratio of the expansion fraction to the compression fraction. For isotropic materials, Poisson's ratio typically falls within the range of -1 to 0.5 [29]. Isotropic materials maintain consistent properties when tested in different directions [30].

However, it is important to highlight that the specific value of Poisson's ratio may vary depending on the material in question. In the case of a biodegradable polymer like PCL, the Poisson's ratio is approximately 0.3 [31].

With the Young's modulus and Poisson's ratio determined, the process of developing the meshes commenced. All the meshes are developed from medical-grade PCL and share common dimensions, featuring a length of 40 mm, a width of 10 mm, and utilizing a beam element "B21."

Numerous mesh variations were created in an attempt to match the load-displacement values of vaginal tissue (Figure 2.6) using the software Abaqus®. These models were generated by modifying filament thickness, adjusting pore geometries and sizes, and introducing additional filaments around specific areas of the mesh models.

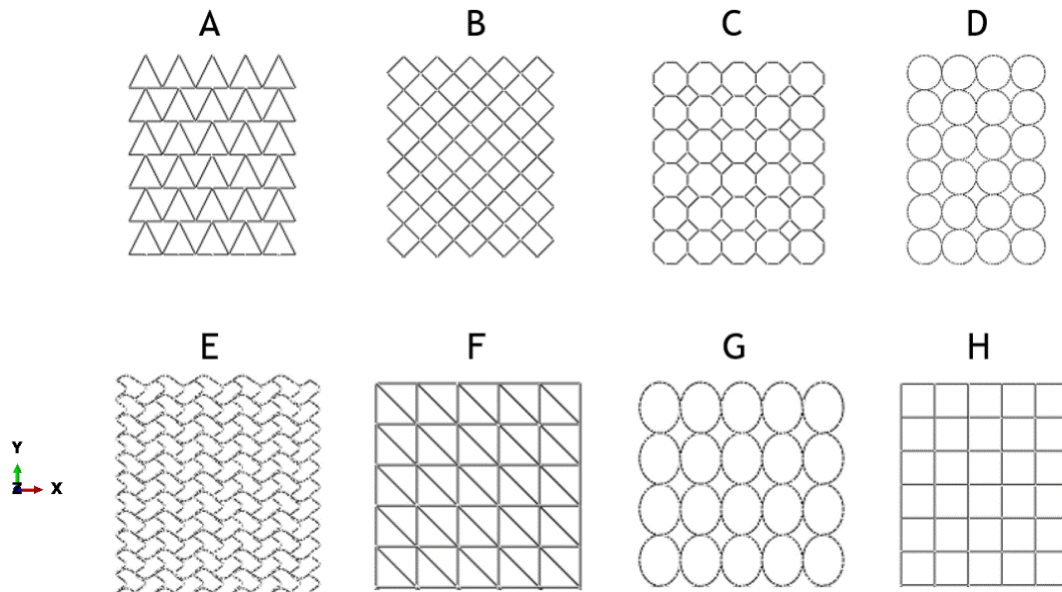
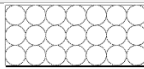
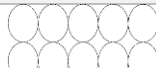
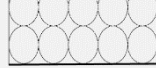
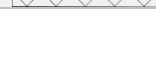


Figure 2.6 Examples of the developed meshes. Mesh names: A - Triangle, B - Diamond, C - Octagon, D - Circular, E - Sinusoidal, F - Diagonal, G - Oval, and H - Square.

The Table 1 shows the number of nodes and elements for each computational model of the meshes. The element type applied for these meshes was the beam element “B21”.

Table 1 Number of nodes and elements for each computational model of the meshes.

Type of Mesh		Number of nodes	Number of elements
Sinusoidal		16258	17076
Square		4401	4500
Circular without the filament around the mesh, and with 2.00 mm pore diameter		6197	6372
Circular with the filament around the mesh, and with 2.00 mm pore diameter		7175	7400
Circular without the filament around the mesh, and 2.50 mm pore diameter		4990	5098
Circular with the filament around the mesh, and 2.50 mm pore diameter		5975	6123
Circular without the filament around the mesh, and 1.50 mm pore diameter		8726	9070
Circular with the filament around the mesh, and 1.50 mm pore diameter		9684	10096
Diagonal		7101	7300
Octagon without the filament around the mesh		6750	7100

Octagon with the filament around the mesh		7314	7714
Oval		5597	5736
Oval with the filament around the mesh		6581	6762
Triangle		6225	6400
Triangle with the filament around the mesh		7081	7300
Diamond		5425	5600
Diamond with the filament around the mesh		6375	6600

The meshes were designed with varying pore sizes, including 1.50 mm, 2.00 mm, and 2.50 mm, to investigate the impact of pore size on load and displacement outcomes. The target pore size fell within the range of 1.00 mm to 2.00 mm, which led to the creation of meshes with pore diameters of 1.50 mm and 2.00 mm. Additionally, meshes with slightly larger pores measuring 2.50 mm were generated to assess pore deformation and its effects on results. In the case of specific pore geometries like the sinusoidal pore represented by the letter E in Figure 2.6, determining the exact size was challenging due to its shape. Hence, the pore size was approximated at 1.58 mm by measuring the distance between the two farthest points from its centre. To mitigate pore distortion and enhance results, filaments were strategically placed around certain areas of the meshes, as depicted in Figure 2.7. Three filament diameters, namely 0.08 mm, 0.16 mm, and 0.24 mm, were employed for each geometry.

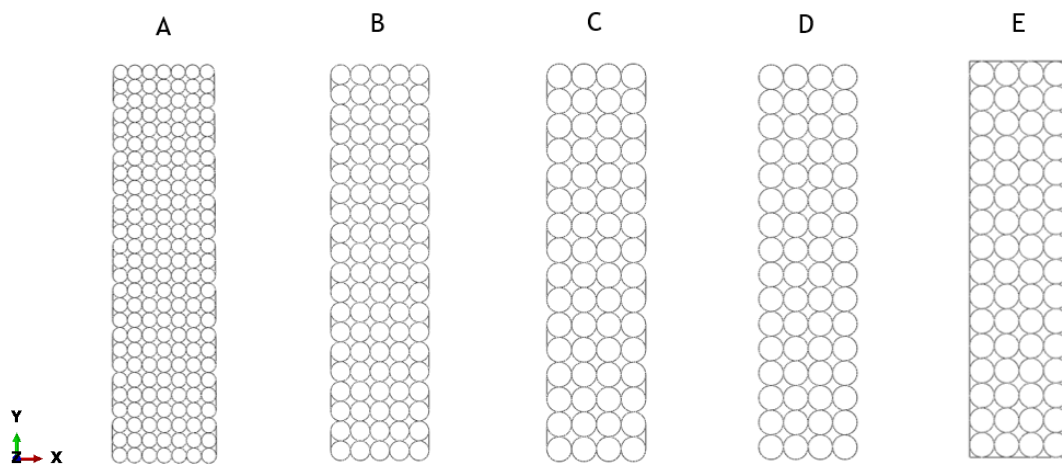


Figure 2.7 Computational models of the circular pore meshes. A - Mesh with 1.50 mm pore diameter and filaments around the mesh in certain areas, B - Mesh with 2.00 mm pore diameter and filaments around the mesh in certain areas, C - Mesh with 2.50 mm pore diameter and filaments around the mesh in certain areas, D - Mesh with 2.50 mm pore diameter and without a filament around the mesh, and E - Mesh with 2.50 mm pore diameter and a filament around the mesh.

Afterwards, the idea of creating meshes with diverse filament thicknesses in different sections was introduced to enhance the obtained outcomes. Filaments measuring 0.08 mm or 0.16 mm in diameter were employed for the mesh's edges, while a diameter of 0.24 mm was adopted for the remaining columns, as illustrated in Figure 2.8.

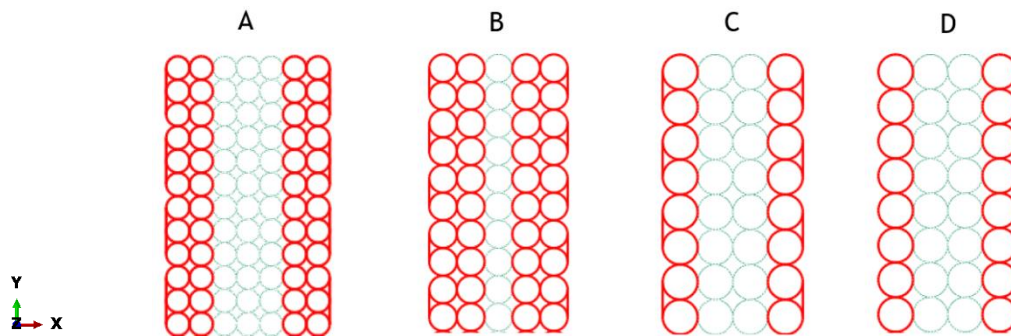


Figure 2.8 Distribution of filament thickness in the meshes with 1.50 mm, 2.00 mm, and the last two with 2.50 mm pore diameter, respectively. The red columns represent the filaments with a diameter of 0.08 mm or 0.16 mm, and the remaining columns have 0.24 mm of thickness.

Next, to replicate the uniaxial tensile test, boundary conditions were established. The nodes at the lower extremity of the mesh were set as fixed, while a displacement was applied to the upper edge a displacement of 40% of the mesh length, as depicted in Figure 2.9.

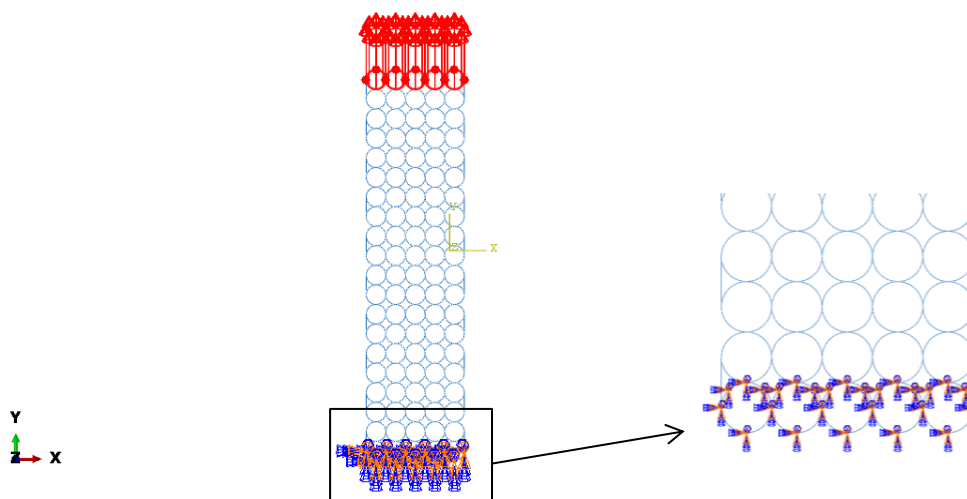
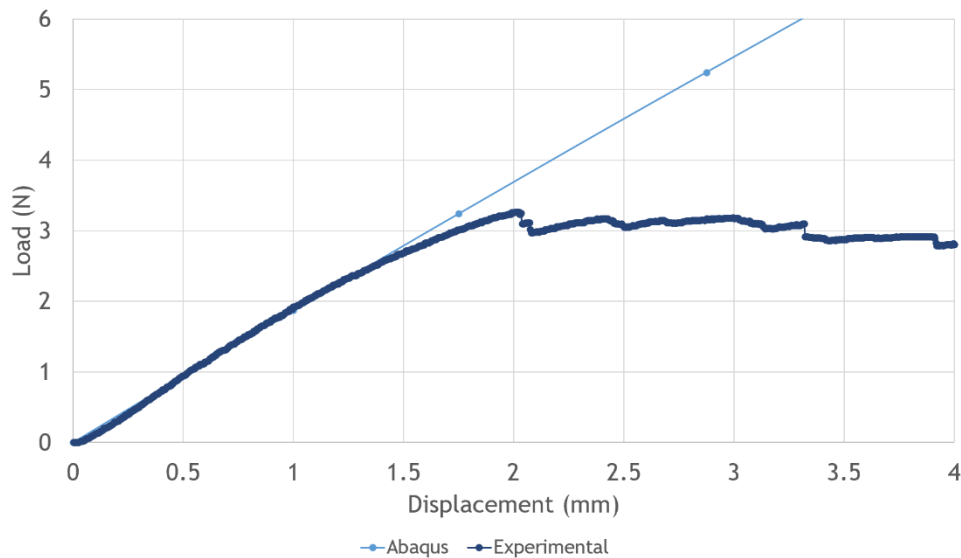


Figure 2.9 Definition of the boundary conditions of the circular mesh with 2.00 mm of pore diameter.

3. Results and Discussion

3.1 Printed Mesh and the Computational Model

In the beginning, to validate the simulation results in Abaqus®, a comparison was made between the load and displacement values obtained through simulation and those obtained experimentally. These experimental values were derived from the average stress-strain data collected from three uniaxial tensile tests conducted on three medical-grade PCL meshes.



3.1 Load and displacement values obtained from the developed model and the experimental mesh, both with rectangular pores of 2 mm and 0.24 mm of filament diameter.

As observed in the obtained graphic (Figure 3.1), the magnitude of the values is the same and the lines display similar behaviour. As anticipated, the developed model exhibits greater stiffness compared to the experimental model. These findings are grounded in square pore mesh models. It is crucial to acknowledge that outcomes may vary based on the mesh's geometry and properties. The computational model was built and simulated based on experimental results from a medical-grade PCL mesh produced through MEW. The results indicate a remarkably close alignment between the experimental and computational tests. Notably, a discrepancy emerges during the uniaxial tensile test when the filaments rupture, leading to plastic behaviour in the experimental scenario, while the simulation maintains elastic behaviour, as it does not account for yield stress.

3.2 Computational Models

Before diving into the analysis of the simulation results, it is important to emphasize that the graphics represent outcomes in the safety zone, while the images displaying distorted pores pertain to the comfort zone.

3.2.1 Absence and Presence of the Filament around the Mesh

Firstly, it was compared the load and displacement values of the computational models without a filament around them, all with a pore dimension of approximately 2.00 mm (except for the sinusoidal mesh). These values were then compared with the load and displacement values of the vaginal tissue, as illustrated in Figure 3.3. The computational models corresponding to the results in Figure 3.3 are depicted in Figure 3.2.

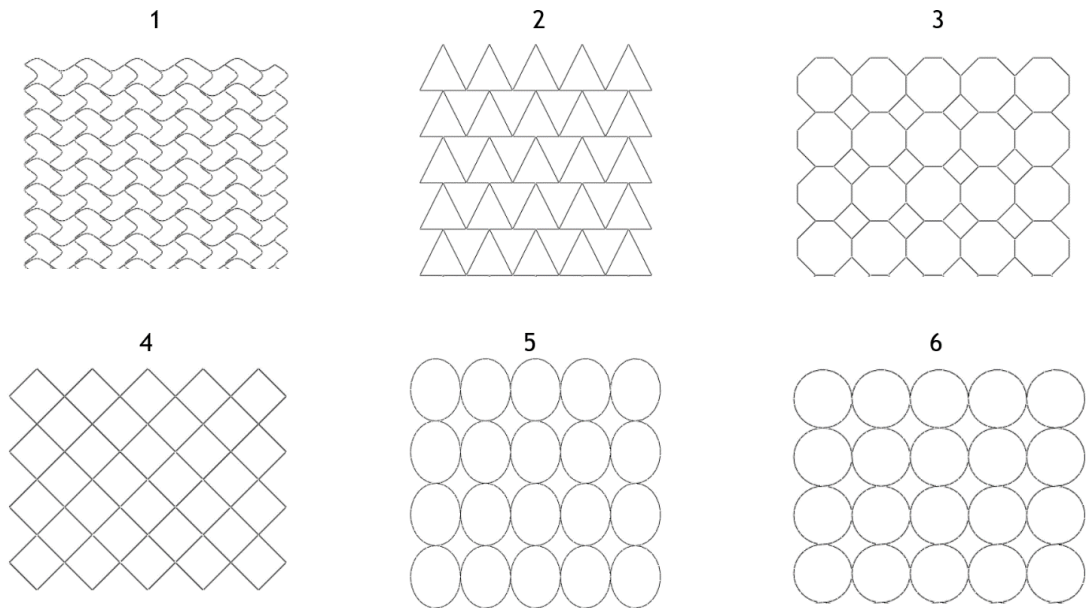


Figure 3.2 Computational models developed without a filament around the mesh. 1 - Sinusoidal with a 1.58 mm pore size. 2 - Triangular with a 2.06 mm pore size. 3 - Octagon with a 2.10 mm pore size. 4 - Diamond with a 2.00 mm pore size. 5 - Oval with a 2.00 mm by 2.50 mm pore size. 6 - Circular with a 2.00 mm pore size.

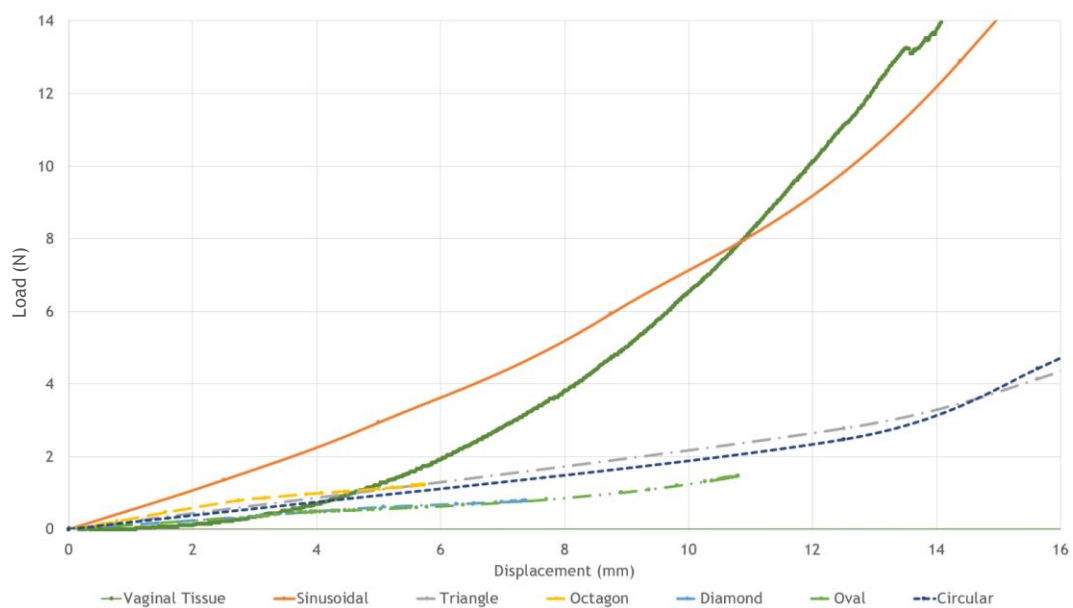


Figure 3.3 Load-displacement curves of the computational models created without the filament around them.

Upon analysing Figure 3.3, it becomes apparent that meshes without a filament around them exhibit lower load values for the same displacement values as the vaginal tissue, except for the sinusoidal mesh, which displays a nonlinear mechanical behaviour resembling that of the vaginal tissue.

In addition to these findings, it is also essential to scrutinize the pore deformation in the computational models. To accomplish this, it was examined the pore distortion in the mesh that demonstrated the best results, namely the sinusoidal mesh, as depicted in Figure 3.4.

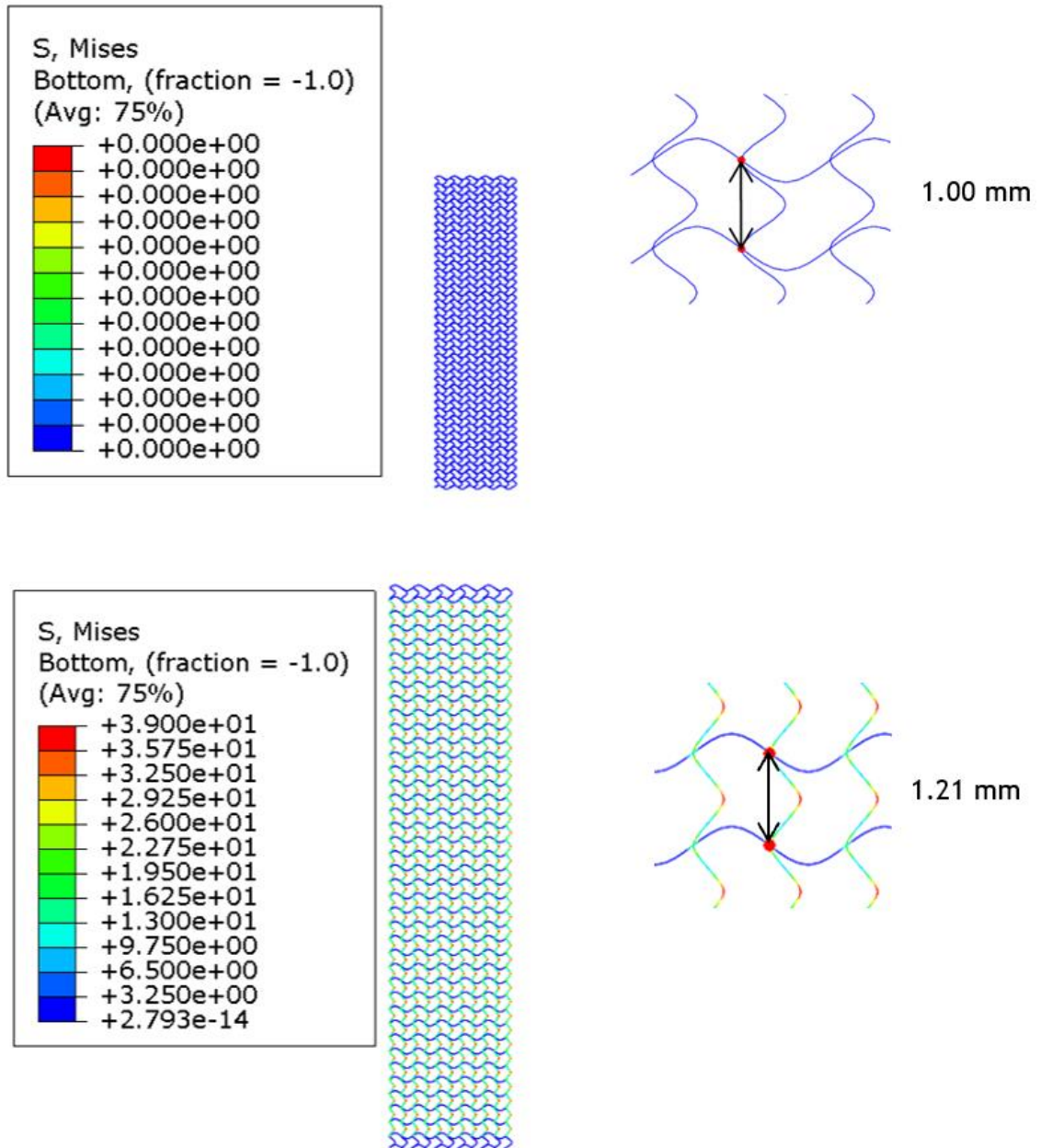


Figure 3.4 Difference between the pores of the sinusoidal mesh before and after the simulation.

As evident from the uniaxial tensile test, the horizontally positioned filaments have minimal impact on the overall outcome. In this test, the vertically positioned filaments bear the majority of the applied force on the mesh. Consequently, when focusing solely on the pores, you can observe a transformation in the filament's original sinusoidal shape, resulting in a vertical elongation of 21.60%. This transformation alters the pore dimensions, as illustrated in Figure 3.4. On the horizontal plane, the filament experiences minimal alteration, approximately 1%, transitioning from 1.00 mm to 0.99 mm. In summary, the filament's geometry and shape deform, leading to a departure from its initial configuration.

While it is crucial to consider load and displacement values, it is equally vital to examine the deformation of each mesh after it undergoes a specific level of load. Excessive deformation can render a mesh unusable due to its degree of distortion.

To address this, an attempt was made to enhance load values and minimize pore deformation by adding a filament around the meshes, as depicted in Figure 3.5. The results of simulations conducted on these modified meshes are presented in Figure 3.6.

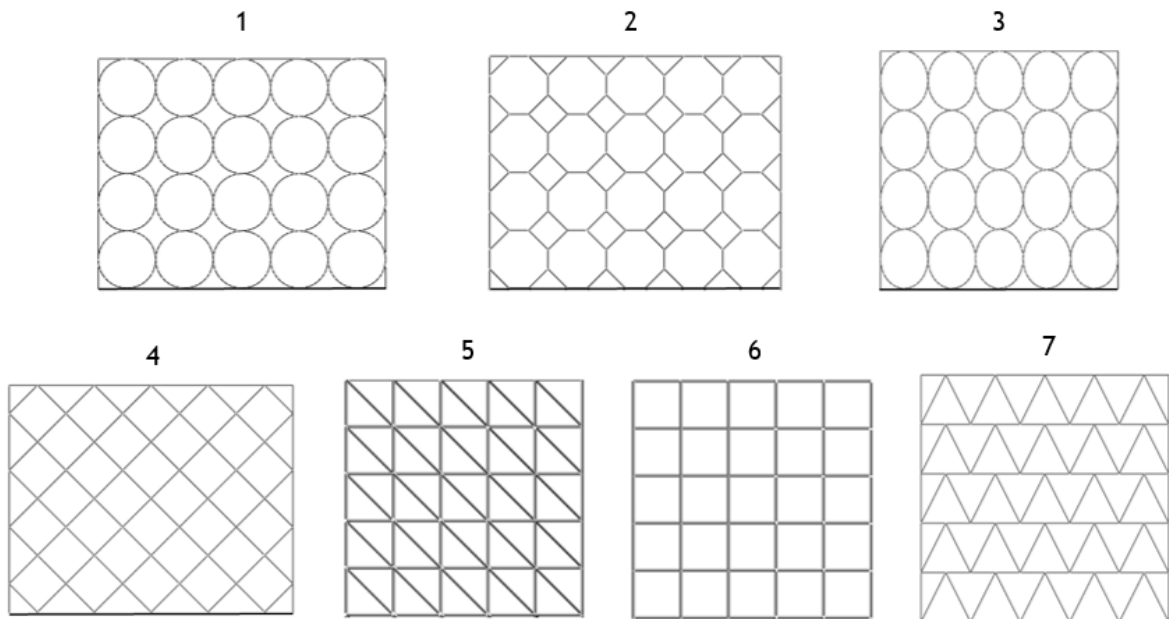


Figure 3.5 Computational models developed with a filament around the mesh. 1 - Circular with a 2.00 mm pore size. 2 - Octagon with a 2.10 mm pore size. 3 - Oval with a 2.00 mm by 2.50 mm pore size. 4 - Diamond with a 2.00 mm pore size. 5 - Diagonal with a 2.00 mm pore size. 6 - Square with a 2.00 mm pore size. 7 - Triangular with a 2.06 mm pore size.

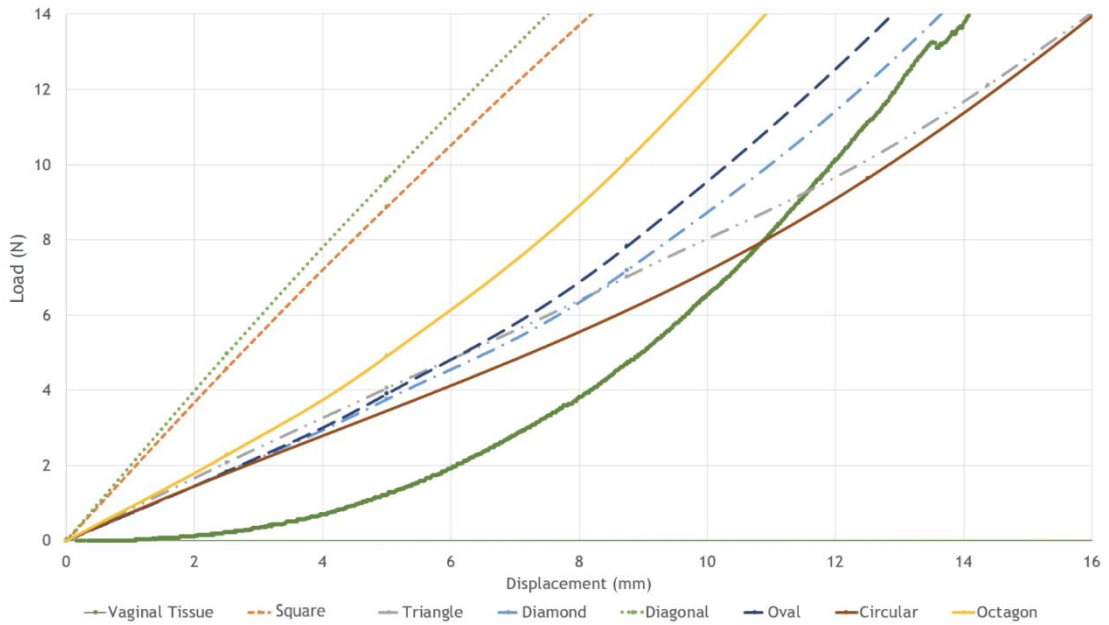


Figure 3.6 Load-displacement curves of the computational models created with the filament around them.

As depicted in Figure 3.6, it becomes evident that meshes with a filament incorporated around them exhibit higher load values compared to meshes without this added feature. This indicates that the presence of a filament surrounding the mesh significantly influences the load values obtained.

Analysing the obtained results allows us to eliminate square and diagonal meshes from further consideration. These meshes demonstrate considerably higher load values than vaginal tissue when subjected to the same displacement, suggesting that they may not be the ideal choice for POP repair.

Among the remaining computational models, the circular mesh shows particularly promising results, with mechanical behaviour closely resembling that of vaginal tissue.

Finally, an examination of pore deformation within the circular mesh was conducted, as it exhibits values resembling those of vaginal tissue, as illustrated in Figure 3.7.

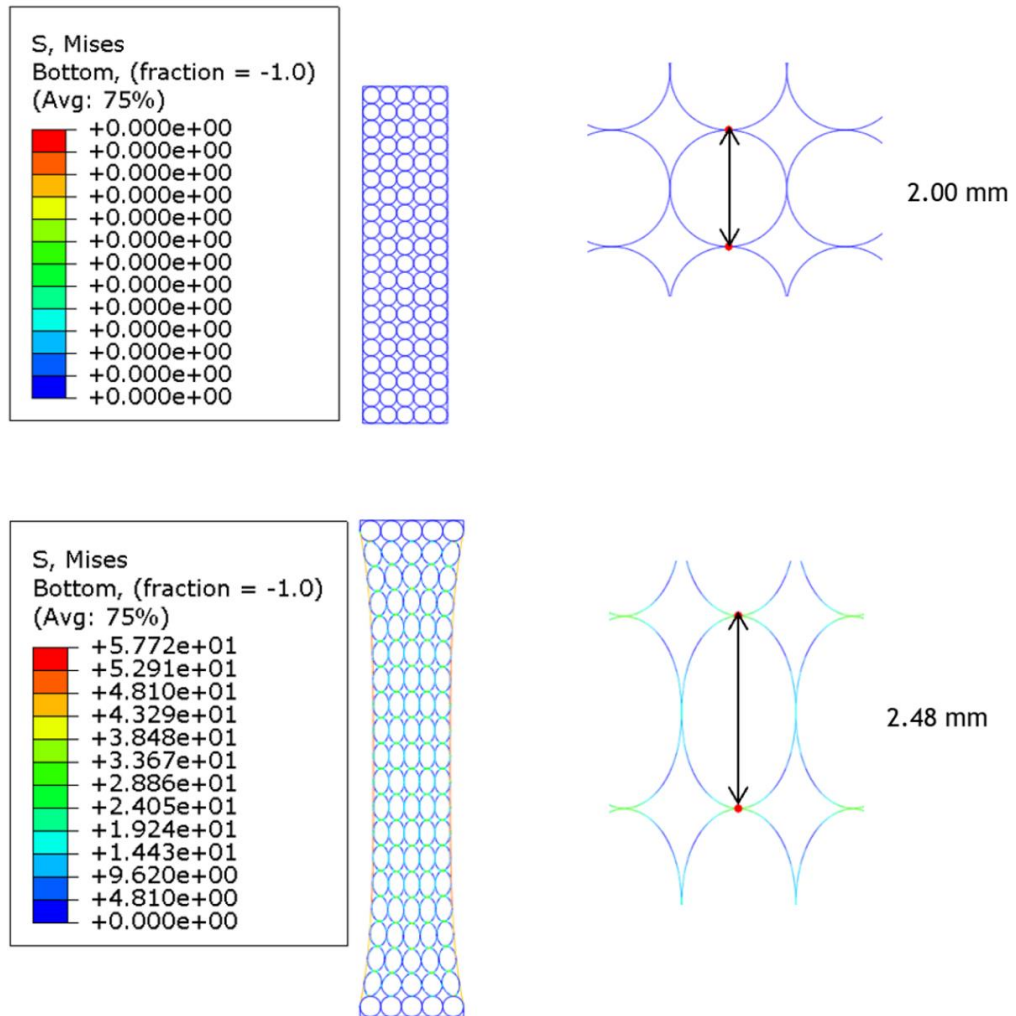


Figure 3.7 Difference between the pores of the circular mesh before and after the simulation.

The Figure 3.7 highlights a significant contrast in pore deformation within this mesh when compared to the sinusoidal mesh. It is important to note that pore deformation is not uniform across the entire mesh. Near the fixed regions, pores experience minimal deformation, while at the mesh's centre, there is a more substantial deformation of 24.15%, as depicted in Figure 3.8. In this context, the areas capable of withstanding most of the force applied during the uniaxial test are the filaments surrounding the mesh and the regions where the pores are interconnected.

In conclusion, while the inclusion of filaments around the computational models has demonstrated potential in reducing pore deformation and improving load-displacement values, it is crucial to explore alternative approaches and adjust various mesh characteristics to further enhance the obtained results.

3.2.2 Pore Dimension

To improve the performance of the meshes, it was investigated how altering the dimensions of the pores could influence the load and displacement values. To achieve this, three models with

circular pores were developed: one with 1.50 mm diameter, another with 2.00 mm, and a third with 2.50 mm diameter (Figure 3.8). It is worth noting that all these meshes were created using a 0.24 mm filament thickness.

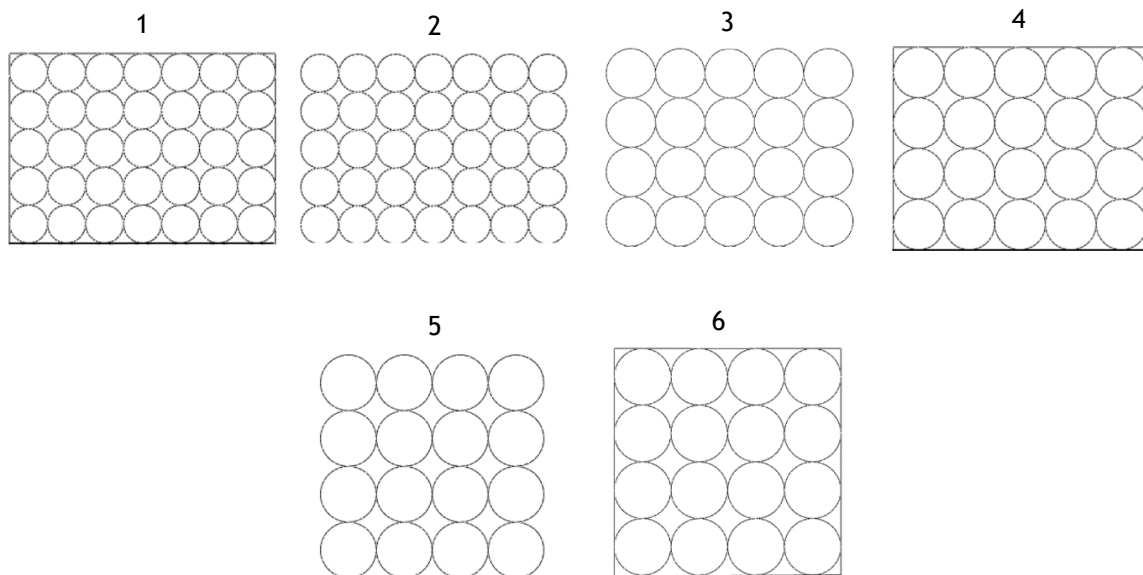


Figure 3.8 Circular pore meshes developed with and without a filament around the mesh. 1 and 2 - Meshes with 1.50 mm pore diameter. 3 and 4 - Meshes featuring a pore diameter of 2.00 mm. 5 and 6 - Meshes possessing a pore diameter of 2.50 mm.

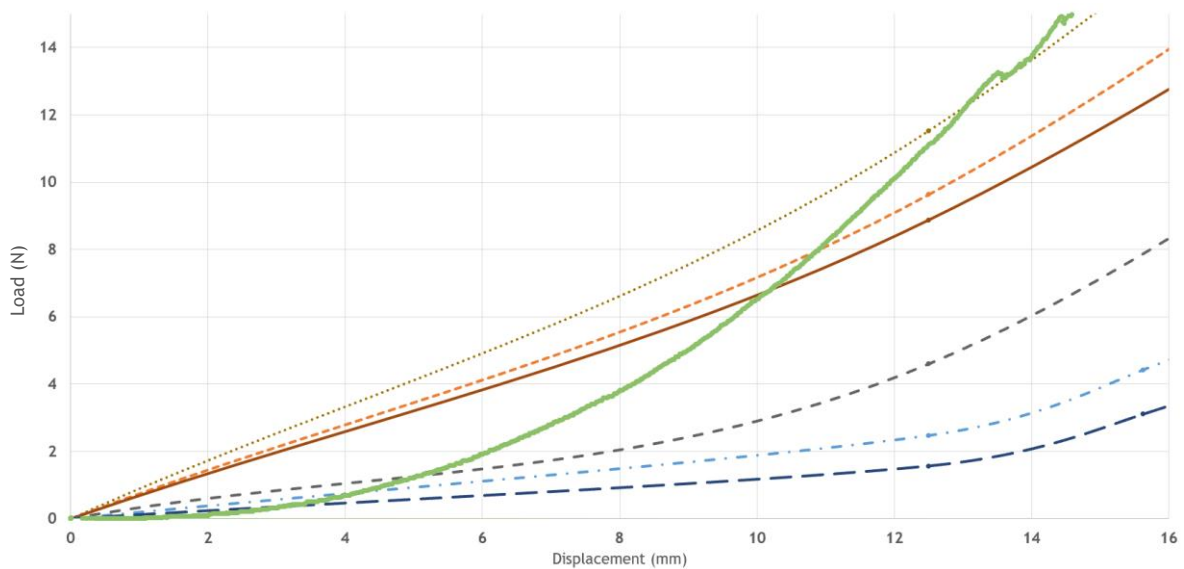


Figure 3.9 Load-displacement curves of the circular meshes created with different pore sizes.

Upon analysing the graphic (Figure 3.9), a clear relationship emerges between the mesh's pore size and the resulting load values. Specifically, the mesh with the smallest pore diameter, 1.50 mm, exhibits higher load values compared to the other meshes.

This experiment has led to the conclusion that as the mesh's pore size decreases, the number of mesh columns increases. Consequently, the mesh becomes more resistant to the applied force, resulting in higher load-displacement values.

Based on these results, a potential strategy emerges: the concept of designing meshes with strategically positioned filaments in specific regions to achieve load values within a desired range while minimizing pore distortion. Subsequent to this discussion, it will be presented the outcomes of meshes designed with such strategically placed filaments.

3.2.3 Filament Thickness

Filament thickness is another critical factor to consider when designing meshes. For the previously mentioned pore geometries in the subsection 3.2.1 and 3.2.2, it was created meshes with varying filament diameters. Each pore geometry resulted in three meshes with different filament thicknesses: 0.08 mm, 0.16 mm, and 0.24 mm. While three meshes were produced for each pore geometry, it will only be presented the results in the following graphic for the meshes that exhibited behaviour similar to vaginal tissue.

In Figure 3.10 below, you can see the results obtained from simulations performed on different mesh models that showed the most promising results, namely, the sinusoidal mesh and the circular mesh with a pore diameter of 2.00 mm, featuring a filament around it.

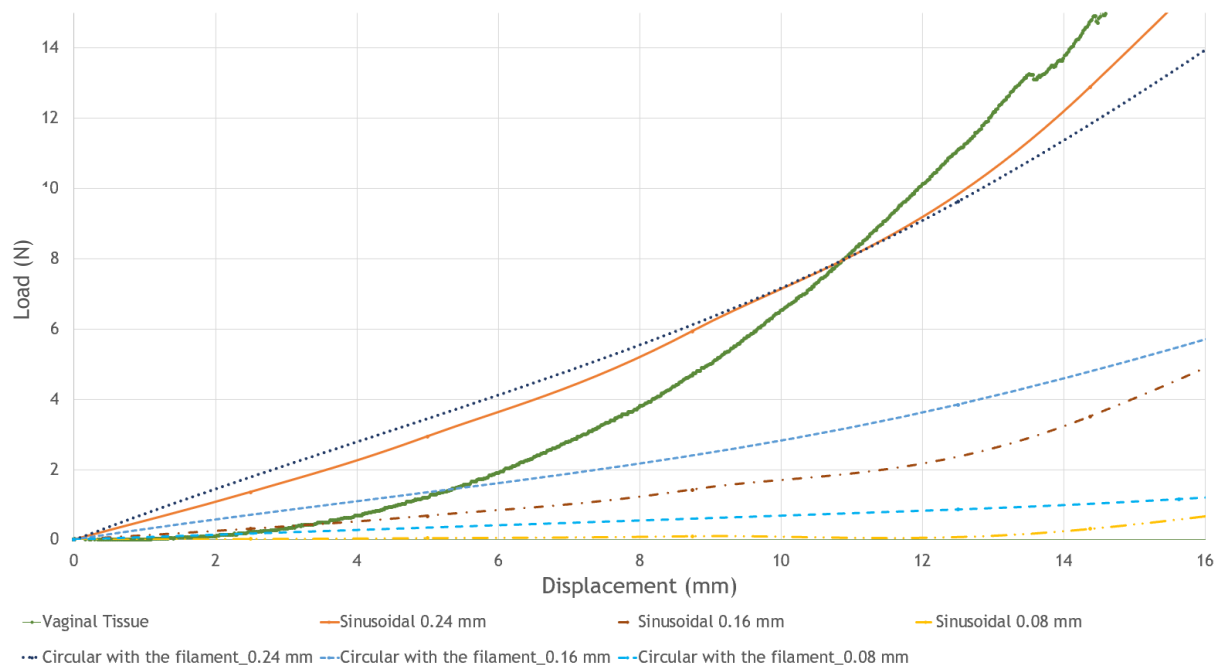


Figure 3.10 Load-displacement curves of the sinusoidal meshes and the circular meshes with a pore diameter of 2.00 mm and a filament around it.

As expected, reducing filament thickness corresponds to lower load-displacement values. Notably, the meshes delivering the most favourable outcomes are those equipped with filaments measuring 0.24 mm in diameter. These results align with the previous findings, specifically

regarding the sinusoidal mesh and the circular mesh with a 2.00 mm pore diameter, which also featured 0.24 mm diameter filaments.

Throughout this study, it was explored three crucial attributes of the meshes: pore geometry, the presence of a filament around the mesh, and filament thickness. Based on the findings, the meshes that closely mimic the behaviour of vaginal tissue include the sinusoidal mesh with a 1.58 mm pore size and 0.24 mm diameter filaments, along with the circular mesh featuring pore diameters of 1.50 mm and 2.00 mm, 0.24 mm diameter filaments, and a filament surrounding the mesh.

However, in the quest to further improve results and design meshes capable of effectively repairing prolapse, it was introduced a novel concept. This involves crafting meshes with filaments present only in specific regions, and varying filament thickness throughout the mesh, departing from the uniform thickness seen in the previous models. These new meshes feature circular pores with diameters of 1.50 mm, 2.00 mm, and 2.50 mm, as illustrated in Figure 3.11.

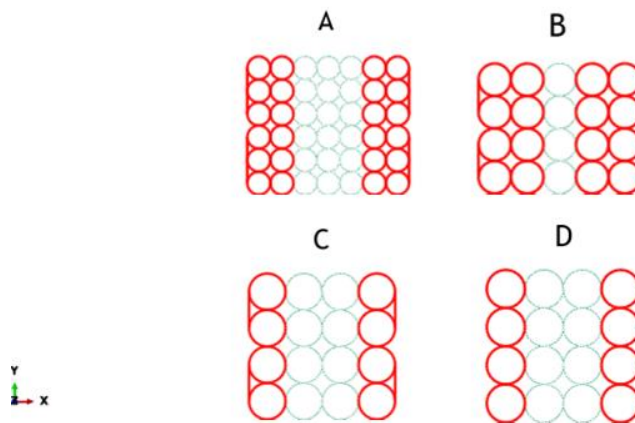


Figure 3.11 Distribution of filament thickness in the circular meshes. A - Mesh with 1.50 mm pore diameter, B - Mesh 2.00 mm pore diameter, C - Mesh 2.50 mm pore diameter, D - Mesh with 2.50 mm pore diameter. The red columns represent the filaments with a diameter of 0.08 mm or 0.16 mm, both cases were simulated, and the remaining columns have 0.24 mm of thickness.

This innovative approach stems from the mesh's primary objective of replacing damaged ligaments, muscles, or connective tissues that can no longer adequately support the tissues. It is essential to acknowledge that the mesh, when attached to structures like bone (e.g., the sacrum), exhibits a more rigid behaviour and undergoes property changes as it approaches the uterus. Therefore, by incorporating filaments of varying thicknesses across different regions of the mesh, its ability to withstand exerted forces will differ based on filament thickness. In this scenario, the central part of the mesh, equipped with 0.24 mm diameter filaments, can endure higher force values.

In the following section, it will be compared the meshes that demonstrate the most promising results with the load-displacement values of the uterosacral ligament. The graphic below (Figure 3.12) illustrates the outcomes obtained from the simulations conducted on these new meshes.

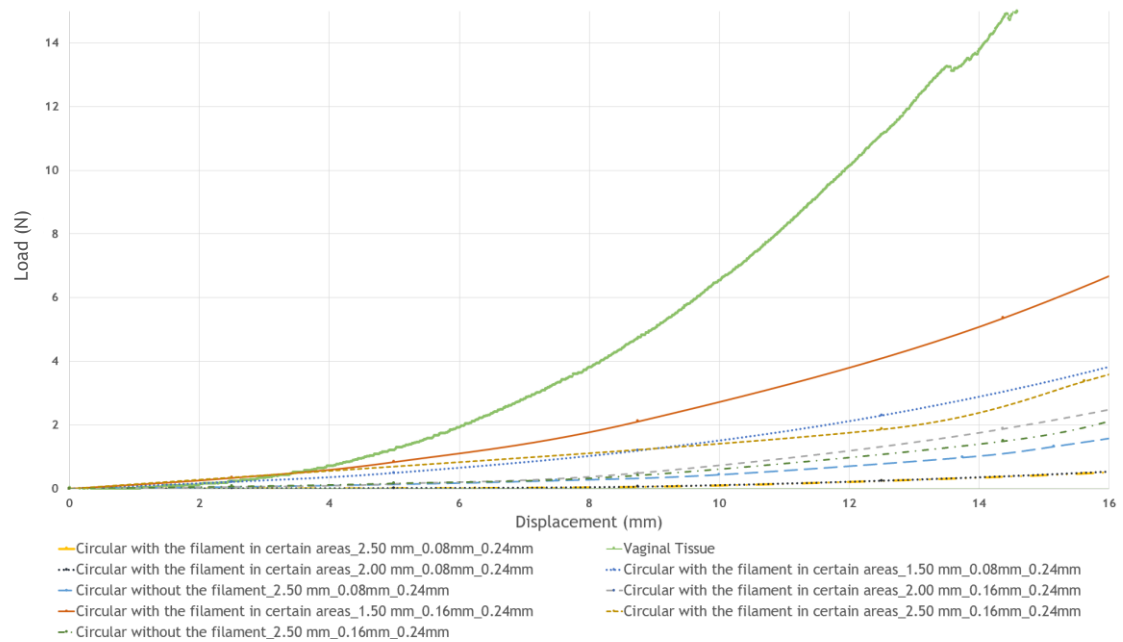


Figure 3.12 Force-displacement curves of the circular meshes with and without a filament around it in certain areas, and with the different filament thickness.

As evident from the graphic, the mesh that exhibits a more similar behaviour to the vaginal tissue features a pore diameter of 1.50 mm, along with filaments around specific areas, and incorporates filaments with 0.16 mm of diameter in the end columns and filaments with 0.24 mm diameter in the central columns.

As done previously, the deformation of the mesh pore that closely mimics the behaviour of vaginal tissue was analysed (Figure 3.13).

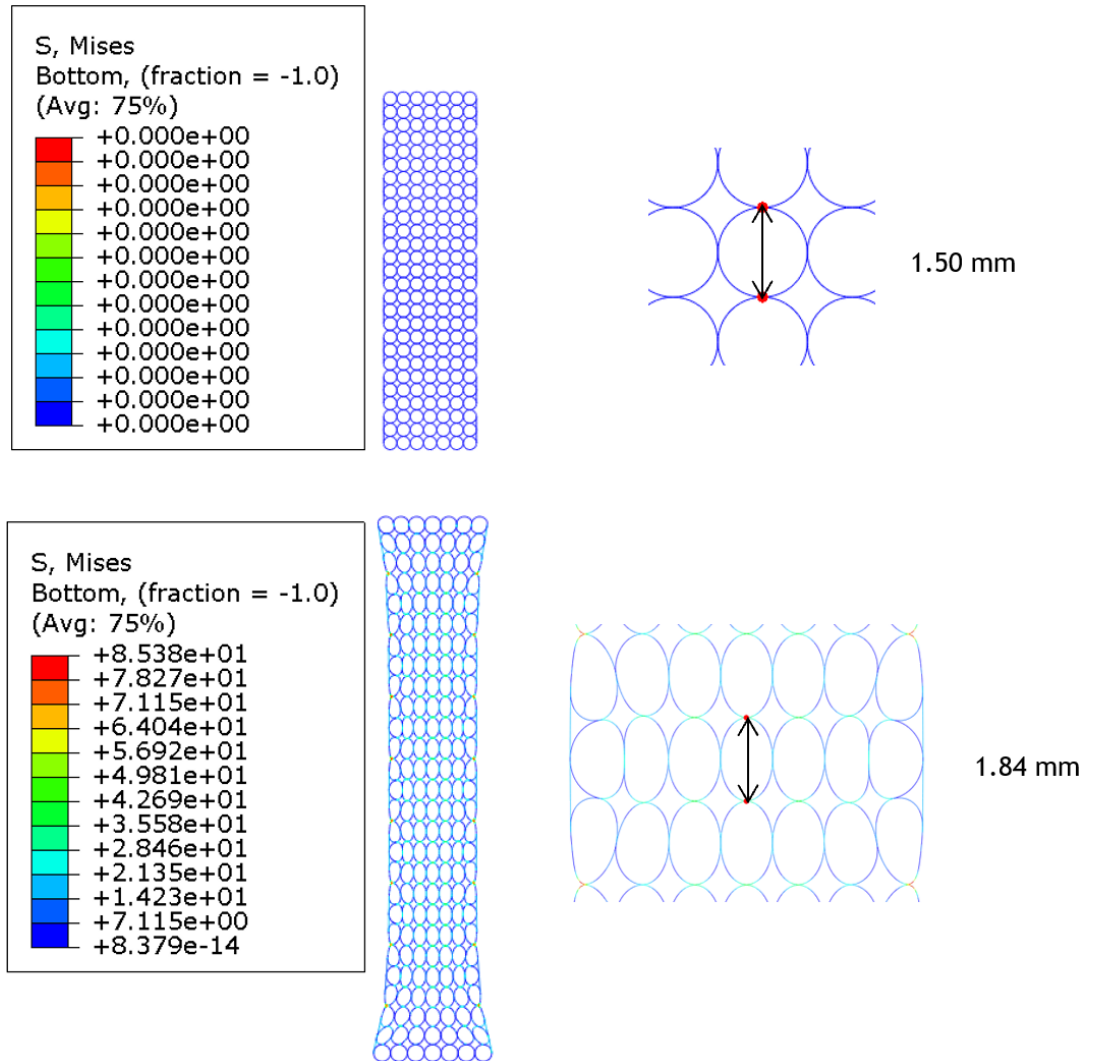
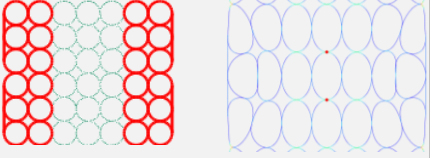
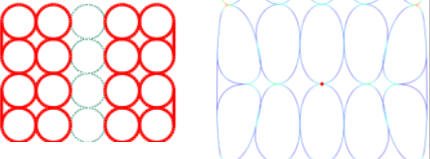
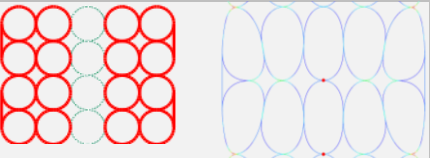
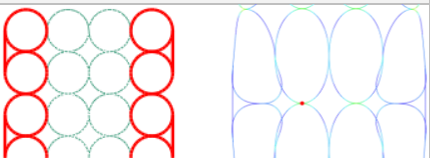
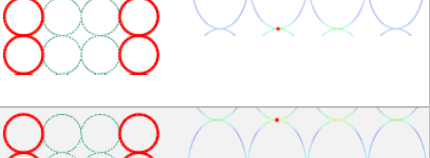


Figure 3.13 Difference between the pores of the circular mesh with a filament around it in certain areas, and with the different filament thickness before and after the simulation.

As depicted in Figure 3.13, it can be inferred that the recent alterations made to the meshes have led to a decreased pore deformation of 22.89% while achieving a maximum load value of 1.75 N within the comfort zone. This brings the results closer to replicating the behaviour of vaginal tissue.

The values of pore deformation and maximum load achieved within the comfort zone are presented in Table 2.

Table 2 Values of pore deformation and maximum values of load in the comfort zone for the circular pore meshes with different filament thickness.

Type of Mesh	Pore	Pore deformation (%)	Load (N)
Circular with the filament in certain areas_1.50 mm_0.08mm_0.24mm		22.50%	0.99
Circular with the filament in certain areas_2.00 mm_0.08mm_0.24mm		24.96%	0.04
Circular with the filament in certain areas_2.00 mm_0.16mm_0.24mm		24.63%	0.39
Circular with the filament in certain areas_2.50 mm_0.08mm_0.24mm		25.60%	0.32
Circular with the filament in certain areas_2.50 mm_0.16mm_0.24mm		25.19%	0.57
Circular without the filament_2.50 mm_0.08mm_0.24mm		24.94%	0.29
Circular without the filament_2.50 mm_0.16mm_0.24mm		25.42%	0.36

As evident from the information presented in Table 1, there is a direct correlation between increasing pore size and higher pore deformation, which is coupled with a decrease in the maximum load attained within the comfort zone.

3.3 Final Remarks

Considering the results obtained, the following graphic (Figure 3.14) illustrates the load-displacement values of the meshes that exhibited the most promising outcomes within the comfort zone. It also compares these values with the behaviour of the vaginal tissue, the uterosacral ligament, and the Restorelle® mesh [32][13].

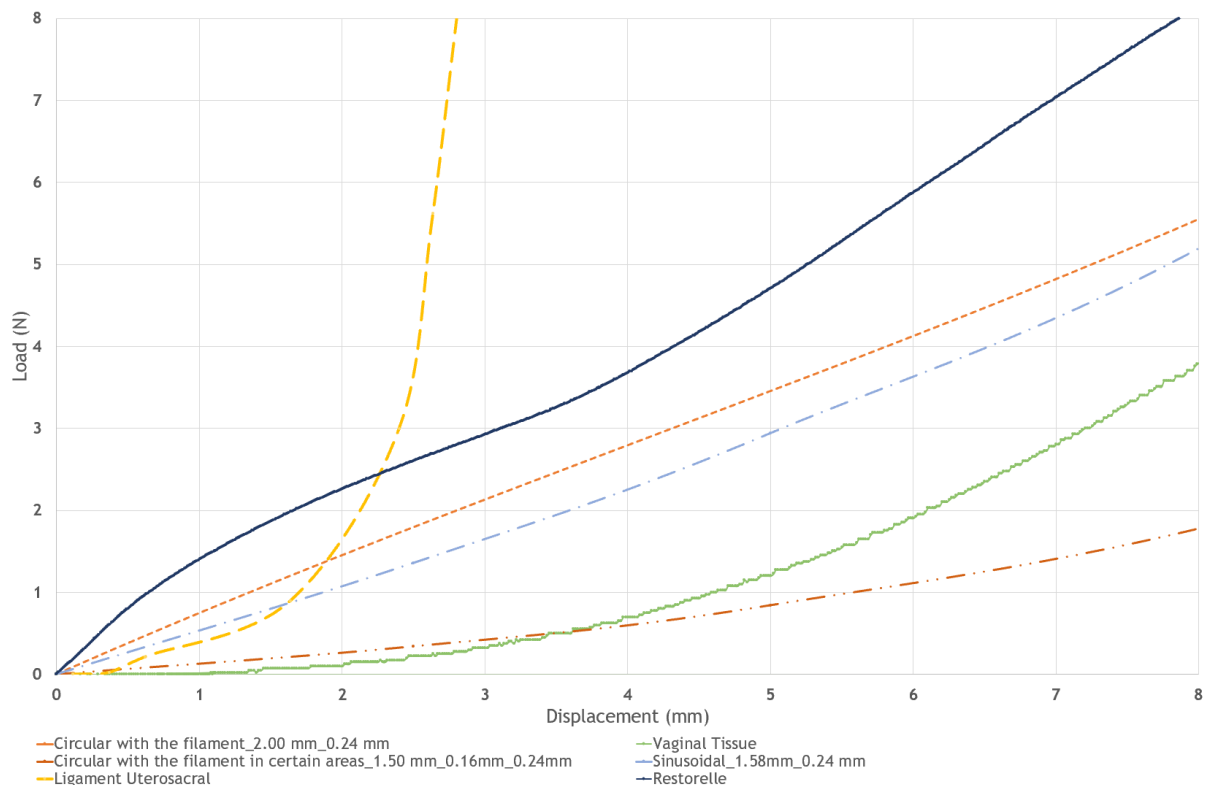


Figure 3.14 Load-displacement curves of the best mesh results obtained, the vaginal tissue, the ligament uterosacral, and the Restorelle® mesh.

As observed in Figure 3.14, the mesh that closely replicates the behaviour of vaginal tissue possesses specific characteristics, including a pore diameter of 1.50 mm, strategically positioned filaments around the mesh, and filaments with a diameter of 0.16 mm at the end columns and 0.24 mm in the central columns.

Despite the excellent results obtained by the sinusoidal and circular meshes with a 2.00 mm diameter and 0.24 mm filament thickness, it is worth exploring the possibility of combining the sinusoidal pattern with a circular pore design. These new meshes would incorporate 0.16 mm thick filaments in the end columns and 0.24 mm thick filaments in the central columns while maintaining a pore diameter of 1.50 mm. These meshes are expected to yield even closer load-displacement values to the vaginal tissue and minimal pore deformations, considering the sinusoidal pores exhibited the least distortion during the uniaxial tensile test.

The results were also compared to the load-displacement values of the uterosacral ligament, which possesses a more rigid behaviour compared to the vaginal tissue. While it is anticipated

that the selected meshes will not behave identically to the ligament, some resemblance can be observed between the load-displacement values of the sinusoidal mesh and the circular mesh with specific area filaments, particularly at the beginning of the graphic, demonstrating a partial likeness to the ligament's behaviour. Therefore, a future endeavour could involve investigating meshes capable of embodying both ligament and tissue properties.

Regarding the Restorelle® mesh, it is evident that this mesh does not exhibit behaviour similar to that of vaginal tissue or the uterosacral ligament. This dissimilarity is likely a major factor contributing to issues and tissue damage when this mesh is implemented in patients.

3.4 Main Conclusions

Key conclusions drawn from all the conducted work are as follows:

- The outcomes establish a strong correlation between experimental and computational tests, indicating that the simulations provide accurate representations of the mesh behaviour.
- Meshes lacking a filament around them tend to exhibit lower load values for equivalent displacement values compared to vaginal tissue, with the exception of the sinusoidal mesh.
- Beyond load and displacement values, the deformation of each mesh after specific force exposure is vital to consider, as excessive distortion can render a mesh unusable. Generally, meshes with a filament around them experience reduced pore deformation.
- The mesh's pore size directly influences load values, with smaller pore diameters, such as 1.50 mm, leading to higher load values. This suggests that a decrease in pore size results in an increase in the number of mesh columns and greater resistance to applied force, yielding higher load-displacement values.
- Thinner filaments correlate with lower load-displacement values.
- Among the latest meshes developed, the one most closely mirroring vaginal tissue behaviour features a pore diameter of 1.50 mm, strategic filaments in specific areas, and filaments with diameters of 0.16 mm in the end columns and 0.24 mm in the central columns.
- Meshes combining the sinusoidal pattern with a circular pore, along with 0.16 mm and 0.24 mm filament diameters while maintaining a 1.50 mm pore diameter, show promise for closely resembling vaginal tissue load-displacement values. Additionally, due to the minimal distortion observed in sinusoidal pores during the uniaxial tensile test, these meshes are likely to exhibit minimal pore distortion.
- Exploring the design of a mesh that can incorporate both ligament and vaginal tissue characteristics is important for future research.

- The Restorelle® mesh does not exhibit behaviour similar to vaginal tissue or the uterosacral ligament, suggesting it may not be the ideal choice for prolapse repair.

4. Conclusions

POP has a significant impact on the lives of individuals worldwide, underscoring the growing importance of dedicating resources and efforts to develop solutions that can alleviate these issues and improve people's quality of life.

Currently, there are recommended treatments available for managing POP. In its early stages, mild cases of POP can be effectively addressed through minimally invasive approaches, including the use of pessaries, physiotherapy, muscle strengthening exercises, biofeedback therapy, and electrical stimulation therapy. These methods have proven to be effective with minimal invasiveness. For cases where these approaches are ineffective, more invasive treatments are considered, especially for severe POP cases, which may involve surgery using synthetic mesh for permanent correction. However, due to the associated high risks, the FDA has prohibited the sale and distribution of such meshes for transvaginal prolapse treatment, posing a significant challenge in this area. This situation has prompted the development of biodegradable meshes, which offer advantages such as flexibility, malleability, biocompatibility, and the promotion of cell growth.

In essence, the introduction of biodegradable meshes into prolapse treatment is emerging as a highly recommended option, with the potential for improved outcomes while avoiding the risks and drawbacks associated with synthetic mesh use.

Within this context, various computational models of meshes have been created, varying in pore geometries, pore sizes, filament thicknesses, and the addition of filaments around specific areas of the meshes. These models have yielded promising results, demonstrating similarities to the load-displacement values of vaginal tissue. Nevertheless, there is a need for further refinement of these computational models to achieve the best possible meshes for prolapse repair. To this end, new concepts have emerged to advance this work and achieve a behaviour more akin to that of vaginal tissue and ligaments.

Conflict of interest statement

The authors affirm that they have no financial, professional, or any other personal interests in any product, service, or company that could be perceived as influencing their stance or position.

Acknowledgment

The authors thank the Emprego Científico 2021.00077. CEECIND, Funded by FCT. This work was supported by FCT, through INEGI, in the scope of LAETA, project UIDB/50022/2020 and UIDP/50022/2020.

References

- [1] D. Vilas and B. Rodrigues, "Structure Design Optimisation Of Biodegradable Implants For Melt Electrowriting," 2022.
- [2] J. Eric Jelovsek, C. Maher, M. D. Barber, J. E. Jelovsek, and M. D. Barber, "Pelvic organ prolapse," 2007. [Online]. Available: www.thelancet.com
- [3] S. Paramasivam, A. Proietto, and M. Puvaneswary, "Pelvic anatomy and MRI," *Best Pract. Res. Clin. Obstet. Gynaecol.*, vol. 20, no. 1, pp. 3-22, 2006, doi: 10.1016/j.bpobgyn.2005.09.001.
- [4] L. H. NYU, "Diagnosing Pelvic Organ Prolapse | NYU Langone Health." <https://nyulangone.org/conditions/pelvic-organ-prolapse-in-adults/diagnosis> (accessed Jun. 15, 2022).
- [5] C. Persu, C. R. Chapple, V. Cauni, S. Gutue, and P. Geavlete, "Pelvic Organ Prolapse Quantification System (POP-Q) - a new era in pelvic prolapse staging.," *J. Med. Life*, vol. 4, no. 1, pp. 75-81, 2011.
- [6] R. Specialists, "Pelvic Organ Prolapse How is pelvic organ prolapse diagnosed?"
- [7] F. Khorasani *et al.*, "Physiotherapy and pelvic floor muscle exercises for the prevention and treatment of pregnancy-related pelvic floor dysfunctions: A systematic review and meta-analysis," *Int. J. Women's Heal. Reprod. Sci.*, vol. 8, no. 2, pp. 125-132, 2020, doi: 10.15296/ijwhr.2020.20.
- [8] J. Xu and F. Huang, "A study of efficacy of traditional Chinese medicine combined with biofeedback electrical stimulation on postpartum pelvic organ prolapse," *Int. J. Clin. Exp. Med.*, vol. 13, no. 12, pp. 10031-10038, 2020, [Online]. Available: <https://www.embase.com/search/results?subaction=viewrecord&id=L2005768579&from=export>
- [9] "What is a Pessary: Pessary Device 101 | Penn Medicine." <https://www.pennmedicine.org/updates/blogs/womens-health/2016/may/what-is-a-pessary> (accessed Nov. 18, 2022).
- [10] "Pelvic Organ Prolapse (POP): Surgical Mesh Considerations and Recommendations | FDA." <https://www.fda.gov/medical-devices/urogynecologic-surgical-mesh-implants/pelvic-organ-prolapse-pop-surgical-mesh-considerations-and-recommendations> (accessed Jun. 13, 2022).
- [11] M. N. B. da Cunha, R. Rynkevich, M. E. T. da Silva, A. F. Moreira da Silva Brandão, J. L. Alves, and A. A. Fernandes, "Melt Electrospinning Writing of Mesh Implants for Pelvic Organ Prolapse Repair," *3D Print. Addit. Manuf.*, vol. 00, no. 00, pp. 1-10, 2021, doi: 10.1089/3dp.2021.0010.
- [12] B. Chughtai, J. Mao, T. S. Asfaw, C. Heneghan, C. R. Rardin, and A. Sedrakyan, "Long-term Device Outcomes of Mesh Implants in Pelvic Organ Prolapse Repairs," *Obstet. Gynecol.*, vol. 135, no. 3, pp. 591-598, 2020, doi: 10.1097/AOG.0000000000003689.
- [13] C. Maher, B. Feiner, K. Baessler, C. Christmann-Schmid, N. Haya, and J. Marjoribanks, "Transvaginal mesh or grafts compared with native tissue repair for vaginal prolapse,"

- Cochrane Database Syst. Rev.*, vol. 2016, no. 2, Feb. 2016, doi: 10.1002/14651858.CD012079.
- [14] M. E. T. Silva, J. N. M. Bessa, M. P. L. Parente, T. Mascarenhas, R. M. Natal Jorge, and A. A. Fernandes, "Effect of mesh anchoring technique in uterine prolapse repair surgery: A finite element analysis," *J. Biomech.*, vol. 127, no. July, p. 110649, 2021, doi: 10.1016/j.jbiomech.2021.110649.
- [15] J. K. Lunney, A. Van Goor, K. E. Walker, T. Hailstock, J. Franklin, and C. Dai, "Importance of the pig as a human biomedical model," *Sci. Transl. Med.*, vol. 13, no. 621, pp. 1-20, 2021, doi: 10.1126/scitranslmed.abd5758.
- [16] C. Soares, P. Martins, E. Silva, L. Hympanova, and R. Rynkevic, "Cog Threads for Transvaginal Prolapse Repair: Ex-Vivo Studies of a Novel Concept," *Surgeries (Switzerland)*, vol. 3, no. 2, pp. 101-110, 2022, doi: 10.3390/surgeries3020012.
- [17] M. Isabel and A. Pinto, "Melt electrowriting prototype optimization for medical-grade polycaprolactone mesh printing Melt electrowriting prototype optimization for medical-grade polycaprolactone mesh printing," no. september, 2022.
- [18] R. Dwivedi *et al.*, "Polycaprolactone as biomaterial for bone scaffolds: Review of literature," *J. Oral Biol. Craniofacial Res.*, vol. 10, no. 1, pp. 381-388, 2020, doi: 10.1016/j.jobcr.2019.10.003.
- [19] J. C. Kade and P. D. Dalton, "Polymers for Melt Electrowriting," *Adv. Healthc. Mater.*, vol. 10, no. 1, 2021, doi: 10.1002/adhm.202001232.
- [20] U. of P. Perelman School of Medicine, "Uniaxial Testing." <https://www.med.upenn.edu/pcmd/uniaxial-testing.html> (accessed Jun. 04, 2023).
- [21] R. Rynkevic, M. E. T. Silva, P. Martins, T. Mascarenhas, J. L. Alves, and A. A. Fernandes, "Characterisation of Polycaprolactone Scaffolds Made by Melt Electrospinning Writing for Pelvic Organ Prolapse Correction- a Pilot Study," *SSRN Electron. J.*, 2022, doi: 10.2139/ssrn.4036396.
- [22] M. N. B. Cunha, "Optimisation of a MEW prototype for mesh implants fabrication," 2020.
- [23] K. M. Knight, P. A. Moalli, and S. D. Abramowitch, "Preventing Mesh Pore Collapse by Designing Mesh Pores with Auxetic Geometries: A Comprehensive Evaluation Via Computational Modeling," *J. Biomech. Eng.*, vol. 140, no. 5, pp. 1-8, 2018, doi: 10.1115/1.4039058.
- [24] K. Baylón, P. Rodríguez-Camarillo, A. Elías-Zúñiga, J. A. Díaz-Elizondo, R. Gilkerson, and K. Lozano, "Past, present and future of surgical meshes: A review," *Membranes (Basel)*, vol. 7, no. 3, pp. 1-23, 2017, doi: 10.3390/membranes7030047.
- [25] H. Elsaghir, "R Econstructive S Urgery of the T Horacolumbar," *Neurosurgery*, vol. 51, no. November, pp. 118-122, 2002.
- [26] Coloplast, "'Restorelle Flat Mesh.'" <https://products.coloplast.us/coloplast/implantable-devices/womens-health-wh/pelvic-floor-repair/restorelle/restorelle-flat-mesh/> (accessed Jul. 23, 2023).
- [27] S. Eshraghi and S. Das, "Mechanical and microstructural properties of polycaprolactone scaffolds with one-dimensional, two-dimensional, and three-dimensional orthogonally oriented porous architectures produced by selective laser sintering," *Acta Biomater.*, vol. 6, no. 7, pp. 2467-2476, 2010, doi: 10.1016/j.actbio.2010.02.002.
- [28] Corbion, "Purasorb® DL - Product Specification Data Sheet," no. September. pp. 1-2, 2019. [Online]. Available: <https://www.corbion.com/static/downloads/datasheets/20d/purasorb-dl.pdf>
- [29] G. N. Greaves, A. L. Greer, R. S. Lakes, and T. Rouxel, "Poisson's ratio and modern materials," *Nat. Mater.* 2011 1011, vol. 10, no. 11, pp. 823-837, Oct. 2011, doi: 10.1038/nmat3134.
- [30] H. Marsh and F. Rodríguez-Reinoso, "Activated Carbon (Origins)," *Act. Carbon*, pp. 13-86, 2006, doi: 10.1016/B978-008044463-5/50016-9.
- [31] E. Characterization and F. Element, "applied sciences Experimental Characterization and Finite Element Modeling of the E f f ects of 3D Bioplotting Process Parameters on Structural and Tensile Properties of Polycaprolactone (PCL) Sca ff olds".
- [32] P. Martins, "Experimental and Numerical Studies of Soft Biological Tissues," vol. I, no. 1577, pp. 333-339, 2010.